UNIVERSIDADE DE BRASÍLIA – UNB

FACULDADE DE TECNOLOGIA / FACULDADE DO GAMA

PROGRAMA DE PÓS-GRADUAÇÃO EM INTEGRIDADE DE MATERIAIS DA ENGENHARIA

COMPARATIVE STUDY OF OPTIMIZATION ALGORITHMS FOR PARAMETER IDENTIFICATION OF THE SIGMOID MODEL IN MR DAMPERS

DAVI MATIAS DUTRA DA SILVA

ADVISOR: PROF. DRA. SUZANA MOREIRA ÁVILA

CO-ADVISOR: PROF. DR. MARCUS VINICIUS GIRÃO DE MORAIS

UNIVERSIDADE DE BRASÍLIA – UNB
FACULDADE DE TECNOLOGIA / FACULDADE DO GAMA

COMPARATIVE STUDY OF OPTIMIZATION ALGORITHMS FOR PARAMETER IDENTIFICATION OF THE SIGMOID MODEL IN MR DAMPERS

DAVI MATIAS DUTRA DA SILVA

ADVISOR: PROF. DRA. SUZANA MOREIRA ÁVILA
CO-ADVISOR: PROF. DR. MARCUS VINICIUS GIRÃO DE MORAIS

MASTER THESIS IN INTEGRITY OF MATERIALS ENGINEERING

ISSUE: 104A/2023

BRASÍLIA/DF, JUNE 2023

UNIVERSIDADE DE BRASÍLIA - UNB
FACULDADE DE TECNOLOGIA / FACULDADE DO GAMA
PROGRAMA DE PÓS-GRADUAÇÃO EM INTEGRIDADE DE MATERIAIS DA ENGENHARIA

COMPARATIVE STUDY OF OPTIMIZATION ALGORITHMS FOR PARAMETER IDENTIFICATION OF THE SIGMOID MODEL IN MR DAMPERS

DAVI MATIAS DUTRA DA SILVA

MASTER'S THESIS SUBMITTED TO THE POSTGRADUATE PROGRAM IN INTEGRITY OF MATERIALS ENGINEERING AT UNIVERSITY OF BRASILIA, AS PART OF THE REQUIREMENTS FOR OBTAINING A MASTER'S DEGREE.

APPROVED BY:

PROF. DRA. SUZANA MOREIRA ÁVILA
ADVISOR

PROF. DR. MARCUS VINICIUS GIRÃO DE MORAIS
CO-ADVISOR – FACULDADE TECNOLOGIA/UNIVERSIDADE DE BRASÍLIA

PROF. DR. ANDRÉ MURILO DE ALMEIDA PINTO
EXAMINER – FACULDADE DO GAMA/UNIVERSIDADE DE BRASÍLIA

PROF. DR. ALDEMIR APARECIDO CAVALLINI JUNIOR
EXAMINER– FACULDADE ENGENHARIA MECÂNICA/UNIVERSIDADE FEDERAL DE UBERLÂNDIA

RELATÓRIO (ATA) DE DEFESA DE DISSERTAÇÃO ASSINADO ELETRONICAMENTE PELA BANCA AVALIADORA, VIA SISTEMA ELETRÔNICO DE INFORMAÇÕES - SEI, DOCUMENTO 9844121, PROCESSO 23106.058529/2023-34.

BRASÍLIA/DF, JUNE 2023

CATALOGRAPHIC CARD

SILVA, D. M. D.

Comparative Study of Optimization Algorithms for Parameter Identification of the Sigmoid Model in MR Dampers [Distrito Federal], 2023.

151 p. 210 x 297 mm (FGA/FT/UnB, Master in Integrity of Materials Engineering, 2023).

Master Thesis – University of Brasília. Faculty of Technology.
Faculty of Gama.

1 MR Damper
2. Parameter Identification
3. Optimization
4. Sigmoid

I. ENC/FT/UnB
II. Title (series)

REFERENCE

SILVA, D. M. D. (2023). Comparative Study of Optimization Algorithms for Parameter Identification of the Sigmoid Model in MR Dampers. Master's Thesis in Integrity of Engineering Materials, Publication 104A/2023, Postgraduate Program, Faculty of Technology, University of Brasília, Brasília, DF, 151 p.

Assignment of Rights

Author: Davi Matias Dutra da Silva

Title: Comparative Study of Optimization Algorithms for Parameter Identification of the Sigmoid Model in MR Dampers.

Degree: Master

Year: 2023

davimatiasbra@gmail.com

Brasília, DF – Brasil

ACKNOWLEDGMENTS

I want to express my heartfelt gratitude to my mother, Rose, for her unwavering support and unconditional love. Her guidance and teachings have shaped me into who I am today, not only during my master's program but throughout my entire life.

I am deeply thankful to God for watching over me and caring for every detail throughout my life.

A special thanks go to my sisters, Susi and Raquel, for their love, encouragement, and unwavering belief in my abilities. Their support has been a constant source of motivation throughout my academic journey.

I extend my sincere appreciation to my supervisors, Prof. Suzana and Prof. Marcus, for their invaluable guidance, continuous support, and patience during my master's studies. Their immense knowledge and extensive experience have been instrumental in my academic research and daily life.

I want to acknowledge the support and resources provided by the Laboratory of Control Systems (SISCO) and the Vibrations Laboratory (GDS). The collaboration and access to their facilities significantly contributed to the success of my research.

I would also like to acknowledge Professor Fábio Comes de Castro, the supervisor of the Mechanical Testing Laboratory, for playing an essential role in overseeing the execution of the experiments. His expertise and guidance ensured the proper setup of the equipment and adherence to experimental protocols, contributing to the accuracy and reliability of the results obtained.

Finally, I would like to acknowledge the financial support provided by CAPES, FAP-DF, and DPG, which has been crucial in developing this work.

ESTUDO COMPARATIVO DE ALGORITMOS DE OTIMIZAÇÃO PARA IDENTIFICAÇÃO DE PARÂMETROS DO MODELO SIGMOIDE EM AMORTECEDORES MR

RESUMO

Este trabalho tem como foco a identificação de parâmetros de um amortecedor magneto-reológico (MR) comercial. O comportamento não linear do amortecedor MR foi modelado utilizando o modelo parametrizado sigmoid proposto por Wang, baseado no comportamento dinâmico experimental de um amortecedor MR utilizando técnicas de ajuste para funções senoidais simétricas e não simétricas. Dois métodos de otimização foram utilizados como algoritmos de minimização são eles: método de busca simplex de Nelder-Mead e a evolução diferencial. O desempenho dos métodos de otimização foi comparado. A dependência da frequência de excitação, do deslocamento do pistão, da corrente aplicada na bobina do amortecedor e a temperatura de operação do amortecedor MR também foram avaliadas. A validação do modelo paramétrico foi alcançada comparando-se os resultados experimentais com os valores simulados. Os resultados mostraram que a metodologia proposta é eficaz na identificação de parâmetros do amortecedor MR e pode ser utilizada para aprimorar o desempenho do sistema de suspensão semiativa.

Palavras-chave: Amortecedor MR, Identificação de Parâmetros, Otimização e Sigmoid.

ABSTRACT

This study focuses on the parameter identification of a commercial magnetorheological (MR) damper. The nonlinear behavior of the MR damper was modeled using the numerically parameterized sigmoid model proposed by Wang, which utilized the experimental dynamic behavior of a commercial MR damper and applied a method to fit symmetric and asymmetric sigmoid functions using experimental data. Two optimization methods, namely the Nelder-Mead simplex search method and the differential evolution (DE), were proposed as minimization algorithms. The performance of the optimization methods was compared. The dependency of frequency excitation, piston displacement, current applied in the coil, and the operating temperature of the MR damper were also evaluated. The model parameter was validated by comparing experimental results with identified values. The results show that the proposed methodology effectively identifies the parameters of the MR damper and can be used to improve the performance of the suspension system.

Keywords: MR Damper, Parameter Identification, Optimization and Sigmoid.

CONTENTS

LIST OF TABLES

LIST OF FIGURES

LIST OF NOMENCLATURES AND ABBREVIATIONS

EQ	Equation.
ER	Electrorheological.
ERF	Electrorheological Fluid.
LORD	Lord Corporation.
MR	Magnetorheological.
MRF	Magnetorheological Fluid.
MTS	MTS Corporation.
FIG	Figure.
TAB	Table
DE	Differential Evolution.
GA	Genetic Algorithm.
ES	Evolutionary Strategies.
EP	Evolutionary Programming.
F-V	Force-Velocity Behavior.
$\boldsymbol{\tau}$	Shear Stress.
$\boldsymbol{\tau_y}$	Yielding Stress.
$\boldsymbol{\mu}$	Newtonian Viscosity.
$\dot{\boldsymbol{\gamma}}$	Shear Strain rate.
$\boldsymbol{u}$	Displacement.
$\boldsymbol{f}$	Frequency.
$\boldsymbol{A}$	Amplitude.
$\boldsymbol{T}$	Time.
$\boldsymbol{\phi}$	Phase Angle.
$\boldsymbol{V}$	Voltage.
$\boldsymbol{F_D}$	Damping Force.
$\boldsymbol{c_0}$	Viscous Coefficient.
$\boldsymbol{k_0}$	Stiffness.
$\dot{\boldsymbol{u}}_{\boldsymbol{1}}$	Damper Velocity.
$(\boldsymbol{u} - \boldsymbol{u_0})$	Displacement in the x direction.
$\boldsymbol{\alpha z}$	Hysteretic Variable.
$\dot{\boldsymbol{u}}$	Damper Velocity.

$\ddot{u}$	Damper Acceleration.
v_m	Peak Velocity.
a_m	Sigmoid Amplitude.
ω	Frequency.
v_h	Zero-force Velocity Intercept.
v_d	Offset Velocity.
ω	Frequency.
ϵ_u	Residue Function.
$I^l(x_m)$	Lower Bound.
$I^u(x_m)$	Upper Bound.
R_{noise}	White Noise.
P_{DE}	Initial Population.
x_{rand}	Randomly Population.
x_{best}	Best Adapted Population.
x_{trial}	Vector of Mutation Process.
CR	Crossing Probability.
A	Ampere.
w	Watt.
H	Height.
W	Width.
D	Depth.
Kg	Kilogram.
D	Depth.
Hz	Hertz.
mm	Millimeters.
℃	Celsius.
S	Objective Function.
C	Relative Residual Sum.

1 INTRODUCTION

The concept of vehicle suspension systems dates back to the 19th century when the first automotive suspension system consisted of a few leaf springs. Since its introduction in 1903 by the Mors brothers, the first automobile equipped with shock absorbers inspired by suspension systems used in horse carriages, vehicle suspension technology has undergone significant advancements (Riazi 2021).

Suspension systems (Figure *1*) play a crucial role in the automotive industry, providing stability, comfort, and safety by absorbing and controlling the forces and vibrations during vehicle motion. A suspension system maintains optimal contact between the tires and the road surface, ensuring improved handling, reduced vibrations, and enhanced ride quality (Goodarzi and Khajepour 2017). An ideal suspension system should rapidly absorb road shocks generated by the vehicle and gradually return it to its normal position while maintaining optimal contact between the tire and the road surface (Yaakub et al. 2020).

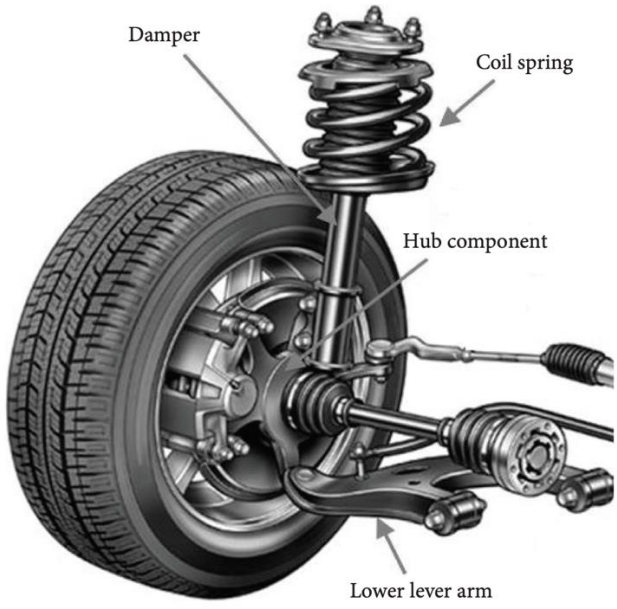

Figure 1 – Automotive Suspension System (Nguyen and Nguyen 2023)

Three types of suspension systems are employed in vehicles, each with its characteristics and advantages. Commonly used suspension systems include passive suspensions, active suspensions, and semi-active suspensions (Dixon 2007).

The semi-active suspension system is a promising alternative to passive and active suspensions. Semi-active suspensions combine the advantages of both passive and active systems by employing controllable dampers that can adjust their damping characteristics based on the driving conditions. This improves ride comfort while reducing complexity and cost compared to fully active suspensions (Fischer and Isermann 2004).

One type of damper commonly used in semi-active suspensions is the magnetorheological (MR) damper. MR dampers utilize magnetorheological fluid, which changes its viscosity and damping properties when subjected to a magnetic field. This unique property enables MR dampers to provide real-time damping adjustments, making them suitable for semi-active suspension systems. MR dampers in semi-active suspensions have gained significant attention in recent years due to their ability to provide adaptive and precise control of the suspension response. These dampers can quickly adjust their damping forces based on sensor inputs, offering improved ride comfort and handling performance in various road conditions (Karkoub and Zribi 2007).

The field of semiactive control dampers for structural vibration control has experienced significant advancement in recent years. Researchers have been focusing on investigating and exploiting some gaps and drawbacks in implementing magnetorheological dampers for vibration control. The MR damper has emerged as a highly promising technology solution for vibration control in several applications, such as building protection from seismic events (Jung et al. 2006; Sun et al. 2018), automotive suspension (Feng et al. 2020; Pepe, Roveri, and Carcaterra 2019; Soliman and Kaldas 2019), aircraft landing gear system (Kang et al. 2020; Luong, Jang, and Hwang 2020), knee prostheses (Fu, Pan, and Xu 2019; Ochoa-Diaz et al. 2014), precise manufacturing machines (Kim et al. 2018), seat suspension (Du et al. 2018) and high-speed railway vehicle suspension (Jin et al. 2020a; Liao, Liu, and Yang 2019).

When working with MR dampers, there are various challenges and issues that researchers and engineers must address to ensure optimal performance and reliability. These challenges arise from the unique properties and behaviors of MR fluids used in these dampers. One common challenge is the formation of hard cake, which refers to solidifying particles within the MR fluid. This can lead to reduced performance and hinder the effective operation of the damper. Another issue is the clumping effect, where particles agglomerate and create uneven distribution within the fluid, resulting in inconsistent damping characteristics. Fluid Particle Separation (FPS) is another concern, as the particles within the fluid can separate under certain conditions, leading to changes in the fluid's properties and affecting its performance.

Additionally, the oxidation of particles due to exposure to oxygen can degrade the fluid over time, necessitating measures to mitigate this effect. Ensuring the stability of the MR fluid is crucial, as it needs to maintain its consistency and properties under different operating conditions. Sealing issues must also be addressed to prevent leakage and preserve the integrity of the damper system. Temperature effects are significant, as MR fluids can exhibit different properties with temperature changes. Understanding and managing these temperature-dependent behaviors is essential for optimizing the performance of MR dampers. Other challenges include interior wall incrustation, erosion, characterizing the yield stress of the MR fluid, addressing instabilities in pressure-driven flow, managing in-use thickening, and optimizing the time response of the damper (Glaser et al. 2016; Kumar et al. 2019).

Semi-active suspension, also known as electronic suspension, has several advantages over conventional vehicle suspension systems. However, it also has some disadvantages. Here are some of them:

1. Cost: Semi-active suspension is more expensive than conventional suspension systems. This is due to the use of additional sensors, actuators, and electronic components required to control the suspension in real time. Therefore, replacing or repairing the system can be more costly (Soliman and Kaldas 2021).
2. Complexity: Semi-active suspension is a complex system with sophisticated electronic and control components. This means it requires specialized maintenance and, in case of failure or malfunction, can be

more challenging to diagnose and repair than a conventional suspension system (Theunissen et al. 2021a).

3. Power dependency: Semi-active suspension relies on electrical power to function. This means that if there is a failure in the vehicle's electrical system or if the battery is discharged, the suspension may not work correctly. In contrast, conventional suspension systems do not require electricity (Zhao et al. 2023).
4. Need for calibration and configuration: Semi-active suspension requires proper calibration and configuration to adapt to the vehicle and driver's preferences. This may require initial and periodic adjustments over time. Additionally, each manufacturer may have a semi-active suspension system, which means that calibration and configuration procedures may vary between vehicles (Theunissen et al. 2021a).

Controlled suspension in mass-market automobiles can be traced back to the 1960s when Citroen introduced hydro-pneumatic active suspension in its luxury cars. The introduction of controlled suspension has significantly impacted the mass market for vehicles. Controlled suspension systems are still expensive, restricting this option to luxury cars (Soliman and Kaldas 2019).

This work aims to reproduce a phenomenological approach to modeling the nonlinear dynamic behavior of the MR damper for semi-active automotive suspension systems. The approach is based on replicating the methodology proposed by (Santade 2017), which utilizes the parametric sigmoid model and Nelder-Mead Simplex method for optimization. By applying this approach, the study seeks to provide a comprehensive understanding of the MR damper's behavior and its potential applications in semi-active suspension systems. The replication of Santade's work is a foundation for investigating the sigmoid model's effectiveness and reliability in capturing the MR damper's complex behavior.

By focusing on the context of the vehicle suspension system and the advancements in MR dampers, utilizing the parametrized sigmoid model in simulations, which demonstrated remarkable conformity with experimental results and indicated a good correlation, this works aims to contribute to the development of more efficient and effective semi-active suspensions. Accurately representing the MR

damper's non-linear hysteretic behavior is crucial for designing controllers that enhance its performance. Hence, selecting an appropriate model becomes essential for achieving this goal. The proposed phenomenological approach seeks to improve the understanding and modeling of the MR damper's nonlinear dynamics, facilitating its optimized integration into suspension systems and improving vehicle performance and comfort.

1.1 Motivation

In the last few years, the automotive industry has focused on developing more advanced and efficient suspensions to enhance comfort and safety for users. Among the available technologies, semi-active suspension with magnetorheological dampers has emerged as a promising option due to its ability to adapt to varying vehicle operating conditions dynamically.

However, despite recent advancements, there still needs to be more in our knowledge regarding the behavior and performance of these semi-active suspensions under different usage conditions. In this context, this thesis aims to explore the application of MR dampers in semi-active suspensions by utilizing a parametric model for parameter identification. The primary objective is to accurately estimate the model parameters using experimental data, which can contribute to a better understanding of the system's behavior and facilitate the development of more precise models and control strategies. Employing a parametric model can simulate and analyze the system's response to various inputs, offering valuable insights for optimizing its performance. Ultimately, applying a parametric model for parameter identification can lead to improvements in the overall design and control of the system.

1.2 Research Objectives

1.2.1 General Objectives

Designing an optimal suspension system is challenging, especially considering the need to control multiple parameters. The general objective of this study is to replicate a phenomenological approach for modeling the nonlinear dynamic behavior of MR dampers in semi-active automotive suspension systems. Drawing inspiration

from Santade's work (Santade 2017), the focus is on utilizing the parametric sigmoid model. The main goal is to compare and evaluate the performance of two optimization algorithms, namely the Nelder-Mead Simplex method and the differential evolution algorithm, in accurately identifying the parameters of the sigmoid model.

1.2.2 Specific Objectives

a) Impact of Frequency and Stroke Displacement: Further investigate the impact of increasing frequency and stroke displacement on the behavior of the MR damper system. Conduct experimental studies to analyze how these factors affect the damping force, velocity, and hysteresis behavior. This analysis will provide insights into the system's dynamic response and help optimize its performance under different operating conditions.

b) Temperature Effects and Magnet Saturation: Conduct a comprehensive study on the effects of temperature, focusing on the impact of magnetic saturation on the maximum damping force of the MR damper. Perform experiments under varying temperature conditions and measure the resulting damping force. This analysis will help understand the thermal behavior of the MR damper and its implications for practical applications.

c) Error Analysis and Validation of the Sigmoid Model: Implement a detailed error analysis to validate the accuracy of the parametrized Sigmoid model. Compare the simulated results obtained from the model with experimental data to assess its conformity. By quantifying the error and conducting statistical analyses, the reliability and applicability of the model can be evaluated, demonstrating its potential for designing controllers to enhance MR damper performance.

d) Sensitivity Analysis of Identified Parameters: Perform a sensitivity analysis on the identified parameters within the parametrized sigmoid model. Determine which parameters have the most significant impact on the model's behavior and output. This analysis will provide valuable insights into the key parameters that must be accurately identified and considered in future modeling and control strategies.

e) Comparison of Optimization Algorithms: Discuss the advantages and limitations of the Nelder-Mead simplex search method and the differential evolution algorithm used for parameter identification. Analyze the discrepancies observed in the optimization outcomes of specific parameters and provide insights into the algorithm's performance for different parameter sets. This analysis will help researchers understand the strengths and weaknesses of each algorithm and guide the selection of appropriate optimization methods in future studies.

1.3 Plan of Dissertation Sections

In order to achieve the objectives of this investigation, five steps were performed. The second step of the study involved conducting a background and literature review on various subjects, including the suspension system of vehicles, semi-active suspensions, control strategies, MR dampers, and MR landing gear. These subjects are presented in chapter 2 of this thesis. Initially, general definitions of vehicle suspension are provided.

The third step focused on designing the experimental procedure, which aimed to replicate and validate results from existing literature. The parametric sigmoid model was selected for this work. A sinusoidal signal was chosen to obtain the excitation signal required by this model. A servo-hydraulic actuator in the universal testing machine (MTS) was used to generate the signal, which allowed precise control of the excitation signal’s frequency, displacement, and current applied to the damper coil. Additional details on these experimental parameters can be found in Chapter 3 of this thesis.

In the fourth step of the study, algorithms for parameter identification based on the sigmoid model were implemented. Two optimization techniques, namely the Nelder-Mead simplex search method and differential evolution, were utilized to minimize the normalized errors between experimental and numerical data. The results obtained from these techniques were subjected to a statistical error analysis using a Gaussian distribution to evaluate the randomness of the errors. They provided a comprehensive analysis and verification of the results. Important aspects were

highlighted, which warrant further investigation in future research. More detailed information on these results is available in Chapter 4 of this thesis.

The final step consisted of drawing conclusions from the study and providing suggestions for future work. Based on the findings and analysis, several key observations were made regarding the behavior of the MR damper and its application in semi-active suspensions.

2 THEORETICAL REVIEW

This chapter aims to establish a theoretical review for studying semi-active suspension systems in automotive applications. It encompasses various topics, including automotive suspension, semi-active suspension, semi-active dampers, commercial vehicles equipped with semi-active suspension, and the current state of the art in this field. By covering these subjects, the chapter provides the necessary background information and context for the subsequent exploration of practical implementation and optimization strategies in the following chapters.

2.1 Automotive Suspension

Over the past few years, the competition within the automotive industry has intensified, leading to an increased focus on developing superior automotive suspension systems. These systems aim to efficiently absorb road disturbances the vehicle generates, swiftly restoring it to its normal position while ensuring optimal contact between the tire and the road surface (Yaakub et al. 2020).

The suspension system plays a vital role as it serves as the connection between the vehicle body/frame and the road surface, encompassing the wheels and tires as integral components. While many people primarily associate the suspension with providing a comfortable ride, it fulfills three essential functions (Murata 2011):

I. Vibration and Shock Absorption: One of the primary objectives of the suspension system is to isolate passengers and cargo from road vibrations and shocks. To achieve optimal comfort, the system must effectively absorb shocks and dampen vibrations caused by uneven road surfaces.

II. Enhanced Mobility: The suspension system is crucial in improving the vehicle's mobility. It ensures sufficient clearance between the road and the vehicle's underside. Additionally, it provides lateral and longitudinal stability, countering chassis roll and promoting better maneuverability.

III. Vehicle Control: Another vital function of the suspension system is facilitating vehicle control. It responds to tire forces induced by acceleration, braking, and steering, helping to maintain proper steer and

camber angles relative to the road surface. Furthermore, it endeavors to keep all four tires in contact with the road during maneuvers.

The passive suspension system is the most commonly used in the automotive industry due to its simple structure, high reliability, and low cost. This system consists of a structure composed of a hydraulic shock absorber, spring, and linkages that connect a vehicle to its wheels (Abdelkareem et al. 2018).

There are three significant kinds of vehicle suspension according to the level of robustness.

- Passive Suspension: Passive suspension refers to a suspension system not incorporating electronic or computer-controlled components. It relies on mechanical components, such as springs and dampers, to absorb shocks and vibrations from the road. The characteristics of the suspension are fixed and cannot be adjusted in real time (Issa and Samn 2022).
- Semi-Active Suspension: Semi-active suspension is a suspension system that combines passive and active suspension elements. It uses electronic controls to adjust the damping characteristics of the suspension in response to changing road conditions. While it can adapt to varying needs, it cannot actively control the suspension system in real-time (Jin et al. 2020b).
- Active Suspension: Active suspension is an advanced suspension system that employs electronic sensors and computer-controlled components to control the suspension in real time actively. It continuously monitors the road conditions and driver inputs and adjusts the suspension settings accordingly. This enables precise control over the suspension's behavior, providing improved comfort, stability, and handling (Joshua Robert et al. 2022).

Figure *2* shows a quarter suspension vehicle models (a) Passive, (b) Semi-active, and (c) Active

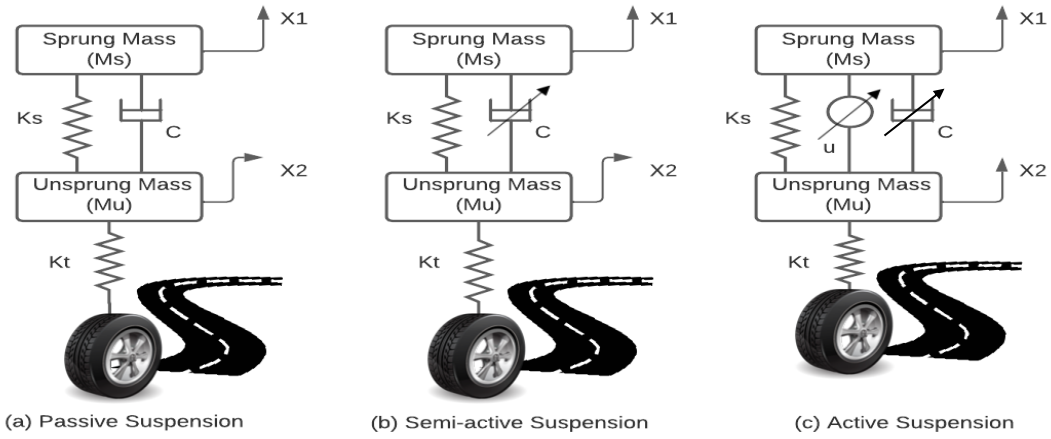

Figure 2 - Suspension System Classification (adapted from Omar et al. 2017)

These suspension elements support the vehicle and transfer its weight to the wheels. In conventional road vehicle suspension systems, passive components such as springs and dampers suppress the vibration. The suspension spring can store energy through load and deflection (Narayan, Alsagri, and Gupta 2019), while the shock absorber is the energy-dissipating device.

To design a suspension system capable of absorbing road disturbances, bumps, and vibrations, a trade-off between two conflicting parameters must be made: road holding and passenger comfort ride. Ride comfort is subjective and depends on human perception. The vibration transmitted to the human body is measured by the comfort rating and is evaluated against established standards (Mitra et al. 2016).

Vehicle vibrations are primarily caused by road roughness, most noticeable in the vertical direction. The impact of vibrations becomes detrimental when they occur at frequencies related to the resonances of road vehicles or the human body (Krauze 2013). In practice, vehicle natural frequencies are typically, observed to be around 1-2 Hz (Dixon 2007a).

The typical force–velocity for a passive suspension is displayed in Figure 3.

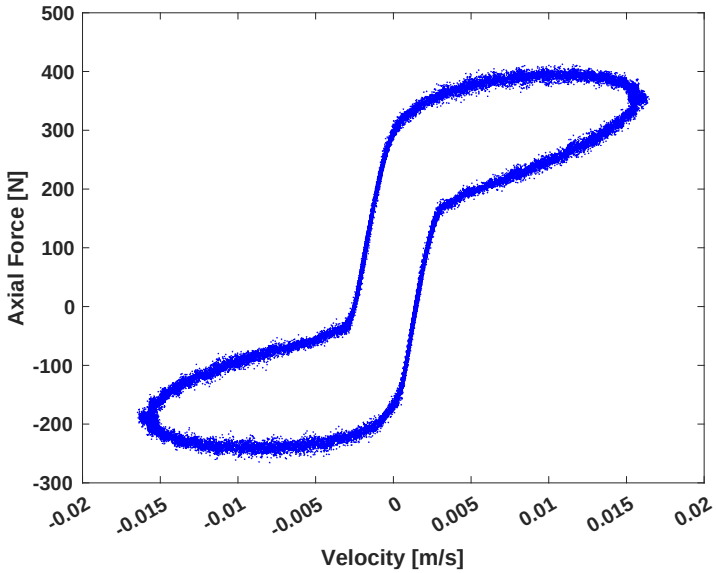

Figure 3 - Typical Force – Velocity response passive damper

The ideal suspension should align with comfort, handling, and safety principles. Various commercial technologies are utilized to enhance or replace conventional passive suspension systems.

To be considered an ideal suspension, it should be able to rapidly absorb road shocks independently while gradually returning the vehicle to its original position without being perceptible to the passengers. In terms of passenger comfort, it is generally assumed that overall comfort is improved when the following conditions are minimized (Gysen et al. 2010):

I. motion sickness: ~1Hz
II. head toss: 2 - 8 Hz

2.1.1 Active Suspension

In a passive suspension system, the dynamic response is governed by fixed stiffness and damping parameters. However, the system is exposed to different external excitations across various frequency ranges, including deterministic factors like track layout and stochastic factors like track irregularities. Designing a passive suspension system with fixed parameters becomes challenging as it requires striking a compromise solution for different operating conditions. On the other hand, an active suspension system provides the opportunity to achieve a "global optimum solution" by

incorporating variable suspension parameters using sensors, controllers, and actuators (Fu et al. 2020).

One significant drawback of many active suspension systems is their high energy consumption. However, in the case of linear electric motors, this disadvantage can be mitigated by the ability to recover and store energy for subsequent use when needed. This feature enables more efficient energy utilization within the system (Hyniova et al. 2009).

Active suspension technologies can be categorized into two types based on their location: active primary suspension and active secondary suspension (Fu et al. 2020).

I. Active primary suspension.
II. Active secondary suspension.

Active primary suspension systems are primarily focused on improving the stability, guidance, and curve negotiation behavior for wheelsets, whether they are solid-axle wheelsets (SW) or independently rotating wheels (IRW). These suspension systems are designed to enhance the performance of the wheels in terms of stability and maneuverability during cornering or navigating curves. On the other hand, active secondary suspension systems aim to improve ride quality and control the quasi-static motion of the car body. They incorporate devices such as the Hold-Off-Device (HOD) to improve the comfort and stability of the car by reducing vibrations and minimizing the impact of road irregularities on the car body. Another application of active suspension can be found in tilting trains, where the car body is tilted to a desired rolling angle in curves. This tilting mechanism helps reduce the lateral acceleration experienced by the passengers, allowing for higher speeds and improved curve negotiation capabilities. By categorizing active suspension technologies based on their location and intended purposes, it becomes easier to understand their specific roles in enhancing stability, ride quality, and overall performance in different types of vehicles (Fu et al. 2020; Liu, Goodall, and Iwnicki 2020; Wang et al. 2020).

To fully control a vehicle's roll and pitch behavior, it is necessary to identify and customize the forces acting on both the unsprung mass (wheels, axles, etc.) and the sprung mass (vehicle body and occupants). An active suspension system can be viewed as the capability to continuously reduce the acceleration of the sprung mass and reduce the suspension deflection. This provides several improvements to the

suspension system, such as enhancing tire grip with the road surface, optimizing brake performance, enabling traction control, and improving vehicle maneuverability (Chen, Liu, and Sun 2005). However, the high energy demand and associated costs hinder the widespread implementation of active suspension systems. These factors pose significant barriers to their adoption of mass-produced vehicles (Stribrsky et al. 2007).

The active suspension system distinguishes itself from the passive suspension system by its capability to inject energy into the system rather than solely storing and dissipating energy. It actively controls the vertical movement of the wheels about the chassis or vehicle body (Yaakub et al. 2020).

When working with an active suspension system, it is essential to consider that this type of system has both advantages and disadvantages in its implementation (Gysen et al. 2010). According to Aboud's classification, active suspensions can be divided into two types: electromagnetic active suspensions and hydraulic active suspensions (Aboud, Haris, and Yaacob 2014).

2.1.1.1 Hydraulic and Pneumatic Suspension

Hydraulic and pneumatic suspensions are active suspension systems that combine springs and hydraulic or pneumatic devices to generate damping forces between the suspended and unsupported masses. Several automotive manufacturers have developed active suspension systems based on these principles. BMW has introduced an active suspension system with a hydraulic stabilizer bar. The system consists of various components such as a hydraulic pump, lateral acceleration sensors, a command emitter, a hydraulic suspension block, and two active stabilizing bars with rotary-hinged devices. Mercedes has developed a hydraulic active suspension system with a hydraulic arc, hydraulic structure, high-pressure accumulator, hydraulic pump, shock absorbers, and a control unit. AUDI has implemented an active pneumatic suspension system that comprises a pneumatic spring, reservoir, control unit, sensors, compressor, and pressure sensor electromagnetic valve block. Compressed air from a compressor or electric motor is used for damping purposes (Marcu et al. 2017).

2.1.1.2 Active Electromagnetic Suspension

The active electromagnetic suspension system combines an electromagnetic device with a mechanical spring. This configuration provides a suspension function and enables energy recovery, reducing vehicle energy consumption. One example is the BOSE suspension, which utilizes a linear electromagnetic motor and a power amplifier for vibration control. The system stores energy generated during suspension compression. By employing an electromagnetic damper, the suspension can compress and relax to a greater extent, minimizing passenger discomfort and enhancing ride comfort (Marcu et al. 2017).

2.1.2 Semi-active Suspension

The semi-active suspension system, illustrated in Figure 2, combines the advantages of both active and passive suspension systems, resulting in a unique hybrid approach. In a semi-active suspension system, the dampers have the capability to enhance the performance of the suspension system across a wide range of frequencies. Even in the event of an electrical system failure, the damper continues to function as a passive hydraulic damping device, ensuring the continued operation of the suspension system device (Yao et al. 2002). In controlled suspension systems used in road vehicles, actuators generate controllable forces between the sprung and unsprung masses (Theunissen et al. 2021b). Semi-active dampers allow the modification of the dynamic properties of the suspension system with lower energy consumption and mechanical complexity. While the semi-active suspension shares the same components as a passive suspension system, the damper has two or more selectable damping rates. The semi-active suspension system can only control the viscous damping coefficient of the shock absorber by changing the applied current. However, this process does not provide energy to the suspension system and is limited in performance because its components can only store or dissipate energy. As a result, it becomes challenging to simultaneously satisfy the requirements of comfort and handling under varying road conditions (Yaakub et al., 2020).

Figure 4 presents a performance comparison of various suspension types produced by Lord Corporation, providing insights into their effectiveness and suitability for specific applications (LORD 2023).

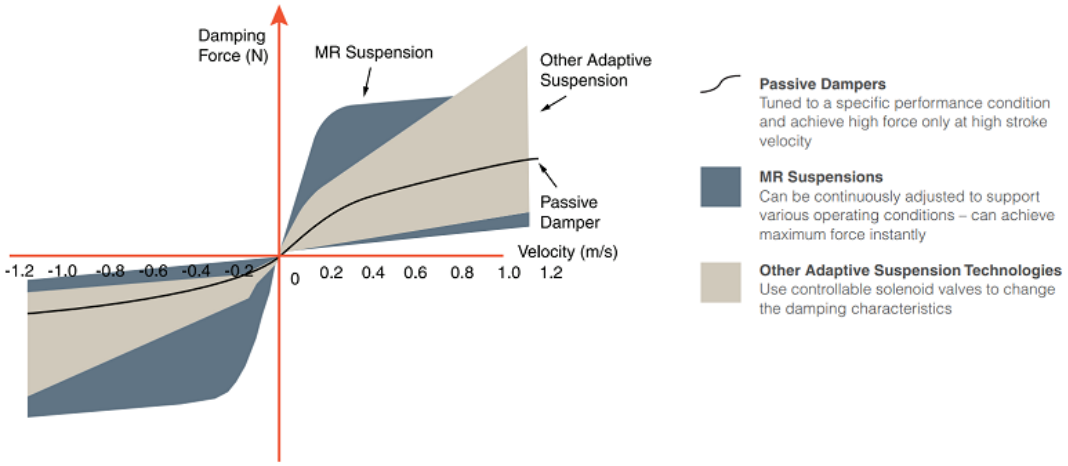

Figure 4 - *MR damper Force – Performance comparison of various suspension types from* (LORD 2023)

Figure 5 is designed to illustrate the force-velocity behavior of both a passive damper and a semi-active damper through experimental testing. The figure compares the force-velocity characteristics of these two dampers to assess their performance under varying velocity conditions. The primary objective is to examine the relationship between the force generated by each damper and the velocity at which it operates.

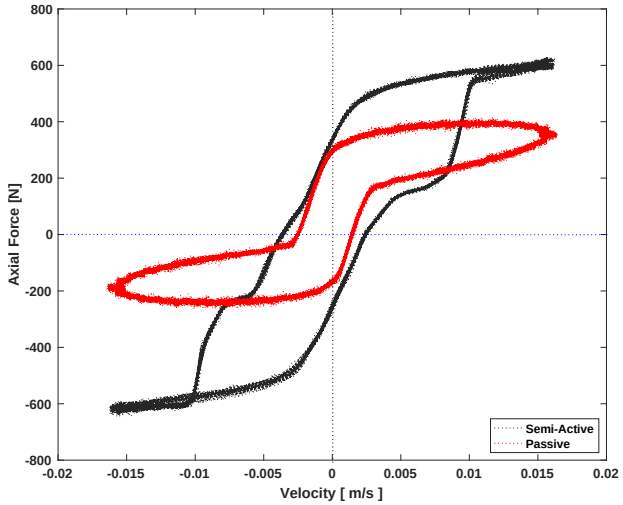

Figure 5 - Experimental Results MR damper vs Passive damper (Force – Velocity performance)

2.2 Semi-active Dampers

The semi-active damper is a component of the semi-active suspension system. It functions as a hydro-mechanical device capable of adjusting the amount of energy

dissipated by the system by controlling the excitation current of the coil. These dampers are designed in a way that the damping force is proportional to the speed (Eslaminasab, 2008). To achieve vibration control using semi-active damping control, various energy-dissipating devices can be used for modulating the damping force. Examples of such devices include (Soliman and Kaldas, 2019):

- Servo/Solenoid valve dampers
- Magnetorheological (MR)
- Electrorheological (ER) dampers

2.2.1 Solenoid/Servo valve dampers

To meet specific requirements, the controllable valve within the damper must operate at its maximum velocity, enabling a flow rate corresponding to the fluid displaced within the damper. Additionally, the controllable valve must rapidly respond to effectively vary the damping force during operation (Soliman and Kaldas 2019).

The classic electrohydraulic model utilized solenoid valves, which can be located either inside or outside the cylinder body of the damper. These valves are capable of changing the damping ratio by adjusting the size of the orifices (Savaresi et al. 2010). Solenoid valves are often considered an alternative to servo valves. While solenoid valves may not offer the same level of quick response or precise feedback as servo valves, they are a more cost-effective option. It is important to note that magnetic saturation should be addressed in many articles when working with solenoid valves. However, the saturation condition should be noticed, as high-speed solenoid valves typically operate in the magnetic saturation region to increase the opening speed (Liu, Gu, and Chen 2008). In the railway vehicles of Japan, semi-active suspension is used to improve the vibration caused by track irregularities. The damping coefficient is controlled by the combination of orifices and high-speed solenoidal valves (Tanifuji, Koizumi, and Shimamune 2002).

2.2.2 Magnetorheological Damper

MR and ER are hydraulic dampers that consist of a hydraulic cylinder containing polarized micro-sized particles called magnetic rheological fluid (MRF). The MRF is a mart material composed of approximately 20-30 % by volume of micro-sized

magnetically polarizable particles suspended in oil (Muthalif, Kasemi, and Rashid 2017), and Rashid 2017), and Rashid 2017), and Rashid 2017), and Rashid 2017).

MR fluids exhibit the behavior of a Bingham plastic fluid, which means they have yield stress and behave as a liquid with viscosity after yielding. The yield stress and viscosity of MR fluid depend on the applied magnetic field, as depicted in Figure 6. When considering the flow of a Bingham material through a circular pipe, no flow occurs for small pressures. Sufficient pressure is required to reach the yielding point, where the material starts flowing (Dixon 2007). This yielding point allows for the division of the material into two rheological domains: the pre-yielding and post-yielding regions. The pre-yielding region demonstrates strong hysteresis, typical of a viscoelastic material that exhibits high viscous damping at low velocities. The post-yield region behaves plastically with a non-zero yield force that depends on the applied current or magnetic field, resulting in low viscous damping at high speeds (Wang and Liao 2011).

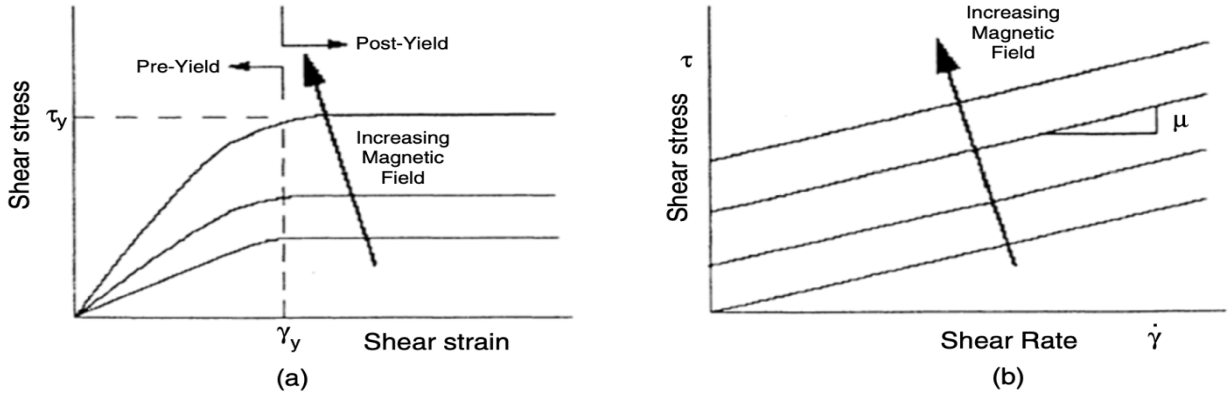

Figure 6 - *Variation of the shear stress and apparent viscosity with shear strain for an MR fluid under different magnetic field strengths: (a) the definition of the pre-yield and post-yield regions, (b) the non-Newtonian post-yield behavior* (Wang and Liao 2011).

where $\boldsymbol{\tau}$ is the shear stress in the fluid, $\boldsymbol{\tau_y}$ is the yielding shear stress controlled by the applied field, $\boldsymbol{\mu}$ is the Newtonian viscosity independent of the applied magnetic field and $\dot{\boldsymbol{\gamma}}$ is the shear strain rate.

Without a magnetic field, the particles in the MR fluid assume random positions, as depicted in Figure *7*. However, when an electromagnetic field is activated, the particles align themselves, creating greater resistance to the piston (Kanarachos et al.

2018). In the presence of an applied magnetic field, the micron-sized particles in the fluid form link and transition from a free-flowing state to a semi-solid state in milliseconds. The particles acquire a dipole moment aligned with the external field that causes particles to form linear chains parallel to the field. The magnetic field results in the formation of linear chains parallel to the field. The magnetic field lines are perpendicular to the flow direction (Wang and Liao 2011). The yield stress refers to the strength required to disrupt the continuous network of particle interaction within the sample (Liu and Liu 2014).

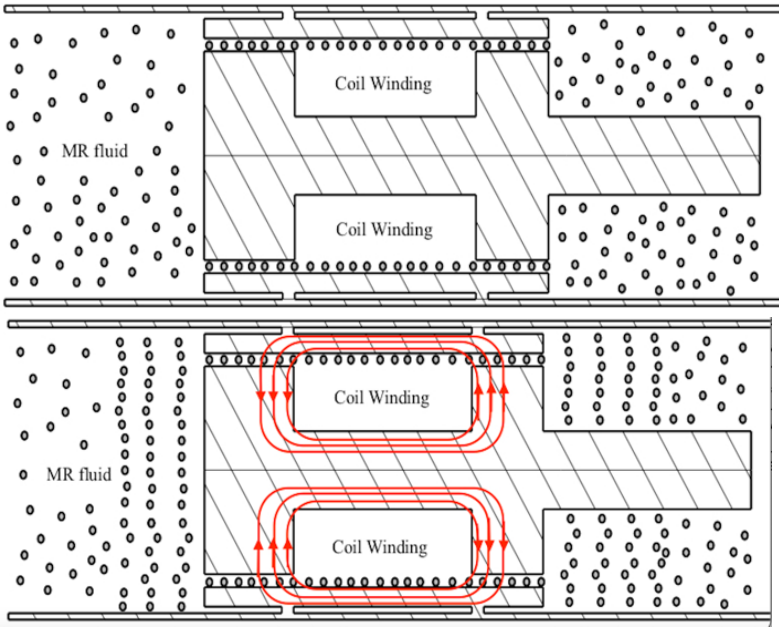

Figure 7 - Cross-sectional view: (a) No magnetic field (b) Presence of magnetic field

Figure 8 depicts a typical commercial MR damper manufactured by Lord Corporation, USA. As stated in the product technical data provided by Lord Corporation on their website, this MR damper is designed for suspension applications across various industries. It offers real-time damping adjustment in response to changes in the magnetic field strength (Desai et al. 2019).

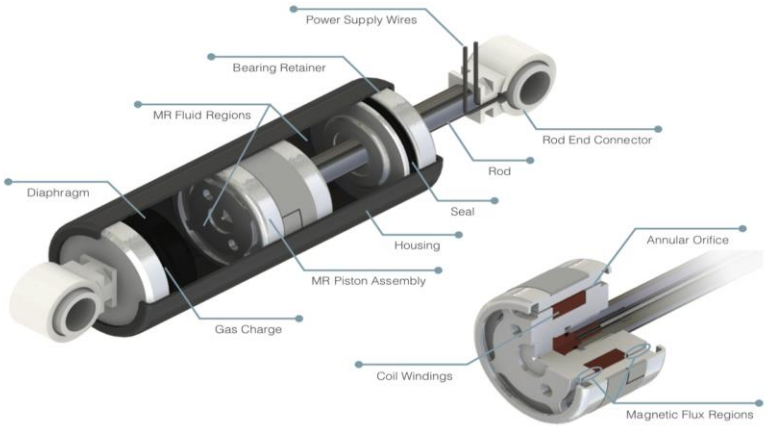

Figure 8 - A (Typical MR damper), B (Typical MR damper Assembly) (LORD 2023)

Many of these technologies have already come onto the market. Below are some models of MR dampers that can already be purchased on the market.

LORD

- LORD 8040-1 (Short Stroke)
- LORD 8041-1 (Long Stroke)

ARUS

- Arus MR Tech

2.2.3 Electrorheological Rheological (ER) Damper

ER dampers, similar to the MR damper, utilize the ER fluid that is sensitive to an electric field. When no electric field or neutral source is present, the particles in the ER fluid assume random positions. However, when an electric field is applied, the particles polarize and align themselves in the direction of the electric field. This causes the particles to redistribute, leading to changes in the viscous properties of the fluid within milliseconds. Unlike MR fluid, ER fluid exhibits non-Newtonian behavior and can be described as a viscoelastic material, specifically a Bingham plastic, with controllable yield stress (Spaggiari et al. 2019).

The ER fluid exhibits viscoelastic plastic behavior at high electric fields and low levels of strain. The ER damper is designed to dissipate energy by channeling the fluid

through narrow laminar ducts with dimensions typically ranging from 0.5 mm to 3 mm. These ducts are energized with a high electric field, typically ranging from 1kV/mm to 6kV/mm. It is worth noting that controlling the flow transient change is crucial in ER damper performance. A notable phenomenon occurs when the electric field is instantaneously removed, causing a transition from a plugged Bingham flow to a Newtonian flow (Gavin, Hanson, and 1996).

ER dampers were discovered before MR dampers; however, they have fewer engineering applications than MR dampers. This is mainly due to ER fluids' lower usable yield stress and the challenge of creating a high magnetic field. It is generally easier to control and generate a high magnetic field for MR dampers (Spaggiari et al., 2019).

The force–velocity characteristic of a commercial ER damper, The Soben damper, is depicted in Figure 9. This figure illustrates the significant behavior and performance of the ER damper.

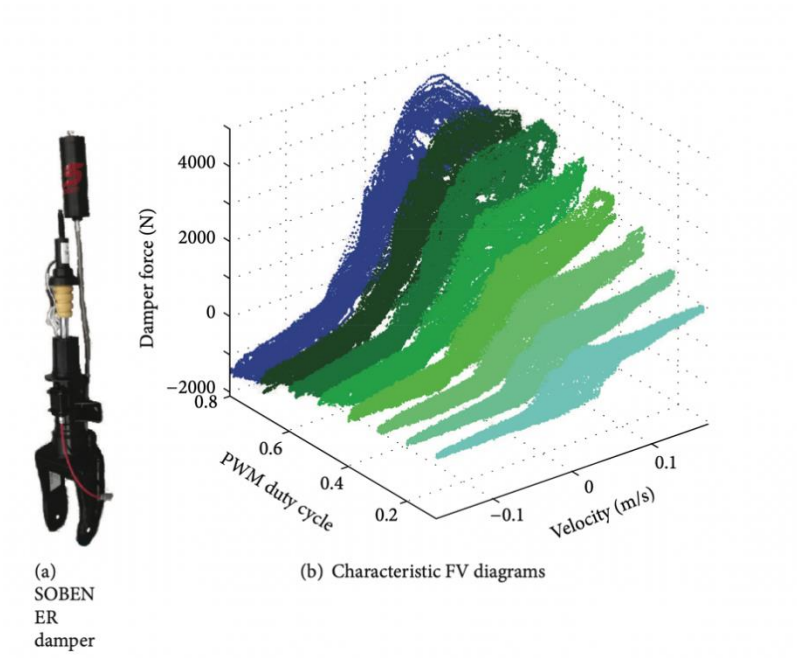

Figure 9 - *Commercial SOBEN ER damper* (Vivas-Lopez et al. 2015)

2.3 Commercial Vehicles with MR dampers

Several models of MR dampers are currently available in the automotive market, as shown in (Table 1). These dampers have been successfully integrated into the

suspension systems of various vehicles as original equipment. This trend highlights the increasing adoption of MR damper technology by automotive manufacturers. By incorporating MR dampers into their vehicles, manufacturers can offer improved suspension performance, enhanced ride comfort, and increased stability during dynamic driving conditions. This widespread integration of MR dampers signifies the industry's recognition of this technology's benefits and potential in advanced damping control. Moreover, the availability of MR dampers in the market allows consumers to directly experience the advantages of this technology directly, further fueling its popularity and widespread use in the automotive industry.

Table 1 - Commercial Vehicles with MR Damper

<table>
<tr><th>Manufacturer</th><th>Technology Model</th><th>Car Model</th><th>Year</th><th>Reference</th></tr>
<tr><td rowspan="11">Arnott</td><td rowspan="5">MR 3435
MR 3436
MR 3568</td><td>Cadillac Escalade</td><td>2007-2014</td><td rowspan="11">(Arnott ®2023)</td></tr>
<tr><td>Chevrolet Avalanche</td><td>2007-2013</td></tr>
<tr><td>Chevrolet Suburban</td><td rowspan="3">2007-2014</td></tr>
<tr><td>Chevrolet Tahoe</td></tr>
<tr><td>GMC Yukon 1500</td></tr>
<tr><td>MR 3437
MR 3438
MR 3439
MR 3440</td><td>GMC Yukon XL 1500</td><td>Cadillac STS</td><td>2007-2010</td></tr>
<tr><td>MR 3441
MR 3442</td><td>Cadillac SRX</td><td>2004-2009</td></tr>
<tr><td>MR 3443
MR 3444
MR 3445</td><td>Cadillac CTS-V</td><td>2009-2015</td></tr>
<tr><td rowspan="2">MR 3447
MR 3448</td><td>Buick Lucerne</td><td rowspan="2">2006-2011</td></tr>
<tr><td>Cadillac DTS</td></tr>
<tr><td>MR 3851
MR 3852</td><td>Audi A3/S3</td><td>2015-2020</td></tr>
</table>

Table 1.1 – Commercial Vehicles with MR Damper

Manufacturer	Technology Model	Car Model	Year	Reference
Arnott	MR 3853 MR 3854 MR 3855 MR 3856 MR 3857	Audi TT/TT RS/TTS	2016-2021	(Arnott ®2023)
Ferrari	SCM MR damping Control 2° generation	Ferrari 599 XX	2006	(Ferrari ®2023)
	SCM – E dual coil system	Ferrari F12 Berlinetta	2012	
	SCM-E FRS with solenoids	La Ferrari	2013	
Lamborghini	ADAS Urus	Aventador S	2016-2021	(Lamborghini ® 2023)
FORD	$\mathrm{MagneRide}^{TM}$ BWI Group	Mustang	2022	(Ford ®2023)
Chevrolet		Camaro ZL1	2019	(Chevrolet ® 2023)
Land Rover		Range Rover Evoque	2020	(Land Rover ® 2023)
		Discovery Sport	2019	
Senator Signature	Generation 3 Magnetic Ride Control (MRC)	HSV	2016	(Senator ® 2023)
		GTS	2016	

2.4 Damper Test Procedures

According to Dixon's (Dixon 2007) classification, the testing dampers can be categorized into three main types: (1) rig testing of the damper's components or the entire assembly, (2) on-road testing of the damper installed on the vehicle, and (3) annual safety certification testing for the vehicle.

In this work, ring testing was conducted using the damper to test the theoretical model and validate the analytical methods specifically. The purpose was to gain confidence in the theoretical framework for design purposes.

The testing was carried out using a hydraulic testing machine called MTS 810, which is based on a single piston that moves the crosshead up and down. This machine is designed for determining stress-strain curves and operates within a specific frequency range of 0 – 100 Hz. The machine performed well at lower frequencies in the experimental configuration with the supports and MR damper, typically between 2 and 3 Hz. The machine's mechanical components effectively responded to the testing requirements within this frequency range. However, it is important to note that the machine may encounter limitations and reduced performance when operating at higher frequencies. This observation is supported by a study conducted by (Wang, Radin, and Laird 1989). To ensure optimal performance of the machine and the MR damper in this specific experimental setup, it is crucial to consider the frequency range and select appropriate operating parameters. When setting frequencies greater than 3 Hz on the universal testing machine with a sinusoidal movement, it was observed that the machine could not provide a sinusoidal movement to the piston, resulting in a triangular waveform. The universal machine features a crosshead-mounted load cell that provides accurate force readings for measurement and control. A displacement transducer integrated into the actuator also allows precise position measurement and control. The machine's control system offers variable signals that can be supplied to the system for control purposes (Dixon 2007):

a) Sinusoidal wave
b) Triangular wave
c) Square wave
d) Random motion
e) External input

2.4.1 Sinusoidal Theory

A symmetrical triangular displacement provides a constant nominal speed throughout the stroke, equal in both directions. However, in this study, sinusoidal movement was employed during testing to characterize the hysteresis behavior of the

damper properly. Using a sinusoidal motion, the aim was to simulate the periodic displacements commonly encountered in automotive suspensions, making the simulation more realistic. If a triangular displacement were used in the testing machine, experiments with varying amplitudes would be required to capture the damper's behavior adequately. However, the choice of a sinusoidal movement was made to approximate better the actual displacements experienced by automotive suspensions in practice. This approach allows for a more realistic simulation and characterization of the damper's performance. (Dixon 2007).

The identified displacement (u) Figure 10 can be identified using the equation $u = Asin(2\pi ft + \phi)$, where A is the amplitude, f denotes the frequency, t represents the time and ϕ is the phase angle. Figure *10* aims to illustrate the angle shift, one of the parameters that require optimization to represent the identified displacement accurately.

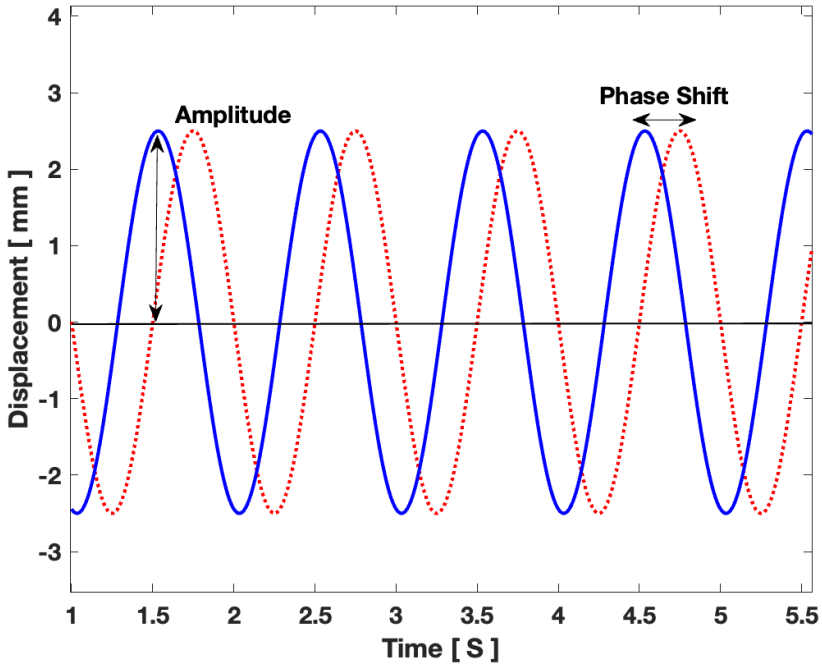

Figure 10 - Sine Displacement

Analyzing errors in experimental results is crucial in the scientific method. These errors can be categorized into two main types: random errors and systematic errors. Systematic errors cause the results to deviate consistently in a particular direction, often due to factors like improperly calibrated instruments or flawed experimental

procedures. On the other hand, random errors are small fluctuations that occur in both positive and negative directions and tend to cancel each other out when analyzed statistically. Repeatability and reproducibility (R&R) are closely related to random and systematic errors. Repeatability refers to the consistency of results obtained when the exact measurement is repeated by the same person using the same equipment and procedure. It is primarily influenced by random errors and remains unaffected by systematic errors. Reproducibility, on the other hand, refers to the consistency of results obtained when the exact measurement is repeated by different individuals or using different equipment or procedures. Random errors also influence it but may be influenced by systematic errors as well. By understanding and analyzing random and systematic errors, researchers can gain insights into the reliability and accuracy of their experimental results. This knowledge allows them to make appropriate adjustments to experimental techniques, improve instrument calibration, and account for potential sources of error, ultimately leading to more robust and valid scientific findings (Attivissimo et al. 2011).

2.5 Parameter Hysteresis Model Identification

The nonlinear and hysteretic behavior of MR dampers necessitates using mathematical models to understand and characterize their physical properties. In the context of parameter identification, the sigmoid model is commonly adopted to process data and minimize discrepancies between measured data and identified responses.

Various mathematical models have been proposed to replicate the characteristic behavior of MR dampers. Researchers have focused on developing parametric models that accurately represent experimental behavior in a mathematical framework. The primary objective of these models is to capture the force-velocity relationship under different conditions, such as the absence of a magnetic field and the application of a power source, and accurately identify the device's response. An ideal model should exhibit sufficient accuracy across different frequencies and applied currents.

Table 2 provides a comparative study of different parametric identification models, highlighting their respective strengths and limitations. This comparison aids researchers in selecting an appropriate model for their specific application and

understand the trade-offs involved in accuracy, complexity, and computational requirements.

2.5.1 Bouc-Wen Model

The Bouc-Wen model is a mathematical model that combines the works of Bouc (1967) and Wen (1976). Bouc initially proposed a mathematical model to describe the nonlinear hysteresis behavior of a sligle-degree-of-freedom system under forced vibrations. Wen later extended this model to random vibration and provided an approximate solution (Mohajer Rahbari et al. 2013). The Bouc-Wen model is particularly suitable for capturing the nonlinear force-velocity response of systems, including MR dampers. It does not exhibit a roll-off behavior in regions where the acceleration and velocity have opposite signs and the magnitude of the speeds is small (Yaakub et al. 2020). This model utilizes a differential equation to describe the non-linear hysteresis of the damper's force-velocity response (SpencerJr. et al. 1997). Figure *11* depicts a schematic representation of the Bouc-Wen model, which helps visualize the underlying structure and components of the model.

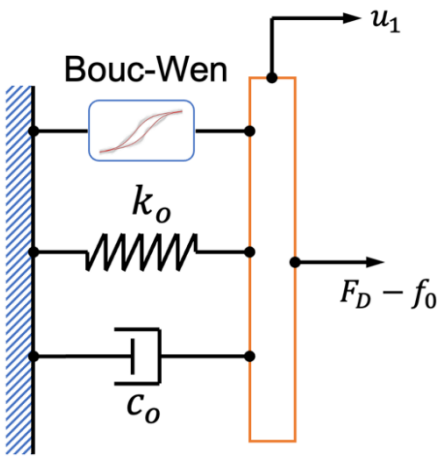

Figure 11 - Bouc-Wen model schematic

The damping force (F_D) present in the Bouc-Wen system is given by response (SpencerJr. et al. 1997):

$$F_D = c_0 \dot{u}_1 + k_0(u_1 - u_0) + \alpha z \quad (1)$$

where F_D is the damping force, c_0 is the viscous coefficient, k_0 is the stiffness, $\dot{u}_1$ is the damper velocity, $(u - u_0)$ is the displacement in the x direction and αz is the hysteretic variable.

$$\dot{z} = A\dot{u}_1 - \beta\dot{u}_1|z|^n - \gamma z|\dot{u}_1||z|^{n-1} \quad (2)$$

$A, \gamma \; and \; \beta$ are model parameters to be identified by adjusting.

2.5.2 Modified Bouc-Wen Model

The modified model to describe the non-linear hysteresis of the damper force/velocity, improving the standard Bouc-Wen model is illustrated in Figure *12*.

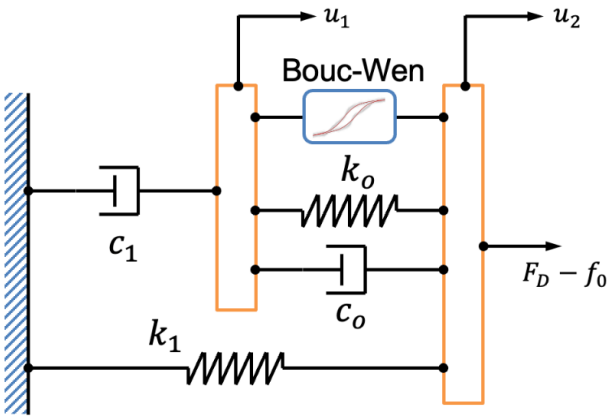

Figure 12 - Modified phenomenological Bouc-Wen model schematic

The damping force (F_D) present in the Modified Bouc-Wen system is given by (Talatahari and Rahbari 2015):

$$F_D = c_0(\dot{u}_2 - \dot{u}_1) + k_0(u_2 - u_1) + k_1(u_2 - u_0) + \alpha z = c_1\dot{u}_1 + k_1(u_2 - u_0) \quad (3)$$

Table 2 - Summary of Previous Studies on MR Suspension System (Yaakub et al., 2020).

Model	Advantages and/or Drawback
Bingham	1. Easy to implement. 2. Only two parameters are needed to characterize MR damper's behavior. 3. The MR damper's performance is better compared to the conventional damper. 4. The hysteresis behavior not considered. 5. The parameter estimation error is 3.8096
Bouc-Wen	1. Predict the force displacement behavior well. 2. It has a smooth transition and strong versatility. 3. Can reflect in all kinds of hysteresis systems. 4. The parameter estimation error is 1.9245 5. Many parameters must be considered.
Modified Bouc-Wen	1. Modified Bouc-Wen model is better as compared to Bouc-Wen model in time settlement. 2. Able to attain its stability within a brief period of time. 3. Predicts the behavior of the damper very well in all regions. 4. Acceleration and Velocity have opposite signs. 5. The parameter estimation error is 1.3770 6. The magnitude of the velocity is small.
Hyperbolic Tangent Function	1. Better in controller design, parameter identification and implementation. 2. The relationship between parameter value and input current is nonlinear. 3. Parameter value can be estimated directly from the estimated equation and the parameter estimation error is 3.3688
Nonlinear Biviscous	1. Cannot describe accurately the F(t) if the current value changes. 2. Disability to perform well with varying input excitation current. 3. The parameter estimation error is 3.8052
Finite Element	1. The flux lines increase as the distance between one flux lines to its adjacent become closer. 2. Provide evidence that the semi-active damper works well. 3. MR semi-active damper also provides ride comfort compared to passive damper.

where c_0 is the viscous coefficient, k_0 is the stiffness, $\dot{u}_i (i = 1,2)$ is the damper velocity, $(u_2 - u_0)$ is the displacement in the x direction and αz is the hysteretic variable.

The hysteretic displacement z is given by

$$\dot{z} = A(\dot{u}_2 - \dot{u}_1) - \beta(\dot{u}_2 - \dot{u}_1)|z|^n - \gamma z|\dot{u}_2 - \dot{u}_1||z|^{n-1} \quad (4)$$

which $\dot{u}_1$ is defined by the following equation according to Figure *12*.

$$\dot{u}_1 = \frac{1}{(c_0 + c_1)}\{\alpha z + c_0\dot{u}_2 + k_0(u_2 - u_1)\} \quad (5)$$

The mathematical modified model of Bouc-Wen needs to receive corrections in fluctuation magnetic fields $\alpha, c_0 \; and \; k_0$ coefficients in Eq. 6 defined as a linear function of the efficient voltage V as given by the following equations to be validated and represent the real model (Talatahari and Rahbari 2015):

$$\alpha(v_1) = \alpha_a + \alpha_b v_1, c_0(v_1) = c_{0a} + c_{0b} v_1 \; and \; c_1(v_1) = c_{1a} + c_{1b} v_1 \quad (6)$$

2.5.3 Parametric Sigmoid Model

There are several reasons to prefer using the parametric sigmoid model over the modified Bouc-Wen model for modeling the behavior of a system, such as an MR Damper. Sigmoid models offer several advantages, including their ability to capture the system's behavior with minimal input parameters, making them computationally efficient and suitable for applications with limited computational resources. Parametric models, like the sigmoid model, can be particularly valuable when specific nonlinearities of the MR damper, such as magnetic saturation and temperature effects, need to be better understood or explicitly accounted for. These nonlinearities play a significant role in the behavior of the MR damper and failing to consider them can lead to inaccurate modeling results. While the sigmoid model provides a simplified

representation of the overall force-velocity relationship, it may not accurately capture these specific nonlinear effects. Therefore, when the objective is to model the MR damper's behavior while considering magnetic saturation, temperature effects, and other particular nonlinearities, the modified Bouc-Wen model may be more appropriate. It offers a more detailed and accurate representation of the system's behavior, allowing for a better understanding of its dynamics.

I. The sigmoid model is simpler and more straightforward to implement than the Bouc-Wen model. Only three input parameters (excitation frequency, piston displacement, and current) must be identified in the sigmoid model. In contrast, the Bouc-Wen model necessitates estimating a more significant number of parameters, making the parameter estimation procedure more challenging and time-consuming.

II. The sigmoid model can frequently provide a satisfactory approximation of the system’s behavior being modeled, primarily for symmetric hysteresis systems. Conversely, the Bouc-Wen model can represent a more extensive range of non-linear behaviors, including asymmetric hysteresis, but may not always offer a better fit than the sigmoidal model.

III. The choice of model may depend on the specific application and the level of accuracy required. For some applications, a simpler model such as the sigmoid model, may be sufficient. In contrast, for others, a more complex model such as the Bouc-Wen model may be necessary to capture the full range of behavior exhibited by the modeled system.

The asymmetric and hysteretic force-velocity characteristics of the MR damper are depicted in Figure *13*. These characteristics describe the nonlinear relationship between the force exerted by the damper and the velocity at which it operates. The force-velocity curve of a damper illustrates how the force changes as the velocity of the damper's motion varies. The hysteresis loop in the curve signifies the energy dissipation that occurs during cyclic loading and unloading. The hysteresis loop is an important feature of the force-velocity curve as it represents the amount of energy the damper absorbs and dissipates. The enclosed area within the hysteresis loop indicates the extent of energy dissipation, providing insights into the damper's ability to absorb and dissipate mechanical energy. Understanding the hysteretic force-

velocity characteristics of a damper is crucial for evaluating its damping performance, predicting its behavior under different loading conditions, and optimizing its design for specific applications.

Research studies conducted by H. Deng et al. (2023) and Wang1 et al. (2003) have contributed to understanding these characteristics, providing valuable insights into the behavior and performance of MR dampers. By analyzing and interpreting the force-velocity relationship, researchers can assess the damping capabilities of MR dampers and make informed decisions regarding their application and optimization in various industries.

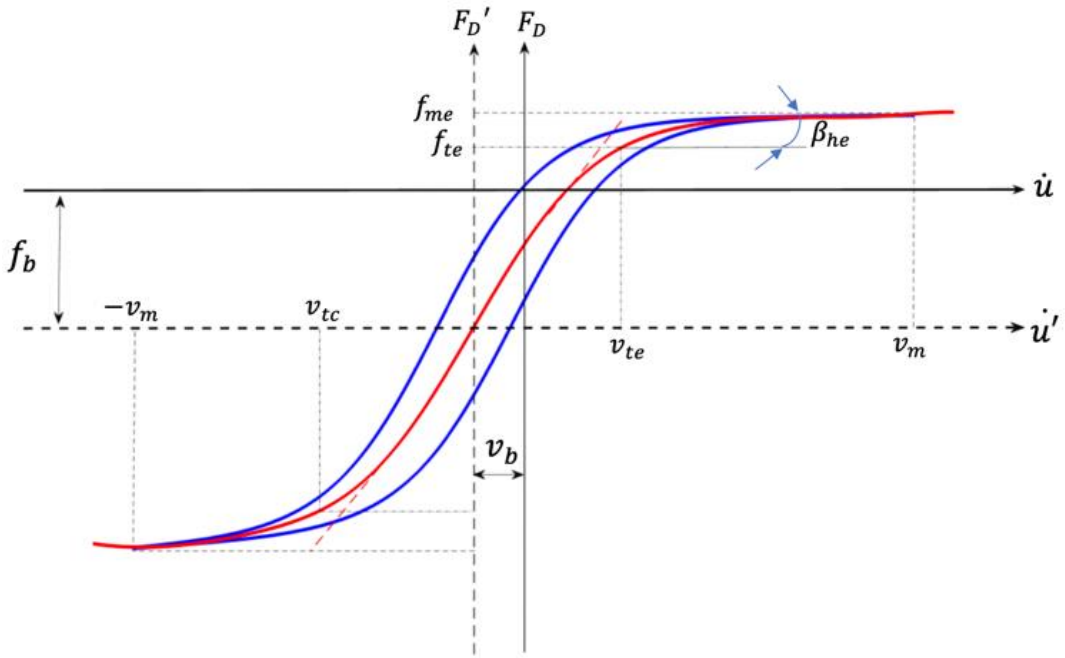

Figure 13 - Generalized hysteretic force-velocity characteristics (adapted from Wang et al., 2004)

The modified Bouc-Wen model is not suitable for capturing the hysteretic force-velocity characteristics of the MR damper under continuous variations in the control current and excitation conditions. In order to reproduce the nonlinear dynamic hysteretic behavior of the MR damper, Wang et al (2004) proposed a parameterized model synthesis approach. This approach involved fitting symmetric and asymmetric sigmoid functions to the experimental data obtained from the MR damper's dynamic behavior.

By adjusting 16 adjustable parameters, the model developed by Wang et al, (2004) provides a robust framework for analyzing and predicting the response of a MR damper. This computational approach allows researchers and engineers to simulate and evaluate the damper's performance in various scenarios, contributing to the advancement of MR damper technology and its applications in areas such as automotive suspension systems, vibration control, and structural engineering.

The magnitude of the peak velocity v_m can be derived from the instantaneous values of position u and acceleration ($\ddot{u}$), $v_m = a_m.\omega = \sqrt{(\dot{u})^2 - \ddot{u}.u}$ (a_m is the amplitude and ω is the frequency) so the transition force can be expressed as

$$f_t = f_0(1 + e^{a_1 v_m})1 + \left(\frac{k_2}{1+e^{-a_2(i+I_0)}} - \frac{k_2}{1+e^{-a_2(I_0)}}\right) \quad (7)$$

The zero-force velocity intercept v_h, offset velocity v_d and force f_d, and constants $\alpha, k_{vc}\ and\ k_{ve}$ can be expressed as:

$$v_h = sgn(\ddot{u})k_4 v_m \left(\frac{k_3}{1+e^{-a_3(i+I_1)}} - \frac{k_3}{1+e^{-a_3(I_1)}}\right) \quad (8)$$

$$\alpha = a_0/(1 + k_0.v_m) \quad (9)$$

$$k_{vc} = k_{1c}e^{-a_4 v_m};\ k_{ve} = k_{1e}e^{-a_4.v_m} \quad (10)$$

$$f_d = k_5 f_t; v_d = k_6 v_m \quad (11)$$

2.6 Literature Review of Magnetorheological Dampers

In recent years, the automotive industry has shown significant interest in developing new vibration control techniques, particularly in semi-active automotive suspension systems. One of the technological solutions gaining attention is the MR damper. Bearing that in mind, researchers have investigated and explored some existing gaps and obstacles to propose a more forceful strategy that allows the implementation of this technological solution. One such effort was presented by Sassi

et al. (2018), who introduced a new concept design for the MR damper. This design applies the excitation circuit and magnetic field externally to the MR chamber. External coils surrounding the body of the damper are used for excitation. Compared to conventional MR damper, this new design offers improved tolerance to temperature elevation caused by the high-intensity current supplied to the coils. The new concept of MR damper was incorporated into a full-car model to investigate the vehicle's vibration performance and stability. Various parameters, such as displacement, acceleration of the sprung mass, and tire deflection were analyzed to evaluate the vehicle's ride comfort and road-holding. The results demonstrated that the new MR damper design led to reductions in these parameters, indicating improved ride comfort and enhanced road holding.

Magnetic saturation is a significant drawback of MR dampers. In order to address this issue and improve the fitting of experimental data, Kanarachos et al. 2018 proposed a new parameters estimation model for the nonlinear mechanical behavior of automotive MR dampers. Their objective was to accurately describe the drawbacks of MR dampers by the influence of the magnetic saturation effect.

Nonmagnetized passages (orifices) in the piston have been a subject of significant research interest. Whether implementing orifices in the piston can improve the damping performance of MR dampers, similar to passive dampers, has intrigued researchers. Oh and Choi 2019 conducted a study to evaluate the relationship between the ride comfort of passenger vehicles and two types of MR damper: one with orifice holes in the piston and one without. The orifice holes in the piston allow for increased MR fluid flow without relying on magnetic effect, as seen in the passive viscose resistance holes. The researchers concluded that the MR damper with orifices in the piston provided a smaller damping force than the convectional MR damper. Similarly, Li and Yang 2020 conducted a study to investigate the behavior of the MR damper and predict the damping force by implementing non-magnetized passages in the piston.

Researchers are interested in developing new optimization algorithms to improve parameter identification in MR dampers. Rosli and Mohamed 2020 proposed a novel optimization algorithm specifically designed to enhance the Bouc-Wen Model. Their algorithm demonstrated superior performance in reaching the fittest solution more

quickly in MR damper applications, outperforming other algorithms such as particle swarm optimization, genetic algorithm, and sine-cosine algorithm. Similarly, Negash et al. 2020 conducted research on a novel genetic algorithm (nGA) implemented for parameter identification of the Bouc-Wen model in MR damper.

In their study, Du et al. (2018) explored using a MR damper to control semi-active scissors linkage in the seat suspension. Their objective was to determine whether this approach could effectively reduce the low-frequency, high-amplitude vibration experienced by drivers or passengers, which can lead to health disorders. Through their investigation, Du et al. (2018) found that by implementing the magnetorheological damper as a control mechanism, human vibration levels were reduced by up to 47.66% compared to an uncontrolled system.

The magnetorheological damper has become one of the most promising vibration control for various such as building protection from seismic events (Jung et al. 2006; Sun et al. 2018), automotive suspension (Feng et al. 2020; Pepe, Roveri, and Carcaterra 2019; Soliman and Kaldas 2019), aircraft landing gear system (Kang et al. 2020; Luong, Jang, and Hwang 2020), knee prostheses (Fu, Pan, and Xu 2019; Ochoa-Diaz et al. 2014), precise manufacturing machines (Kim et al. 2018), seat suspension (Du et al. 2018) and high-speed railway vehicle suspension (Jin et al. 2020a; Liao et al. 2019).

Within the field of magnetorheological (MR) dampers, researchers have made significant contributions to the characterization and development of these dampers. Several notable studies have focused on advancing the understanding and application of MR dampers. Some key researchers and their contributions include:

Guo et. al (2016) have significantly contributed to the characterization and understanding of MR dampers. Their research has focused on studying the behavior of MR dampers under different operating conditions, including analyzing their performance and capabilities. They have also worked on developing control algorithms and strategies to optimize the performance of MR dampers. Turnip et al. (2008) have conducted studies that contribute to the advancement of MR damper technology. Their research has explored various aspects of MR dampers, including material properties, design optimization, control methods, and real-world applications (Abdalaziz et al. 2023; Hu et al. 2022; Wang et al. 2023; Yamin et al. 2022; Yang et al. 2022).

Researchers such as Kumar and Bhushan (2022) have made significant contributions to the field of control strategies for semi-active suspension systems using MR dampers. They have proposed a novel control strategy that aims to optimize the performance of the semi-active suspension system by considering both ride comfort and road handling characteristics. Other notable researchers in this field study include Z. Deng et al. (2023), Li et al. (2023), Yang et al. (2023), Yu et al. (2023). Their research also revolves around control strategies for semi-active suspension systems utilizing MR dampers.

Researchers have explored the use of sigmoid functions to accurately represent the nonlinearity and hysteresis behavior of MR dampers, leading to improved adaptability and reduced model complexity. Here are some notable papers in this area:

Lu et al. (2020) propose a novel invertible model of an MR damper using a sigmoid function. The model aims to accurately capture the damper's nonlinear behavior while ensuring mathematical invertibility. This study focuses on performance tests conducted on a three-coil MR damper and proposes a microstructure-based sigmoid model. The model utilizes microstructural analysis of the MR fluid to enhance the understanding and representation of the damper's behavior. The utilization of microstructural analysis in modeling MR dampers has indeed contributed to enhancing the knowledge and representation of the damper’s behavior. Yang et al. (2020) conducted research on the influence of the microstructure of the MR fluid on the mechanical properties of MR dampers. Their study provides insights into how the microstructure affects damping characteristics and contributes to the development of accurate sigmoid models.

Similarly, Zhang et al. (2017) focused on experimental and numerical studies of a composite MR damper, considering the magnetic saturation effect. Their work investigated the influence of magnetic saturation on damping behavior and proposed a comprehensive model considering the microstructural properties and magnetic saturation effect of the MR fluid. The proposed sigmoid model incorporates various factors to enhance the accuracy and adaptability of the damper model (Zhang, Shi, and Chen 2021).

Overall, these researchers have significantly contributed to the state of the art in the field of MR dampers, advancing our understanding of their behavior, optimizing

their performance, and developing effective control strategies for semi-active suspension systems. Their work serves as a foundation for further advancements and applications in this field.

Designing an optimal suspension system is challenging, especially considering the need to control multiple parameters. The main objective of this work is to investigate the behavior of the MR damper under various operating conditions and develop a parametrized sigmoid model that accurately captures its nonlinear and hysteresis characteristics. Additionally, optimizing the model parameters using the Nelder-Mead simplex method and differential evolution algorithm is performed to minimize the discrepancy between experimental and numerical data.

This research contributes to the state of the art by addressing the following aspects: Firstly, a comprehensive analysis of the MR damper's behavior is conducted under diverse operating conditions, providing valuable insights into its performance in different scenarios. Secondly, implementing a parametrized sigmoid model represents a significant contribution as it accurately represents the damper's nonlinear and hysteresis behavior. This is crucial for designing more efficient and effective suspension systems. Furthermore, the optimization of the model parameters using the Nelder-Mead simplex method and differential evolution algorithm offers a systematic and advanced approach for fitting the model to experimental data. This leads to improved accuracy and predictive capabilities in capturing the behavior of the MR damper across different scenarios, which is of great importance for developing optimized suspension systems. Therefore, the contribution of this work lies in the combination of analyzing the behavior of the MR damper, implementing a parametrized sigmoid model, and employing advanced optimization techniques to fit the model to experimental data. These contributions have the potential to advance current knowledge and provide valuable insights for the design and enhancement of automotive suspension systems.

2.7 Techniques of Parameter Identification

The objective function was optimized using two optimization algorithms the Nelder-Mead simplex search method and differential evolution. The algorithm for solving optimization problems is shown in the flowchart depicted in Figure 14.

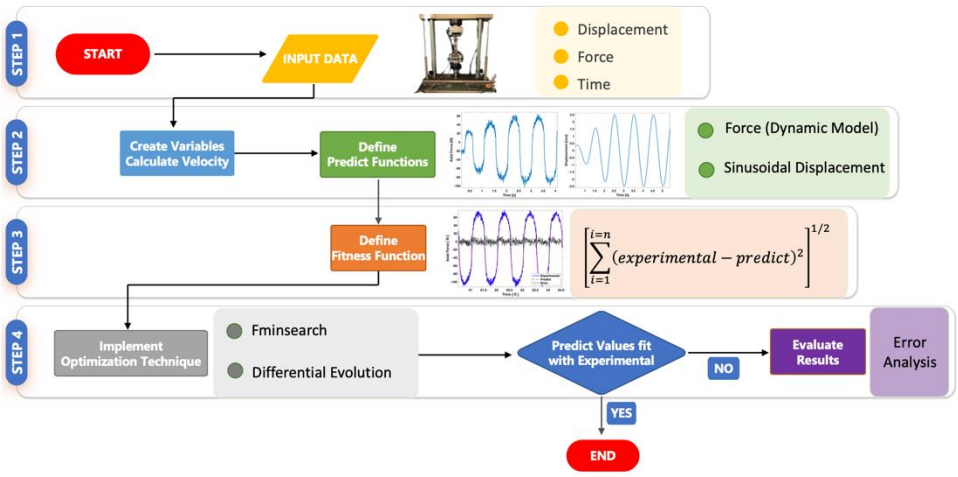

Figure 14 - Optimization Algorithm Flowchart: A Step-by-Step to Solving the Parameter Identification

2.7.1 Nelder-Mead simplex search method

The Nelder-Mead simplex algorithm, initially introduced in 1965, is widely recognized as a popular direct search method for unconstrained multidimensional minimization. Despite its extensive application, more explicit theoretical results concerning the Nelder-Mead algorithm must be provided. The Nelder-Mead algorithm was designed to optimize the minimization of a real-valued function f(x) in the n-dimensional space. To fully define the Nelder-Mead method, four scalar parameters need to be specified: the coefficients of reflection, expansion, contraction, and shrinkage (Lagarias et al. 2006).

The goal of the Nelder-Mead simplex optimization method is to determine the optimal values of variables that satisfy a set of constraints while optimizing a multivariate objective function. This objective function, known as the quadratic residue, is calculated by taking the sum of squared differences between the experimental results and identified sinusoidal displacement and force signals, which are generated using a parametrized sigmoid model.

The error function (objective function) is a quadratic function Eq. 12 of the displacement/force optimized using the Nelder-Mead simplex search method is intended to adjust the parameters in order to find the minimum between the quadratic residue function ϵ_u, given by the square sum of the difference $\left(u_a^i - u^i\right)$ between the

signal of experimental displacement $u(t) = u^i$ and the identified displacement $u_a(t) = u_a^i$. The same procedure was performed for the force error function in order to find the sum of the quadratic residue between experimental force and simulated force.

$$\epsilon_u = \left[\sum_{i=1}^{i=n} \left(u_a^i - u^i\right)^2\right]^{1/2} \tag{12}$$

2.7.2 Differential Evolution

Evolutionary Algorithms (EA) are part of an emerging area of intelligent computing called biologically and nature-inspired computing. EA introduces an important problem-solving tool inspired by evolutionary processes found in nature. Artificial Intelligence (AI) techniques are known for their ability to tackle problems found to be unyielding to traditional mathematical methods. EAs are a collection of algorithms that share the theme of evolution. The main-stream instances of EAs comprise Genetic Algorithms (GAs), Evolutionary Strategies (ES), and Evolutionary Programming (EP) (Beer 2008; Vikhar 2017).

In the real world, individuals within a population often exhibit varying levels of fitness, which can be attributed to their ability to defend themselves against attacks. In evolutionary algorithms (EAs), individuals in a population also differ in fitness due to their unique characteristics. Limited resources mean that the fittest individuals are more likely to survive and pass their favorable traits to their offspring through mating. As a result, the best individuals in the population will continue the cycle of reproducing, fighting for survival, and passing on their genes to the next generation. This cycle is depicted in Figure 15 with the terminal condition being determined by factors such as the number of generations, error tolerance, or other criteria.

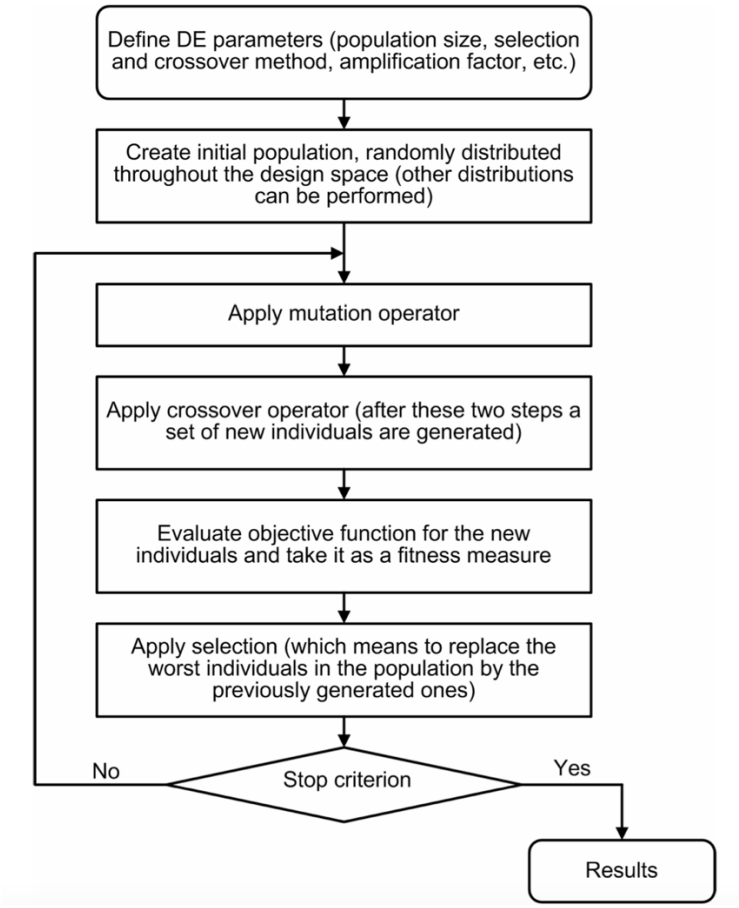

Figure 15 - *Evolutionary Algorithms Procedures* (Viana 2008)

GAs differ from traditional optimization methods because they are based on a population of possible solutions, not just the parameter optimization problem. Using Darwinian selection to evolve the population of potential solutions has an added advantage in solving dynamic problems. As most real-life problems are dynamic in nature, the definition of fitness and the rules governing the problem may change once it has been formalized. However, employing a population of evolving solutions allows individuals to adapt to the new rules of their environment over time. Evolutionary Programming (EP), presented by Fogel et al. (1966), was proposed as an evolution simulation technique that emphasizes mutation to develop a differentiated form of Artificial Intelligence (AI).

Differential Evolution (DE) is an EA optimization approach initially proposed by (Storn and Price 1997a). This method uses procedures derived from biological

processes, such as genetic variation, mutation, natural selection, and crossing. However, unlike what happened historically with genetic algorithms, the main idea behind the Differential Evolution method is not precisely simulating Darwin's theory on the survival and evolution of species (Viana 2008). This method presents a purely mathematical conception based on vector operations, which is considered a structural approach (Coelho 2012).

In the Differential Evolution algorithm, the value of each design variable is represented by a real value, and the optimization procedure is governed by five steps presented in the sequence below (Lobato 2008).

a) Step 1: an initial population is generated (randomly) with feasible solutions for the problem in question, ensuring that the values assigned to the variables are within the boundaries delimited by the designer (design space);
b) Step 2: an individual is selected at random to be replaced. Three (or more; Tab. 1) different individuals are selected as parents (parents), one of which is selected as the primary parent;
c) Step 3: add to the current value of the variable (main parent) the difference between two other variables (or sum of the difference between other variables; Tab. 1) weighted by a disturbance rate F. This procedure represents the mutation operator in Differential Evolution;
d) Step 4: now apply the procedure that represents the crossover operator in the Differential Evolution, carried out according to a crossover probability CR;
e) Step 5: if the resulting vector presents an adaptation function (Fitness) better than the main parent, it replaces it. Otherwise, this vector is kept in the population.

2.7.2.1 Mathematical Formulation

Step 1 regarding the mathematical formalism, comprises the random generation of the initial population P_{DE} with m individuals, also called vectors, covering the entire search space for a problem with n design variables, the dimension of each vector. The

population will generally be an ($m\ x\ n$) matrix, where each row represents an individual in the population.

$$P_{DE} = [x_1 \quad x_2 \quad \cdots \quad x_m]^T \tag{13}$$

where $x_m = [x_1 \quad x_2 \quad \cdots \quad x_n]^T$ is the vector with n project variables of the individual m.

Which individual x_m of the initial population is determined by:

$$x_m = I^I(x_m) + R_{noise}[I^u(x_m) - I^I(x_m)] \tag{14}$$

where $I^u(x_m)\ and\ I^I(x_m)$ are the lower and upper bounds. R_{noise} is the vector correspondent to white noise (with normal distribution in the interval [0,1]).

Therefore, given a population, the three operators to be performed are mutation, crossover, and selection. These three operations will be repeated until a stopping criterion is reached. This criterion can be population convergence, a minimum error reached, or a predefined value of iterations.

2.7.2.2 Mutation

Applying the mutation operator (steps 2 and 3) can be performed using different schemes regarding the choice of vector x_m that will be mutated. This process can be done randomly (randomly chosen vector among members of the current population, type "rand", x_{rand}) or with the vector associated with the best-adapted function (Fitness; type "best", x_{best}). Table 3 shows mutation schemes that are commonly used.

Table 3 - *Differential Evolution method*

Type	Mutation Equation	Alvo	Population
best/1	$x_{trial} = x_{best} + F(x_1 - x_2)$	x_{best}	m > 3
rand/1	$x_{trial} = x_{rand} + F(x_1 - x_2)$	x_{rand}	m > 3
rand-to-best/2	$x_{trial} = x_m + F(x_{best} - x_m + x_1 - x_2)$	x_{best}	m > 5
rand/2	$x_{trial} = x_{rand} + F(x_1 - x_2 + x_3 - x_4)$	x_{rand}	m > 5

*x_{trial} Is the resultant vector of the mutation process.

It is important to emphasize that the scheme type used in this work was the rand/1. This scheme randomly chooses three vectors ($x_{rand}, x_1 and\ x_2$). A subtraction operation is performed from two of them ($x_1 and\ x_2$). The result is multiplied by the disturbance rate F, thus generating a vector with a different module from the original subtraction.

So, the new vector is then added to the x_{rand} vector, providing a new x_{trial} vector as presented in the mutation equation for rand/1 indicating a new position in space. In terms of the Differential Evolution algorithm, this has to do with the generation of a new individual (Lobato 2008). Figure 16 graphically presents what was described (two-dimensional problem). In this work, F was set at 0.8. According to (Viana 2008), satisfactory results are obtained in minimization processes with the disturbance rate varying between 0.5 and 1.0 (the larger the initial population size, the smaller the value of F in this interval).

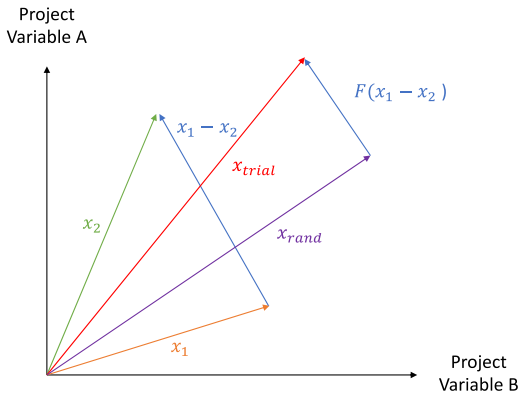

Figure 16 – Theoretical Foundation of the DE (Storn and Price 1997b)

2.7.2.3 Crossover

The application of the crossover operator (step 4) is carried out as shown in Eq. 3. Some of the main parent's design variables (target of Tab. 1) are incorporated into the x_{trial} vector according to a given CR crossing probability. The parameter CR was set at 0.8.

$$x_{trial} = \begin{cases} x_{trial} mutation, rand\ [0,1] < CR \\ x_{trial} \end{cases} \quad (15)$$

where x_{trial} is the vector with some mutated design variables.

2.7.2.4 Selection

Finally, the selection operation is performed. But to talk about selection, first we must know the objective function, also known as fitness. Fitness is the function we want to optimize (minimize in this case). The objective of the optimization is to find the minimum between the simulated and experimental sine function that represents the displacement, as well as the simulated force function in comparison to the experimental values, with that the fitness functions will be the sin and the force. Therefore, it will be our evaluation function from which an error will be generated (the difference between simulated and experimental results).

2.8 Preliminary Parameterization Results

2.8.1 Sinusoidal Signal

The error function Figure 17 is a quadratic function Eq. 15 of the displacement optimized using the Nelder-Mead simplex method search that finds the minimum between the displacement experimental and identified.

The Nelder-Mead simplex search method is intended to adjust the parameters A, f and ϕ in order to find the minimum between the quadratic residue function ϵ_u, given by the square sum of the difference $\left(u_a^i - u^i\right)$ between the signal of experimental displacement $u(t) = u^i$ and the identified displacement $u_a(t) = u_a^i$.

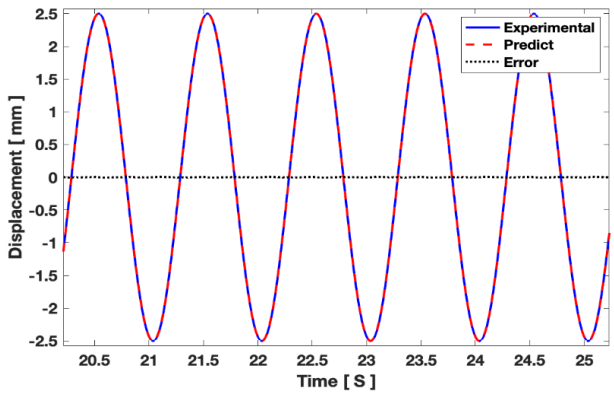

Figure 17 - Sine Displacement Identified with error (Displacement of 2.5 mm, 0 A and Frequency of 1 Hz)

Applying the function histfit (Histogram) makes it possible to see that the error function has a Gaussian distribution Figure *18*, which is a random error.

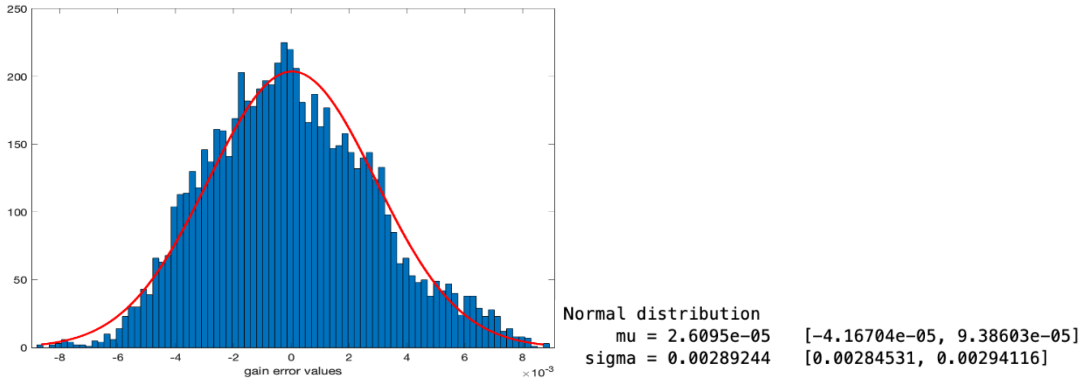

Figure 18 - Displacement error histogram

The identified velocity is the derivative of the displacement function given by the equation $\dot{u} = 2\pi f A cos(2\pi f t + \phi)$.

2.8.2 Parametric Sigmoid Force Signal

To evaluate the performance of the simulated force and compare it with the experimental model, an objective function is defined to quantify the error between the experimentally obtained values and the simulated values. The error is called using Eq. 1, which allows for a direct comparison between the identified and experimental forces. Figure 19 represents the optimization process using the Nelder Mead simplex search method.

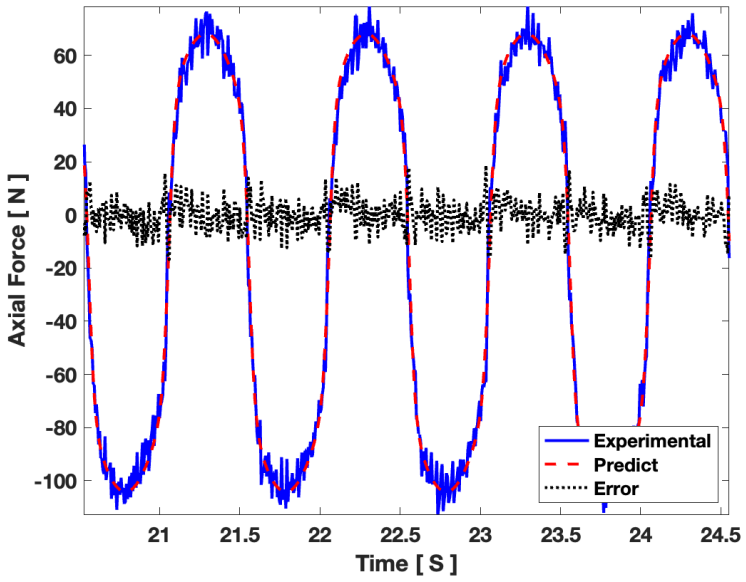

Figure 19 - Comparison between the identified and experimental responses

Applying the function histfit (Histogram), it is possible to see that the force error function has a Gaussian Figure 20.

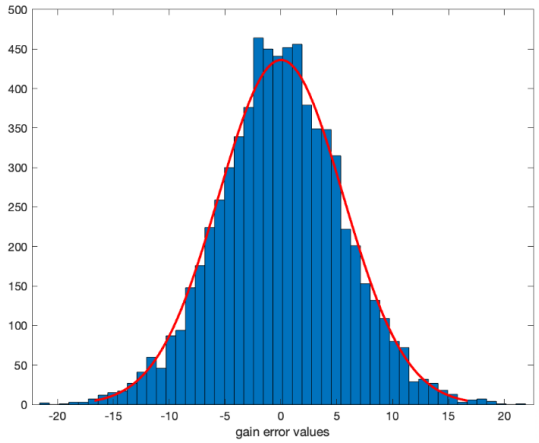


```
Normal distribution
     mu = 0.00258883    [-0.127884, 0.133062]
  sigma =    5.56902    [5.47828, 5.66283]
```

Figure 20 - Force error histogram

Figure 21 highlights a quantile-quantile plot that compares the quantiles of the force error sample with the theoretical quantile values derived from a normal distribution. This plot is a visual tool to assess whether the force error distribution follows a normal distribution pattern. If the data points on the plot form a straight line, it indicates that the force error distribution is approximately normal. Therefore, by observing Figure 21, we can conclude that the force error distribution appears to be normal based on the linear pattern observed in the plot.

Figure 21 - *Force error Quantile-Quantile Plot*

3 EXPERIMENTAL SETUP

This chapter introduces the experimental setup for studying damper characteristics. It covers experimental design, implementation, equipment used, and damper characterization. The chapter emphasizes the importance of a well-planned experiment, provides an overview of the implementation process, describes the equipment utilized, and highlights the specific damper characteristics of interest. This chapter sets the foundation for subsequent data analysis and interpretation in the following chapters.

3.1 Equipment's

Table 4 presents the list of equipment used in the experimental test. The MR damper is tested using the MTS 810 servo-hydraulic test system (Material Testing Machine) manufactured by MTS (Figure 22). The MTS 810 testing machine consists of an upper and lower head with grippers that securely hold the fabricated support (Figure 26) for fixing the MR damper. The lower head is connected to the hydraulic cylinder, allowing vertical movement.

Table 4 - *List of Experimental Equipment*

DESCRIPTION	MODEL	FIGURE
Material Testing Machine	MTS 810	Figure 22
MR Damper	8041-1 LORD	Figure 24
Power Supply	Minipa MPL 3303M	Figure 24
Digital Multimeter	AFR MT 4300	---
Manufactured Support	-	Figure 26

3.1.1 MTS 810 model 318.10

The experimental equipment used in this study included a universal testing machine manufactured by MTS Systems Figure 22, specifically model 318.10. The machine was equipped with a load cell with a maximum capacity of 100 KN, enabling accurate measurements of forces applied during the experiments.

The MTS model 318.10 universal testing machine is widely recognized and a reliable apparatus used for various mechanical tests, including tensile, compression,

and fatigue tests. It features a robust structure and advanced control capabilities enabling precise control and measurement of various mechanical parameters.

The load cell incorporated in the testing machine allowed for measuring the force exerted by the MR damper during experiments. With a maximum capacity of 100 KN, it provided sufficient range and sensibility to capture the forces generated by the damper under different operating conditions. According to the manufacturer's manual from Lord, the MR damper has a maximum force capacity of 2447 N. This specification indicates the upper limit of the force the damper can withstand and exert during its operation.

Figure 22 - MTS 810 (Material Testing Machine)

Figure *23* - MTS 810 (Specifications).Figure 23 illustrates the geometry and technical specifications of the MTS 810, as outlined in the table. The figure serves as an illustrative representation of the physical structure and key features of the MTS testing equipment.

Force capacity (Maximum)	100 KN
Available actuator ratings	15, 25, 50 and 100 KN
Vertical Test space (A)	1308 mm
Working height (B)	889 mm
Column spacing (C)	533 mm
Column diameter (D)	64 mm
Base width (E)	864 mm
Base depth (F)	610 mm
Diagonal Clearance (G)	2718 mm
Overall Height (H)	2540 mm
Stiffnesst	2.6×10^8 N/m
Weight	500 Kg

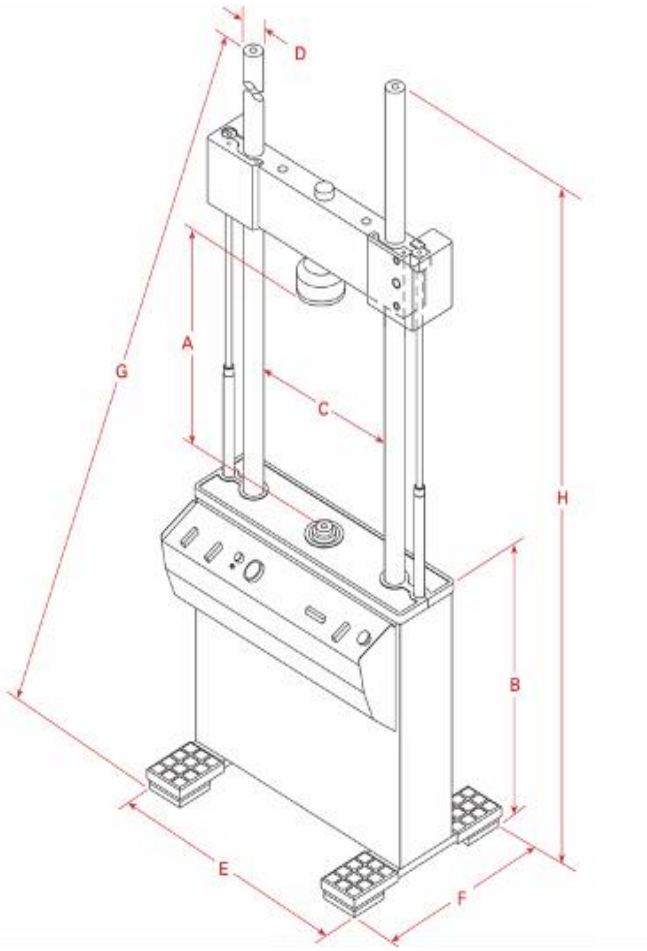

Figure 23 - MTS 810 (Specifications).

3.1.2 Power Supply Minipa

Typically, magnetism is activated in an electromagnetic device by passing a current through a coil around a magnetic material. In this work, a short circuit on channel 1 of the Minipa Power Supply initiated current control. Figure 24 illustrates the connection between the MR damper and the power supply, while Table 5 provides the general specifications of the power supply.

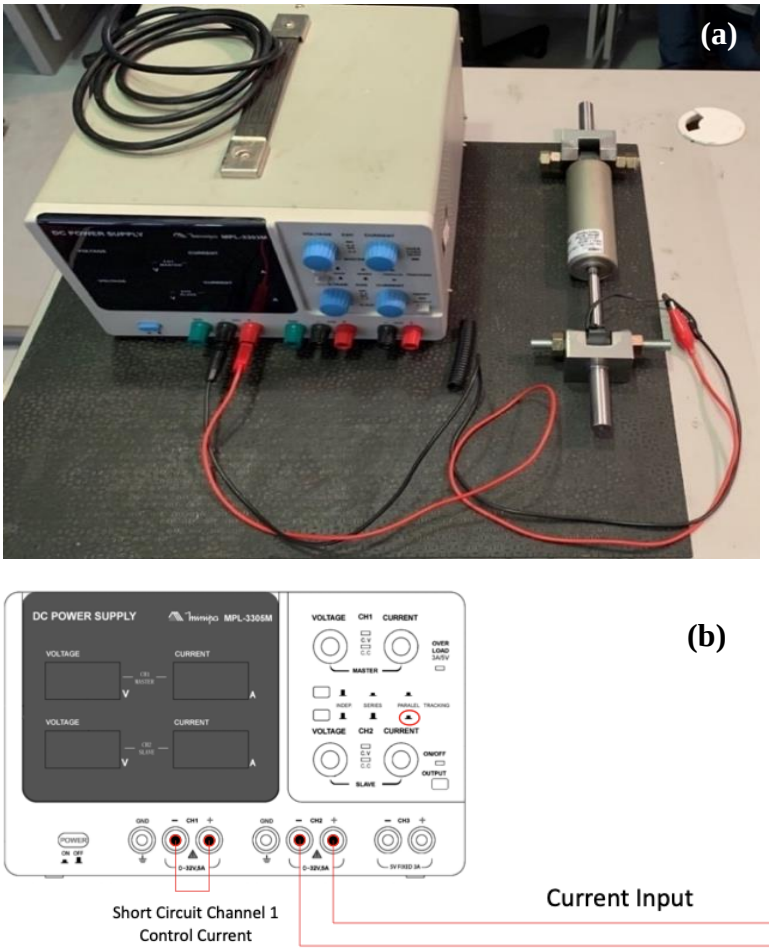

Figure 24 - Description of Minipa Power Supply and MR damper (a) and electric schematics description of constant current input (b).

Table 5 - *Minipa General Specifications*

Characteristics	MPL – 3303 M
Variable Output	2 x 0 ~32 V
	2 x 0 ~ 3 A
Fixed Output	5 V / 3A
Consume maximum (W)	350
Dimension H x W x D (mm)	170 x 260 x 315
Approximate weight (Kg)	10

3.2 Damper Characteristics

The force exerted by a damper, as shown in Figure 25, depends on its velocity and recent operation, which can affect the temperature and fluid properties. The desired behavior of the MR damper's F(u) loop is to have a smooth and gentle shape in its hysteretic response. This requires the valve characteristics to be smooth and prevents cavitation within the typical operating range. In essence, this means that any velocity, whether compression or extension, can be expressed as a corresponding velocity with the appropriate sign. In a typical suspension damper setup, when there is a bump in the suspension, it leads to compression in the damper. Therefore, "bump velocity" can be used interchangeably with compression velocity, while "rebound velocity" can be used for extension velocity (Dixon 2007).

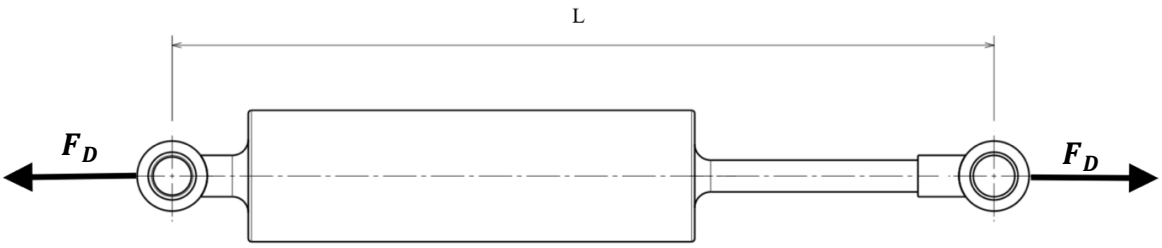

Figure 25 - Positive velocity and force excitation in the MR damper

The RD 8041-1 damper is a monotube shock absorber containing high-pressure nitrogen gas (300 psi) in the gas Figure 8. RD 8041-1 is a MR damper manufactured by Lord Corporation, USA. According to the product technical data provided by Lord Corporation on their website, it is meant for suspension application in industries, and it provides damping, which varies in real-time in response to the varying strength of the magnetic field. A rise in the MR fluid yield strength achieves this. The stroke length of the damper is 74 mm, and the extended length is 248 mm (Desai et al. 2019).

MR damper RD 8041-1 LORD properties are given by Table 6 and Table 7 measured electrical properties.

The axial coil generates the magnetic field, which can be modeled as an electrical circuit. The commercial MR damper of LORD has an electric potential of around 12 Volts and produces a maximum current of 2 A.

Table 6 - *MR Damper Typical Properties (RD 8041-1)*

Stroke	74 mm
Extended Length	248 mm
Body Diameter	42.1 mm
Shaft Diameter	10 mm
Tensile Strength	8896 N
Damper Forces (Peak to Peak)	
5 cm/sec @ 1 A	2447 N
20 cm/sec @ 0 A	2447 N
Operation Temperature	71 °C

Table 7 - *MR Damper Electrical Properties*

Input Current	Input Voltage	Resistance
0.1 A	0.4 V	0.40 Ω
1.0 A	4.9 V	4.90 Ω
1.5 A	7.9 V	5.26 Ω
2.0 A	11 V	5.50 Ω

3.3 Description of Coupling MR-Damper to MTS

The coupling of the MR damper to the universal tensile testing machine (MTS 810) involved the design of support elements. Based on the Von Mises failure criterion, these supports were specifically designed to ensure their structural integrity under the applied loads.

To validate the performance and suitability of the designed supports, numerical analyses were conducted using Ansys software. Figure 26 depicts the configuration used in the analyses.

The results obtained from the numerical simulations confirmed that the supports were appropriately dimensioned to withstand the expected load requirements. This indicates that the coupling between the MR damper and the MTS is robust and capable of effectively carrying out the intended testing tasks.

One of the requirements for characterizing the damper on the universal testing machine was to ensure that the base of the support had a minimum diameter of 15 mm. The technical drawing of the support can be found in Appendix A.

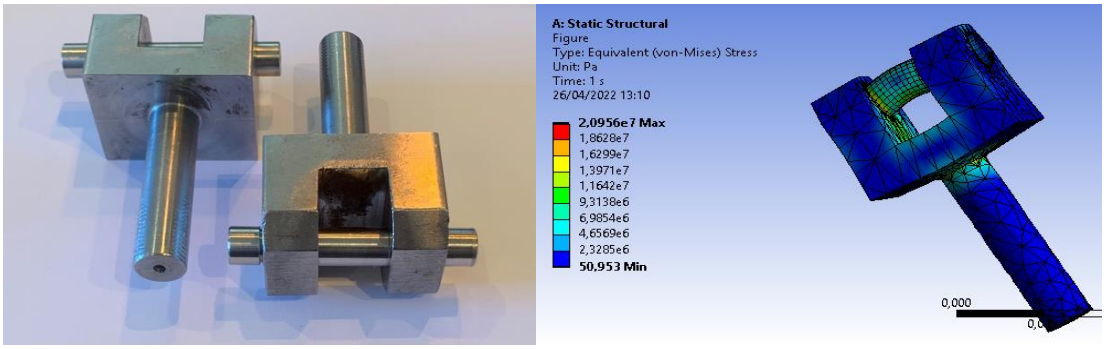

Figure 26 - (a) Manufactured Support (b) Von Mises Failure Simulation

Initially, a discrepancy was observed between the experimental and simulated values. A detailed analysis of the experimental procedure was conducted to investigate this issue further. It was discovered that the source of error was a screw used to fasten the MR damper to the support. This screw caused wear on the internal surface of the damper's mounting area, leading to clearance issues in the system. To rectify this issue, a pin was designed to facilitate the fine adjustment between the mounting support and the damper. This solution provided a more precise connection and eliminated the clearances, improving agreement between the identified and experimental results. Appendix A of this thesis shows the technical drawing of the pin and support.

3.4 Implementation of the experimental program

The experimental methodology adopted imposes a sinusoidal excitation through the servo-hydraulic actuator on the Universal Machine testing. This process is repeated for various magnetic fields over a nominal operation current range of 0 – 1.5 A. The damping force is measured for each current level to generate the final graphic in the presented flowchart in Figure *27*. These currents will be generated by an external alimentation source DC. The universal machine testing is equipped with

internal sensors of displacements and force, which are controlled by an electronic control unit LVDT (Linear Variable Displacement Transducer) able to provide the piston displacement and a cell force for the applied force. The frequency of the sinusoidal wave and the amplitude of the triangular signal were defined according to the literature because, in this way, it will be possible to compare with the experimental values obtained. The velocity is derived from the numerical differentiation of the displacement.

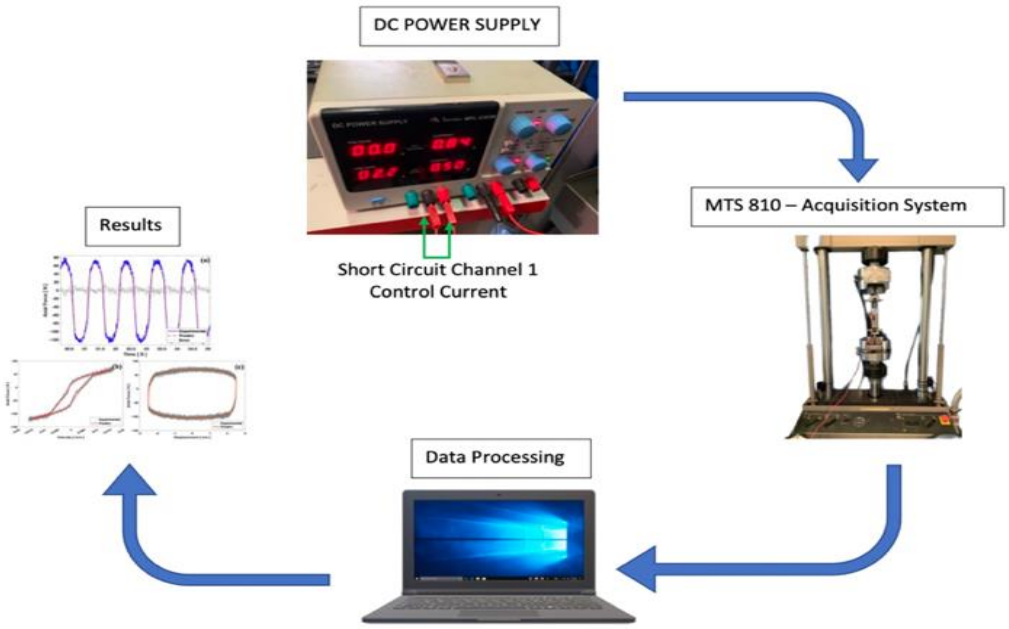

Figure 27 - Data Processing Process

The experimental procedure, as illustrated in Figure 28, involves the use of a DC power supply with two parallel output channels to control the current supplied to the coils of the MR damper. The MR damper is securely attached to the MTS universal testing machine, which is programmed to apply a sinusoidal displacement function. This displacement generates two output signals: displacement and force, recorded over time.

The DC power supply with two parallel output channels enables precise control of the current flowing through the coils of the MR damper. By adjusting the current, the magnetic field strength within the damper can be manipulated, thereby influencing its damping characteristics. This setup allows for the investigation of how variations in the

magnetic field strength impact the behavior of the MR damper in terms of displacement and force responses.

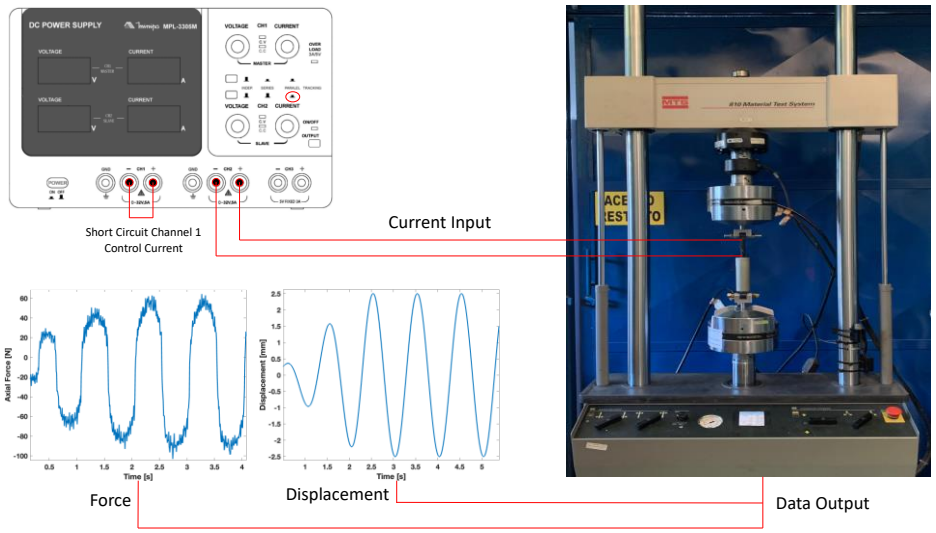

Figure 28 - MTS Output Data Response

The MR damper was securely attached to the clamps of the MTS machine using custom mounting brackets, ensuring proper alignment and fitting of the elements. These brackets were specifically designed to hold the MR damper in place during the experiments securely. In this case, the MTS machine is programmed to execute a fatigue test executing a sinusoidal displacement profile. This means that the machine-generated a controlled oscillating motion, serving as the input to the MR damper for different operating conditions.

Two key output signals are recorded during the experiment: displacement and force. The displacement signal represents the change in the position of the damper over time, indicating its response to the applied input displacement. On the other hand, the force signal measures the resistance and force exerted by the damper as a reaction to the input displacement.

4 RESULTS

This chapter explores the characterization of mechanical behavior, covering topics such as asymmetric and symmetric force behavior, temperature and frequency dependence, displacement effects, error analysis, experimental results fitting, sensitivity analysis, and parameter identification techniques. It offers valuable insights into the behavior of mechanical systems, enabling researchers and engineers to optimize and design controllers with the aim of enhancing system performance.

Description	Topic	Conclusion
Asymmetrical and Force Distribution	4.1	It can be observed that the force distribution for semi-active behavior is almost symmetrical comparing with passive behavior.
Current Dependency	4.2	The immediate effect of increasing current is an increase in the damping force.
Frequency Dependency	4.3	The force exhibited minimal variation and the damper velocity increases as the vibration frequency rises.
Displacement Dependency	4.4	The force and the damper velocity increases as the displacement rises.
Temperature Dependency	4.5	As the temperature increased to 71°C, the damping force decreased by approximately 26% compared to the baseline condition.

Description	Topic	Conclusion
Error Analysis	4.6	The presence of a normal distribution in the force error indicates that the data errors were randomly distributed.
Experimental Results	4.7	Appendix B of this study offers a comprehensive analysis of various operational conditions.
Parameter Sensibility	4.8	Parameters f0, k5, k1c, and k1e were found to be the most sensitive, indicating that small changes in these parameters can lead to significant variations in the damping force.
Sigmoid Model Parameters	4.9	The experimental results were approached and optimized using the Nelder-Mead simplex search method and differential evolution algorithm.

4.1 Asymmetrical and Symmetrical Force Distribution Comparison

Based on the F-V behavior of the MR damper depicted in Figure 29, it is evident that the damper exhibits an asymmetric force distribution when operating as a passive damper with an excitation current of 0 A. Specifically, the maximum force exerted during compression (negative velocity) is greater than the force generated during extension (positive velocity).

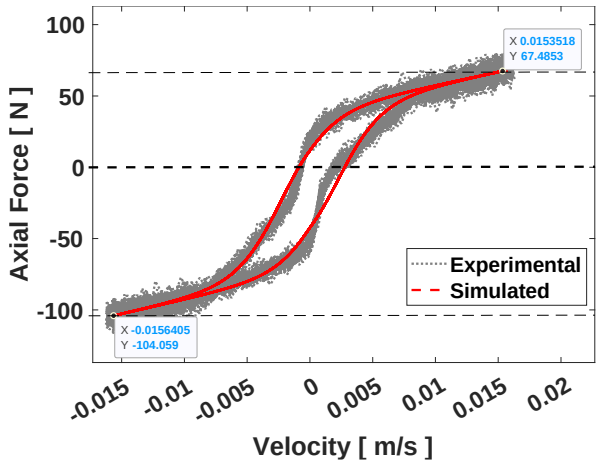

Figure *29* – Hysteretic F-V curve of LORD MR Damper with 0 A

The F-V behavior of the MR damper, as depicted in Figure 30 and subjected to a 0.5 A current, demonstrates an asymmetric force distribution similar to the previous case. The maximum force during compression (negative velocity) remains greater than the force generated during extension (positive velocity). However, a notable difference can be observed when comparing the passive and semi-active behavior of the MR damper. The force distribution for the semi-active behavior shows a higher degree of symmetry. The discrepancies between the extension and compression forces are significantly reduced, with less than 10% differences when considering the peak forces.

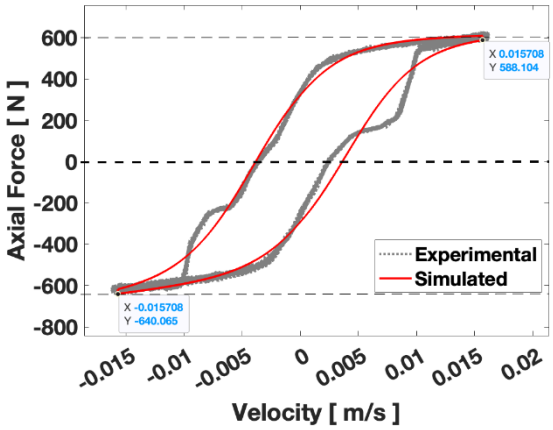

Figure *30* - Hysteretic F-V curve of LORD MR Damper with 0.5 A

4.2 Current Dependency

The force-displacement Figure 31(a) and force-velocity Figure 31(b)characteristics curves depict the experimental values for four different current levels, with an amplitude of 5 mm and a frequency of 1 Hz. As the excitation current in the damper coil increases, there is a corresponding increase in the damping force. This immediate effect of increasing the current level indicates that the MR damper becomes more effective in dissipating energy and providing damping as the excitation current is increased.

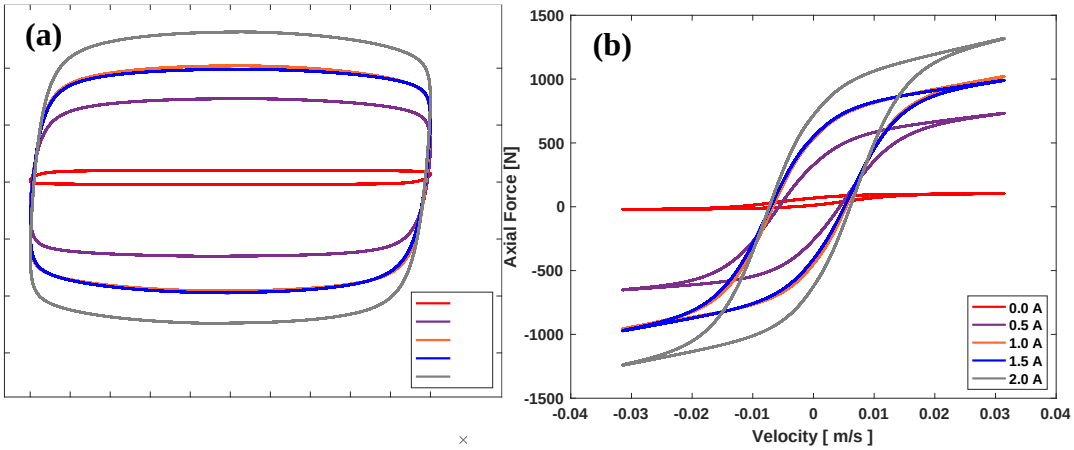

Figure 31 – Numerical (a) Force vs Displacement (b) Force vs Velocity

The immediate effect of increasing the damper coil excitation current is an increase in the damping force. An analysis performed to achieve the sensitivity of the parameters will be shown subsequently in section 4.8, where each parameter was subjected to variation rates of approximately (1%, 5%, 10%, 15%, and 20%) and it was verified that the most sensitive physical parameter is the force f_0.

4.3 Frequency Dependency

The dynamic behavior of a system can be analyzed in both the time and frequency domains. In the case of the sigmoid model used in this study, the characteristic parameters are independent of frequency, amplitude, and current excitations. This means that the identified parameters can define the response of the MR damper under

specific excitation conditions. If a different combination of excitation parameters is desired, the estimated parameters need to be reevaluated (Çeşmeci and Engin 2010).

Figure 32 presents the plots of the damper response force at three different vibration frequencies $f = [1 \quad 3 \quad 5]\, Hz$, while maintaining a magnetic field of I = 0.5 A and an amplitude of 5mm. Consistent with the findings of (Li et al. 2000), the force exhibited minimal variation with changes in frequency. Figure 32(b) illustrates the damper response force plotted against displacement and force at 1 Hz, 3 Hz, and 5 Hz frequencies.

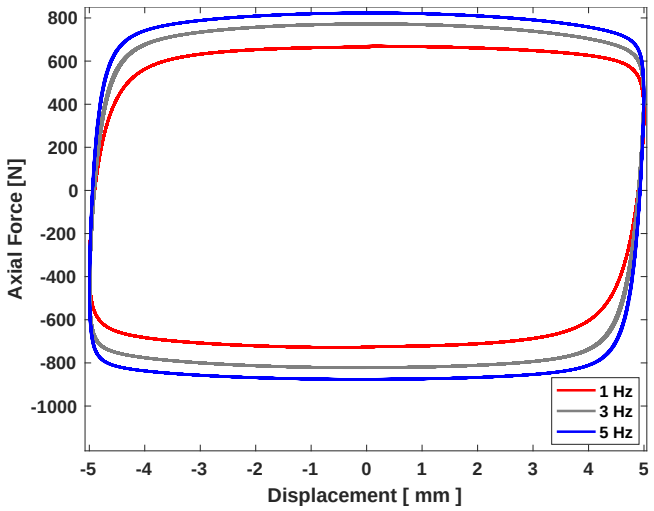

Figure 32 - Numerical Comparison Force vs Displacement (Increasing Frequency)

Figure 33 depicts the force-velocity relationship of the MR damper at three different vibration frequencies $f = [1 \quad 3 \quad 5]\, Hz$, whit a fixed magnetic field of I = 0.5 A and an amplitude of 5 mm. The plot highlights the presence of a nonlinear behavior between force and velocity, with the nonlinearity becoming more evident at higher frequencies. In other words, as the frequency increases, the deviation from a linear relationship between force and velocity becomes more significant. These observations suggest that the dynamics of the damper are influenced by both the frequency and velocity of the input excitation. The nonlinearity in the force-velocity relationship becomes more significant as the excitation frequency increases. It is important to understand and account for this nonlinearity when modeling and controlling the behavior of the MR damper in practical applications (Li et al. 2000).

Based on the findings of (Chen et al. 2022), it can be concluded that the damping force of the MR damper increases as the vibration frequency. The vibration frequency has a noticeable impact on the maximum velocity the damper reaches. However, the hysteresis properties of the MR damper are minimally affected by changes in vibration frequency. These conclusions highlight the influence of frequency on both the damping force and velocity of the MR damper. As the vibration frequency increases, the damping force also increases, indicating a strong resistance to the motion of the damper. Additionally, the velocity of the damper reaches higher values as the vibration frequency increases, as depicted in Figure 33, with an approximate rate of increase of 0.06 m/s every 1 Hz incremented in frequency.

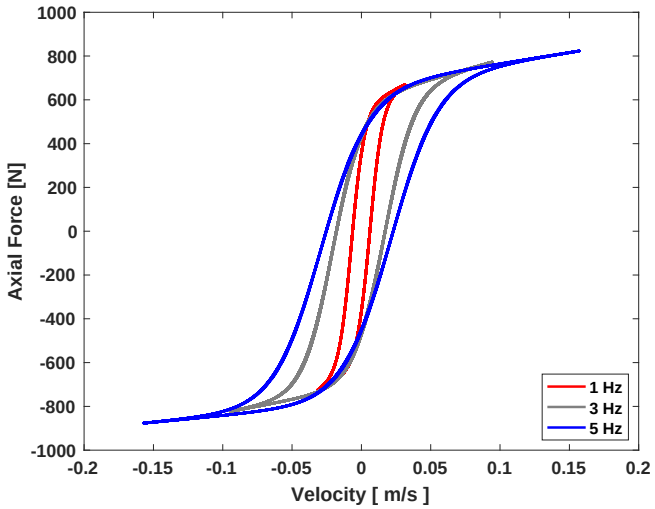

Figure 33 - Numerical Comparison Force vs Velocity (Increasing Frequency)

4.4 Displacement Dependency

Figure 34 displays the plots of the damper response force at three different displacement amplitudes (2.5mm, 5mm, 7.5mm), while maintaining a magnetic field of I = 0.5 A and a frequency of 1 Hz. The results indicate that the peak force increases with the amplitude, which is consistent with the findings of (Li et al. 2000). However, an exception is observed at a displacement of 7.5mm, where a decrease in the peak force is observed. This particular observation warrants further investigation in future studies to determine whether it was an experimental error or if it represents a specific characteristic of this particular damper. These findings suggest that the ideal elastoplastic model may need to explain the experimental results fully.

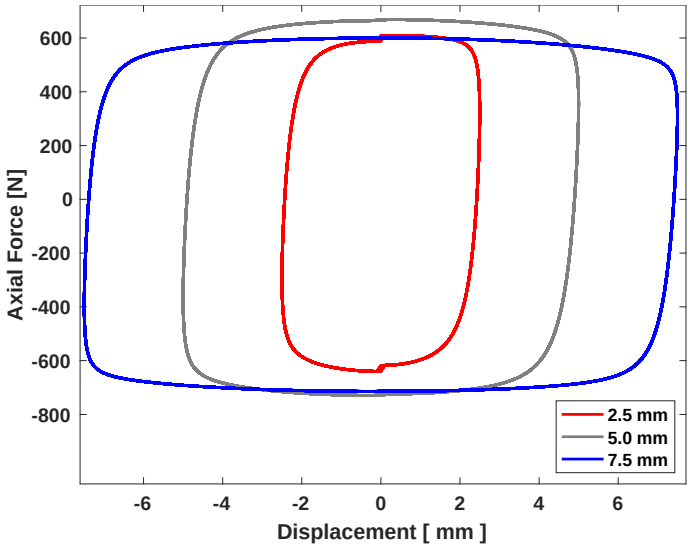

Figure 34 - Numerical Comparison Force vs Displacement (Increasing Frequency)

Figure 35 displays the plots of the damper response force at three different displacement amplitudes (2.5mm, 5mm, 7.5mm), while maintaining a magnetic field of I = 0.5 A and a frequency of 1 Hz. Furthermore, as the displacement increases, it can be concluded that the velocity of the damper also increases, reaching higher values. Based on the data, the rate of increase is approximately 0.015 m/s for every 2.5 mm of displacement increment. This relationship between displacement and velocity highlights the influence of displacement on the dynamic behavior of the damper.

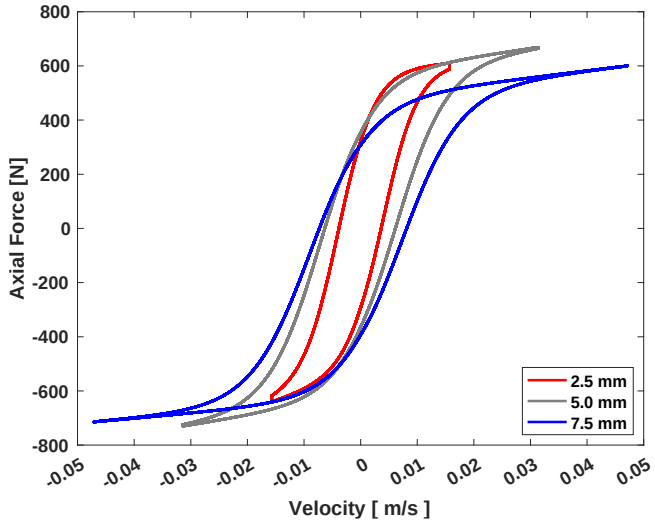

Figure 35 - Numerical Comparison Force vs Velocity (Increasing Displacement)

4.5 Temperature Dependency

According to technical information provided by Lord Corporation, the operational temperature of the MR damper is 71 °C. With an initial temperature of 28°C, the experiment progressed until it reached the operating temperature of 71°C. At this point, the damper experienced a significant reduction in damping force, dropping from 1332 N to 989 N, indicating a variation of approximately 26%, as seen in Figure 36 for an operating condition of 1.5 A and a displacement of 5mm.

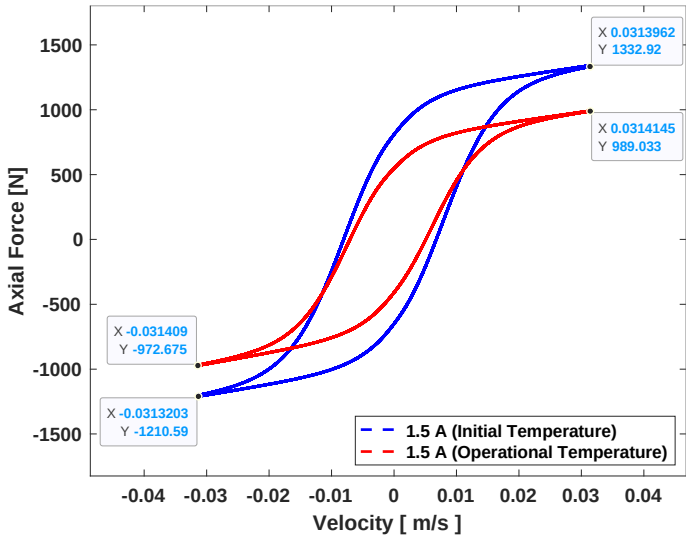

Figure 36 - Numerical Parameters Comparison (Increasing Temperature)

In order to verify the variation of parameters at different operating temperatures, the parameters were identified using the differential evolution technique. A considerable variation was observed in the identified parameters between the initial temperature of 28°C and the operating temperature of 71°C.

Table 8 and

Table 9 - Hysteresis Parameters (Displacement 5.0 mm -1 Hz and 1.5 A)present a comparison of the parameters obtained at these two temperatures. The parameter variation highlights the temperature dependency of the MR damper's behavior.

Table 8 - *Physical Constants (Displacement 5.0 mm – 1 Hz and 1.5 A)*

	$f_0\ (N)$	$I_0\ (amp)$	$I_1\ (amp)$	a_0	$a_1(m/s)^{-1}$	$a_2(amp)^{-1}$	$a_3(m/s)^{-1}$	$a_4(m/s)^{-1}$
Initial Temperature 28°C	8,38	0,34	0,17	236,94	-5,59	-4,04	0,11	-7,22
Operating Temperature 71°C	3,35	-0,51	-1,00	-247,9	1,39	5,00	0,32	-17,42
Difference	**5,03**	**0,85**	**1,17**	**484,86**	**6,98**	**9,04**	**0,21**	**10,2**

Table 9 - *Hysteresis Parameters (Displacement 5.0 mm -1 Hz and 1.5 A)*

	k_0	k_{1c}	k_{1e}	k_2	k_3	k_4	k_5	k_6
Initial Temperature 28°C	0,28	5,09	6,63	-334,23	-5	-0,30	-0,07	0,00
Operating Temperature 71°C	-0,77	5,14	6,99	-118,52	-1,13	-0,22	0,05	0,02
Difference	**1,05**	**0,05**	**0,36**	**215,71**	**3,87**	**0,08**	**0,12**	**0,02**

4.6 Error Analysis

The same error analysis and validation proposed by (Silva et al. 2023) was implemented in this study. Validation is considered an important stage of the model development or implementation process, as it ensures the implemented model's accuracy and reliability in representing the MR damper's nonlinear behavior (Tsioptsias et al. 2016). Figure 37 depicts the approach and the fitting results proposed by (Santade 2017) for compassion and validation purposes. The efficient identification of parameters for a non-linear hysteretic parametrized sigmoid model to represent a MR damper relies heavily on robust experimental methods. However, during the repeatability tests of the experimental results, significant discrepancies in damping force were observed for tests performed under the same conditions. These

discrepancies explain the small difference between the literature and identified results. In contrast, the simulation method strongly agreed with the experimental results, indicating its reliability and dependability.

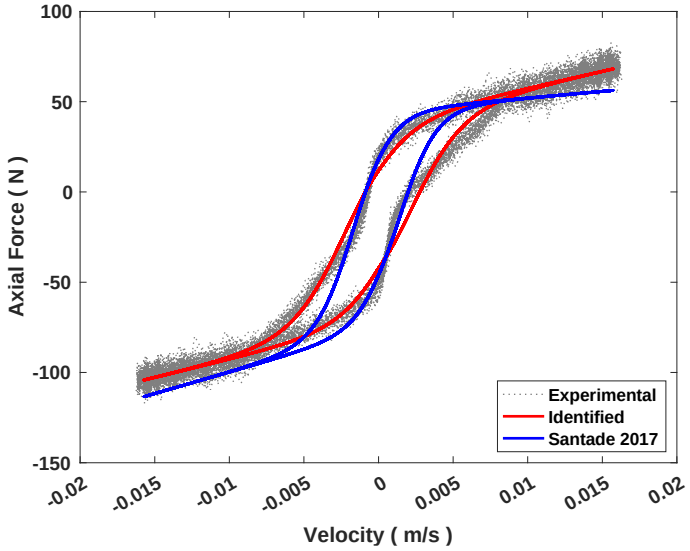

Figure 37 - Comparison of Literature, Experimental, and Identified Values

In general, measurement errors can be classified into two main categories: systematic errors and random errors. Systematic errors are errors whose absolute value and sign remain constant during several measurements carried out under the same conditions for a given value and quantity. They cause the results to deviate consistently from the true value or move away from the actual result in the same direction over time. On the other hand, random errors are small fluctuations that occur in measurements and tend to vary unpredictably. Random errors tend to cancel each other out somewhat, making them suitable for statistical analysis. The probability distribution of random errors, which can shift values in either direction, is called Gaussian distribution, as shown in Figure 38 (Huang et al. 2021).

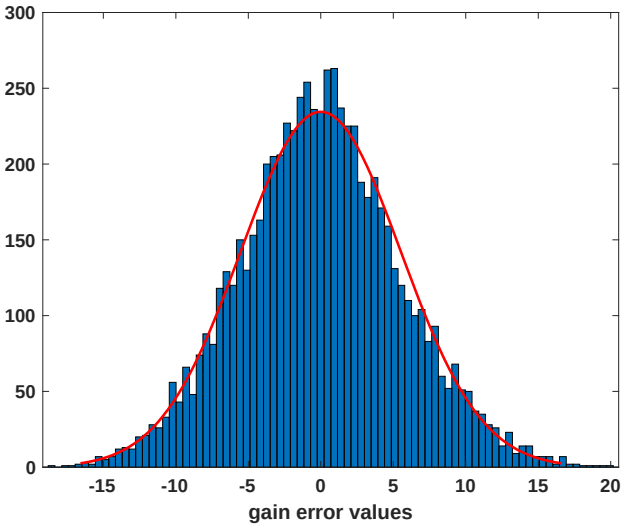

Sample Size	7001
Minimum	-20.9067
Maximum	21.8406
Mean	0.0026
Variance	31.0140

Normal Distribution Force Error	
mu = - 0.00162972	[-0.131098, 0.127839]
sigma =5.52613	[5.43609, 5.61921]

Figure 38 - Error Histogram: Analyzing the Accuracy of the Identified Force

Figure 39 displays a quantile-quantile plot, also known as a QQ plot, which compares the quantiles of the sample force error with the theoretical quantile values from a normal distribution. The QQ plot is a graphical tool used by researchers to assess whether two data sets are derived from populations with common distributions. It provides a visual means of examining the similarities or differences in the distribution of the data sets being compared.

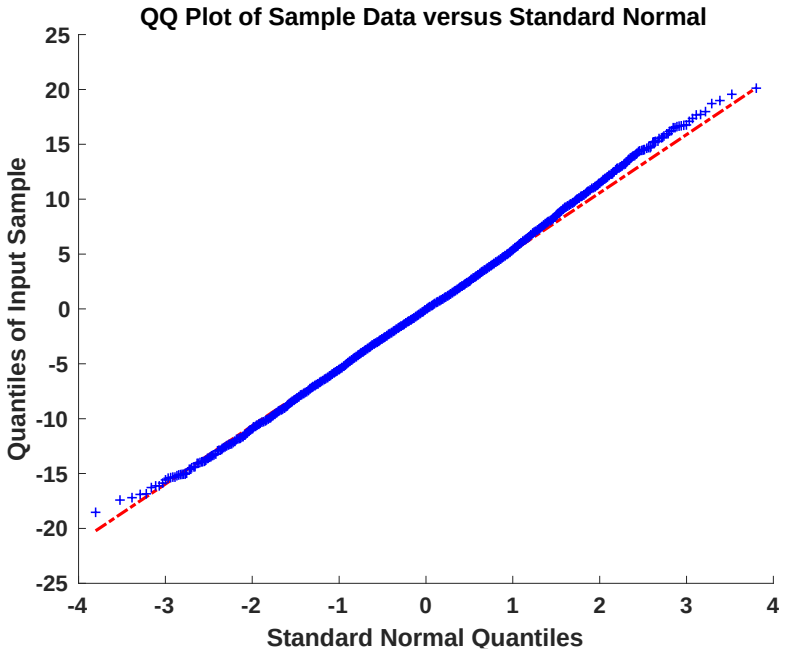

Figure 39 - Force error Quantile-Quantile Plot

The differential evolution method generates different parameter values for each simulation of 500 iterations every time the algorithm is executed. To evaluate the impact of this variation on the simulations, a boxplot graph Figure 40 was produced with the parameter's values for one hundred consecutive simulations. The analyses revealed that almost all parameters showed a variation and the parameters a_0, k_5 and k_6 exhibit a considerable number of outlier points.

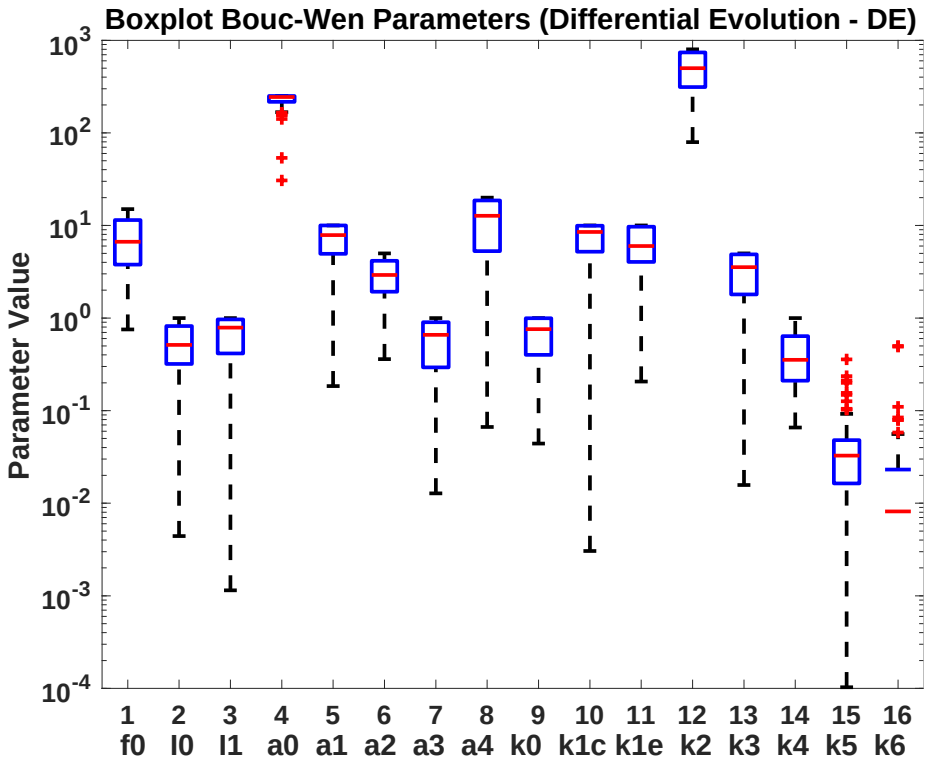

Figure 40 - Statistical Analysis of 16 parameters (Boxplot graph) with the DE method

Table 10 lists the physical parameters, and the maximum, minimum, mean, and variance of each parameter are shown in the subsequent columns. The values in the table are the results of one hundred consecutive simulations using the DE method. The fourth parameter a_0 showed the highest variance, indicating greater variability in its values across the consecutive simulations with the DE method. Variance is a statistical measure of how a set of data is spread out. A high variance indicates that the data points are spread out over a broad range of values, while a low variance indicates that the data points are clustered more closely around the mean. In this case,

the fourth parameter a_0 had a higher variance than the other parameters, indicating its values varied more widely across the simulations.

Table 10 - *Summary of Physical Parameters Analysis Using Consecutive Simulations with DE Method (Displacement 5.0 mm – 1 Hz)*

	5.0 mm	$f_0\ (N)$	$I_0\ (amp)$	$I_1\ (amp)$	a_0	$a_1(m/s)^{-1}$	$a_2(amp)^{-1}$	$a_3(m/s)^{-1}$	$a_4(m/s)^{-1}$
Maximum	**0 A**	15,00	1,00	1,00	250	10	5	1	20
Minimum		0,752	-1,00	-1,00	-250	-10	-5	-1	-20
Mean	**1 Hz**	7,30	0,300	0,17	-30,9	-1,80	-0,18	-0,01	-0,01
Variance		**18,96**	**0,29**	**0,53**	**$5{,}27e^4$**	**56,18**	**10,70**	**0,47**	**189,25**

When subjected to one hundred consecutive simulations, it represents the maximum, minimum, mean, and variance of hysteresis parameters, revealing that the parameter k_2 has the highest variance, indicating its values varied more widely across the simulations.

Table 11 - *Summary of Hysteresis Parameters Analysis Using Consecutive Simulations with DE Method (Displacement 5.0 mm – 1 Hz)*

	5.0 mm	k_0	k_{1c}	k_{1e}	k_2	k_3	k_4	k_5	k_6
Maximum	**0 A**	1,00	10,0	10,0	800	5,00	1,00	0,358	0,5
Minimum		-1,00	-10,0	-10,0	-800	-5,00	-1,00	-0,235	0,00
Mean	**1 Hz**	-0,06	6,45	4,64	15,83	0,18	0,01	0,001	0,02
Variance		**0,55**	**21,32**	**26,64**	**$3{,}09e^5$**	**12,80**	**0,281**	**0,005**	**0,005**

The generated bar graph Figure 41 represents the variance for the 16 obtained parameters when subjected to one hundred consecutive simulations. In this case, the bar graph highlights that the parameters k_2, a_0 and a_4 exhibit a higher degree of variability in their values across the obtained data, as compared to the other parameters.

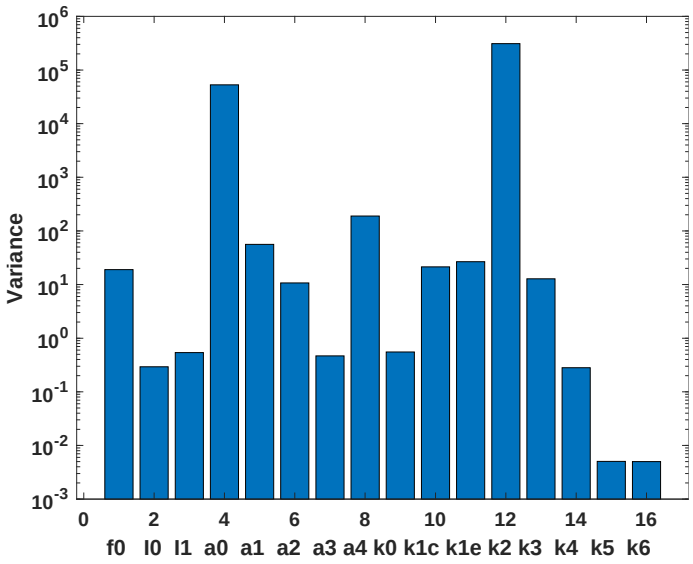

Figure 41 - Variation Analysis of 16 parameters across one hundred consecutive simulations

4.7 **Experimental Results Fitting**

Significant discrepancies were found in relation to experimental tests carried out under the same conditions. As an experimental validation factor, estimates of the repeatability of an assay are necessary to assess the transfer of experimental methods between laboratories.

Table 12 displays the complete experimental conditions and operating combinations tested and analyzed. The table comprehensively overviews the various scenarios and parameters investigated during the experiments.

Appendix B of this work provides a comprehensive analysis of the effect of increasing the excitation frequency on the behavior of the MR damper. It includes simulations for both passive and semi-active modes of the damper.

In the passive mode, it is observed that as the frequency increases, the force and velocity of the damper reach higher values. Additionally, increased displacement leads to a shift in the compressive damping force towards higher values.

For the semi-active mode, simulations were performed with excitation currents of 0.5 A, 1.0 A, and 1.5 A. Similar trends were observed, with the force and velocity increasing as the frequency rises—Moreover, an increase in displacement results in a shift of the compressive damping force towards higher values.

These findings provide valuable insights into the behavior of the MR damper under different operating conditions. They contribute to the understanding of the dynamic response of the semi-active suspension system and can be used to optimize its performance in automotive applications.

Table 12 – Experiment Test Conditions

Displacement	Frequency	Current	Figure
2.5 mm	1 Hz	0 A	Figure 60
		0.5 A	Figure *68*
		1.0 A	Figure *76*
		1.5 A	Figure *84*
	3 Hz	0 A	Figure *61*
		0.5 A	Figure *69*
		1.0 A	Figure *77*
		1.5 A	Figure *85*
	5 Hz	0 A	Figure *62*
		0.5 A	Figure *70*
		1.0 A	Figure *78*
		1.5 A	Figure *86*
5.0 mm	1 Hz	0 A	Figure *63*
		0.5 A	Figure *71*
		1.0 A	Figure *79*
		1.5 A	Figure *87*
	3 Hz	0 A	Figure 64
		0.5 A	Figure *72*
		1.0 A	Figure *80*
		1.5 A	Figure *88*
	5 Hz	0 A	Figure *65*
		0.5 A	Figure *73*
		1.0 A	Figure *81*
7.5 mm	1 Hz	0 A	Figure *66*
		0.5 A	Figure *74*
		1.0 A	Figure 82
		1.5 A	Figure *89*
	3 Hz	0 A	Figure *67*
		0.5 A	Figure *75*
		1.0 A	Figure 83
		1.5 A	Figure *90*

4.8 Parameter Sensitivity Analysis

Real-world problems are often described and analyzed using mathematical expressions that involve various parameters. A model is a simplified representation of specific aspects of a real-life system, often created using mathematical concepts like functions and equations. The process of developing a mathematical model assumes a transition from the real world to the theoretical realm of mathematical concepts, where the model is created and manipulated using mathematical or computational techniques. Eventually, the model is applied to the real world, leading to practical solutions for real-world problems. This iterative process signifies that the analysis begins and ends in the real world, with the mathematical model serving as an intermediate tool for understanding and addressing the underlying problem (Hamby 1994; Latunde and Bamigbola 2018).

Parameter sensitivity analysis is indispensable for examining mathematical models of real-life problems. By conducting a thorough parameter sensitivity analysis, we can explore how changes in a model parameter affect the relevant outputs and generate a range of predictions. In this study, the parameter sensitivity analysis focused on the model's cost function and constraint to assess each parameter's relative significance. Varying each parameter at different rates of variation (1%, 5%, 10%, 15%, and 20%) enabled the determination of the parameter that had the highest impact on the analysis output. By assessing the effect of each parameter variation on the output, it was possible to identify the most sensitive parameter, which exerted the greatest influence on the overall system performance.

Table 13 provides the error values of the error force (fd) for the varied physical parameters. Among the parameters examined, the ones that exhibited the highest sensitivity, resulting in significant changes in the damping force, were f_0, a_0, and a_1.

Table 14 provides the error values of the error force (fd) for the varied hysteresis parameters. Among the parameters examined, the ones that exhibited the highest sensitivity, resulting in significant changes in the damping force, were k_5, k_{1c}, and k_{1e}.

Table 13 – Error fd (Physical Parameters)

Parameter	Error (Fd)	Figure
f_0	$16x10^5$	Figure *42*
a_0	$3x10^4$	Figure 53
a_1	$1.2x10^4$	Figure *45*
a_4	20	Figure 53
I_0, I_1, a_2, a_3	CTE	Figure 43

Table 14 – Error fd (Hysteresis Parameter)

Parameter	Error (Fd)	Figure
k_5	$16x10^4$	Figure *51*
k_{1c}	$7x10^4$	Figure *47*
k_{1e}	$7x10^4$	Figure *48*
k_0	$3.5x10^4$	Figure *46*
k_4	$3x10^4$	Figure *50*
k_6	180	Figure *52*
k_2, k_3	CTE	Figure *49*

After analyzing Table 13 and Table 14, it becomes evident that four parameters, namely f_0, k_5, k_{1c}, and k_{1e}, exhibit the highest error force (fd) values for the damping force. These parameters demonstrate a significant impact on the accuracy and reliability of the damping force estimation. Consequently, it is crucial to pay special attention to these parameters during the analysis and optimization process. By focusing on accurately modeling and effectively controlling the system's damping behavior, the overall performance and behavior of the system can be improved.

4.8.1 Parameter f_0

Upon analyzing Figure 42, it becomes evident that the physical parameter labeled as f_0 plays a crucial role in determining the magnitude of the damping force denoted as f_t. The relationship between these two variables is such that any changes in the parameter f_0 directly affect the resulting damping force. Figure 42 explicitly highlights the distinction between the initial value of the parameter f_0 and its varied counterpart.

This disparity is visualized as the force error, representing the quantitative difference between the expected and actual damping forces resulting from the altered parameter value.

By examining this figure and understanding the force error, it becomes possible to assess the extent to which variations in the physical parameter f_0 impact the system's overall performance. This analysis aids in comprehending the sensitivity of the system's damping force to changes in the parameter f_0, providing valuable insights for optimization and fine-tuning purposes.

By altering the value of the parameter f_0, the behavior of the damping force undergoes changes. Specifically, increasing the parameter f_0 leads to an evident amplification of the minimum and maximum peaks in the damping force. This indicates that higher values of f_0 results in more pronounced fluctuations or oscillations in the force exerted. The relationship between the parameter f_0 and the peaks of the damping force suggests that the parameter f_0 directly influences the magnitude or intensity of these peaks. Understanding this relationship can be crucial in optimizing the system's performance, as controlling the value of f_0 allows for fine-tuning the behavior of the damping force and achieving the desired level of damping or response.

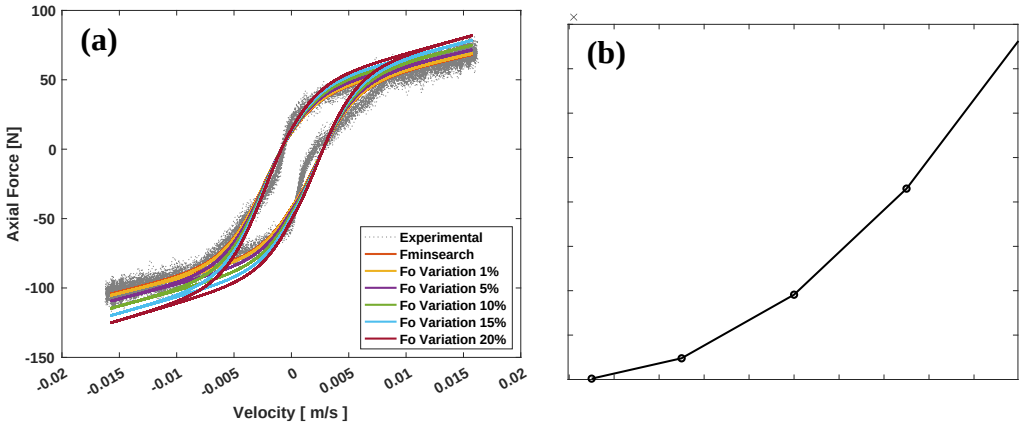

Figure 42 – Percentual variation of f_0 described on (a) F-V curve and (b) sensibility absolute error values of $|F_t - F_{to}|$ with f_0 variation

4.8.2 Parameters $I_0, I_1, a_2,$ and a_3

When subjected to the proposed variation rates in the sensitivity test, the parameters I_0, I_1, a_2 and a_3 did not show any variation in the damping force f_t as seen in Figure 43.

The sensitivity analysis intentionally varied these parameters at different rates (1%, 5%, 10%, 15%, and 20%) to observe their impact on the damping force. However, the results indicated that changes in these specific parameters did not result in any discernible alterations in the damping force. This outcome suggests that the damping force is not sensitive to variations in the parameters I_0, I_1, a_2 and a_3 within the given ranges. It implies that these parameters may have minimal or negligible influence on the overall behavior of the damping force and, consequently, on the system's performance under consideration.

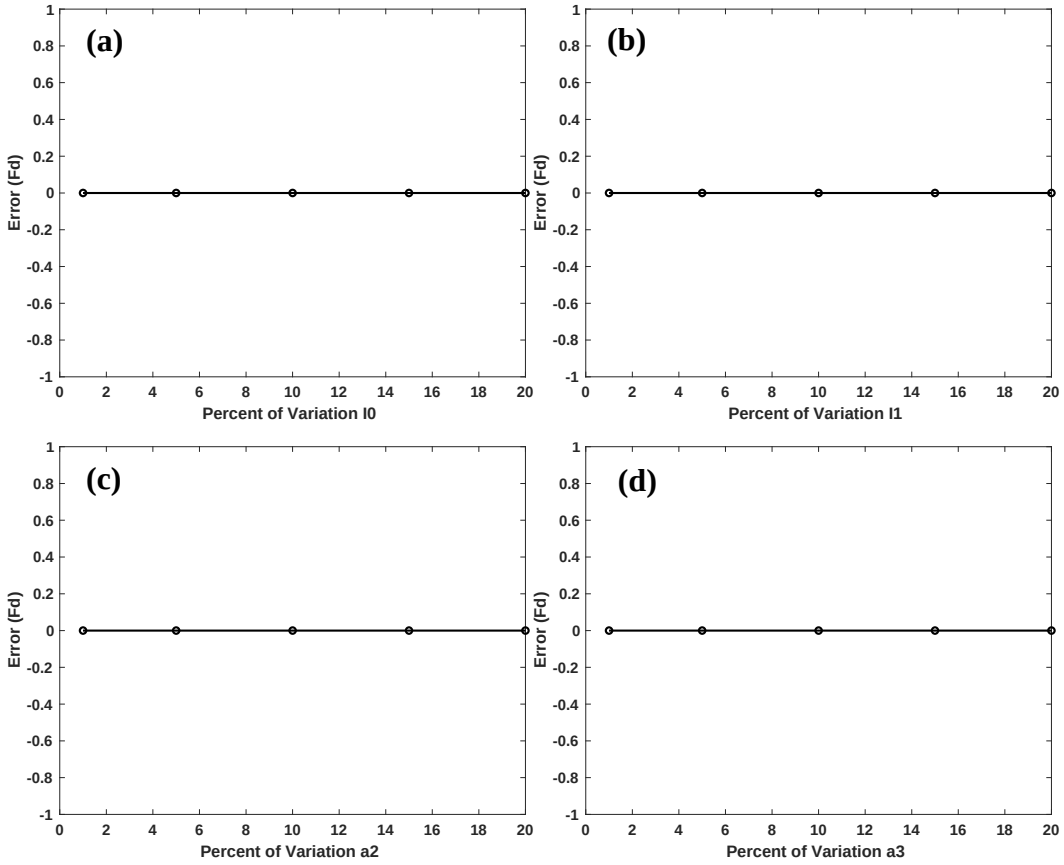

Figure 43 – Sensibility analysis by absolute error values of $|\boldsymbol{F_t} - \boldsymbol{F_{to}}|$ as a function of $\boldsymbol{f_0}$ for variation of physical parameters (a) $\boldsymbol{I_0}$, (b) $\boldsymbol{I_1}$, (c) $\boldsymbol{a_2}$, and (d) $\boldsymbol{a_3}$.

4.8.3 Parameter a_0

Figure 44(a) specifically focuses on the impact of varying the parameter a_0 on the analysis or system under study. The associated error Figure 44(b) highlights the discrepancy between the expected outcomes and the actual results obtained when parameter a_0 is changed. The significant magnitude of this error suggests that the parameter a_0 plays a crucial role in influencing the overall behavior or performance of the system. Consequently, variations in the parameter a_0 result in noticeable deviations from the expected results, highlighting the sensitivity of the system to changes in this specific parameter.

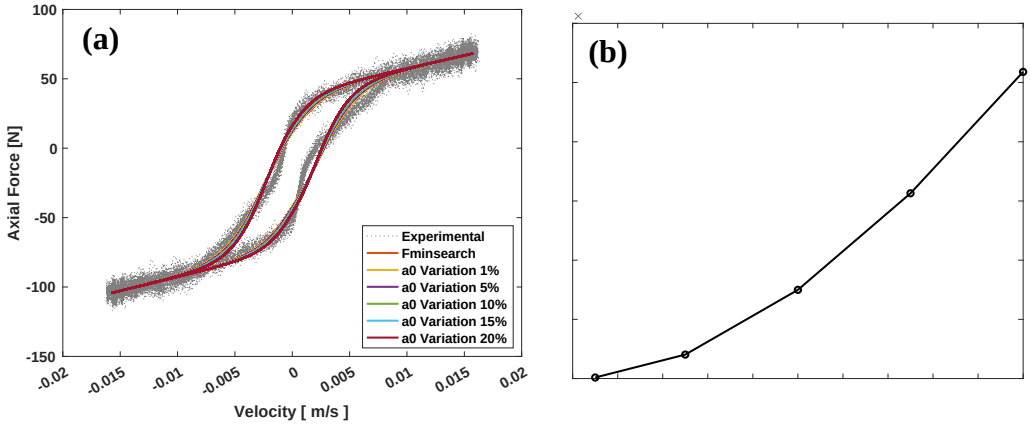

Figure 44 – Percentual variation of $\boldsymbol{a_0}$ described on (a) F-V curve and (b) sensibility absolute error values of $|\boldsymbol{F_t} - \boldsymbol{F_{to}}|$ with $\boldsymbol{a_0}$ variation

4.8.4 Parameter $a_1$and a_4

Figure 45(a) displays the error, which represents the difference between the initial parameter and the variation for parameter a_1. Similarly, Figure 45(b) represents the error for parameter a_4. By analyzing the variation of these two parameters and comparing the magnitude of the errors, it can be concluded that they do not cause a significant variation in the damping force. The comparison of the errors in Figure 45 indicates that changes in parameters a_1 and a_4 have minimal impact on the magnitude of the damping force. The relatively small errors suggest parameter variations result in only minor deviations from the expected or initial damping force values. This conclusion implies that parameters a_1 and a_4 may not be the primary factors influencing the behavior of the damping force in the system under study. Other

parameters or factors may substantially impact the overall performance or characteristics of the damping force.

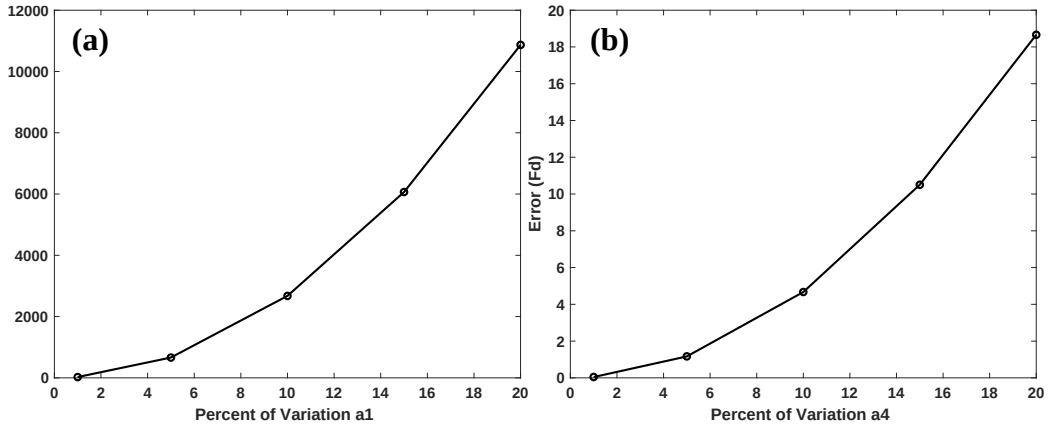

Figure 45 – Sensibility analysis by absolute error values of $|\boldsymbol{F_t} - \boldsymbol{F_{to}}|$ as a function of $\boldsymbol{f_0}$ for variation of physical parameters (a) $\boldsymbol{a_1}$, (b) $\boldsymbol{a_4}$.

4.8.5 Parameter k_0

The error in the variation of the parameter k_0 , as shown in Figure 46(a) and (b) exhibits a similar order of magnitude as the error for the parameter k_4. While it does have an impact on the force f_t, it is not one of the most significant parameters in the analysis, nor does it affect the geometry on the hysteresis side.

The comparable magnitudes of the errors in the variation of k_0 and k_4 suggest that both parameters contribute similarly to the deviations from the expected values of the force f_t. However, it is important to note that other parameters in the analysis have a more substantial influence on the overall behavior and characteristics of the force f_t.

Furthermore, the parameter k_0 does not play a role in altering the geometry on the hysteresis side. This indicates that changes in k_0 do not significantly impact the shape or pattern of the hysteresis loop associated with the system under consideration.

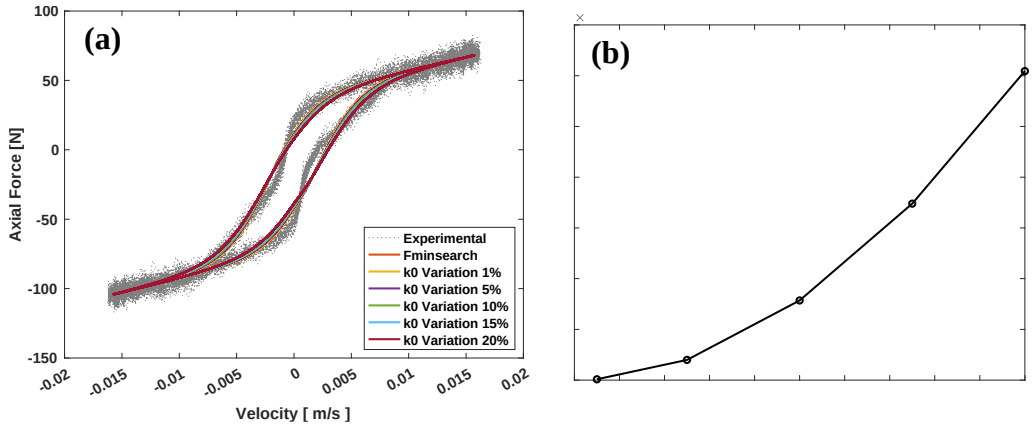

Figure 46 – Percentual variation of $\boldsymbol{k_0}$ described on (a) F-V curve and (b) sensibility absolute error values of $|\boldsymbol{F_t} - \boldsymbol{F_{to}}|$ with $\boldsymbol{k_0}$ variation

4.8.6 Parameter k_{1c}

The sensitivity analysis conducted in Figure 47(a) and (b) demonstrates that changes in the parameter k_{1c} result in notable variations in the damping force f_t. This indicates that the value of k_{1c} plays a crucial role in determining the magnitude and behavior of the damping force within the system under investigation. Moreover, the parameter k_{1c} also influences the geometry of the hysteresis loop. Specifically, it modifies the angle β_{he} associated with the hysteresis loop. This suggests that variations in k_{1c} lead to changes in the hysteresis loop's shape, symmetry, or overall characteristics.

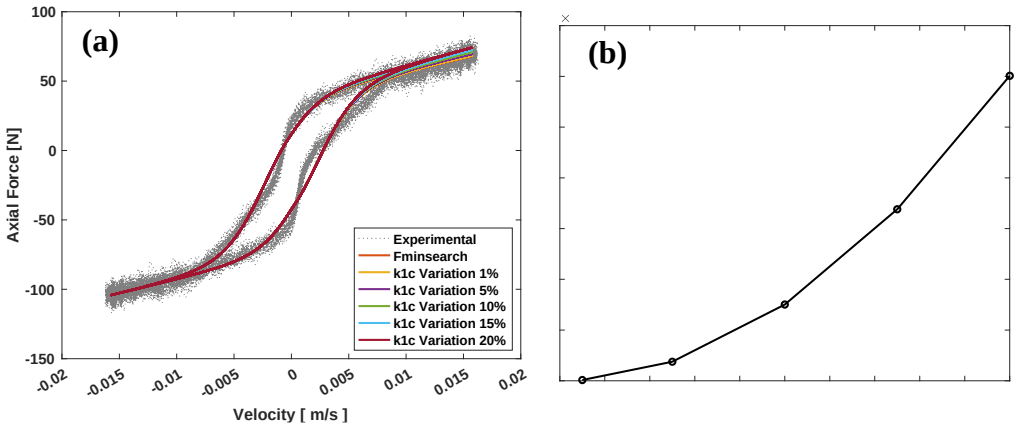

Figure 47 – Percentual variation of $\boldsymbol{k_{1c}}$ described on (a) F-V curve and (b) sensibility absolute error values of $|\boldsymbol{F_t} - \boldsymbol{F_{to}}|$ with $\boldsymbol{k_{1c}}$ variation

4.8.7 Parameter k_{1e}

Figure 48(a) and (b) presents the influence of the parameter k_{1e} on the damping force f_t. Similar to the parameter k_{1c}, the parameter k_{1e} exhibits a significant impact on the damping force with a comparable magnitude. However, the critical difference is that k_{1e} affects the angle β_{hc}. The sensitivity analysis depicted in Figure 48(a) and (b) reveals that parameter k sub 1e variations lead to noticeable changes in the damping force f_t. This suggests that k_{1e} plays a crucial role in determining the magnitude and behavior of the damping force within the analyzed system, similar to the influence of k_{1c}.

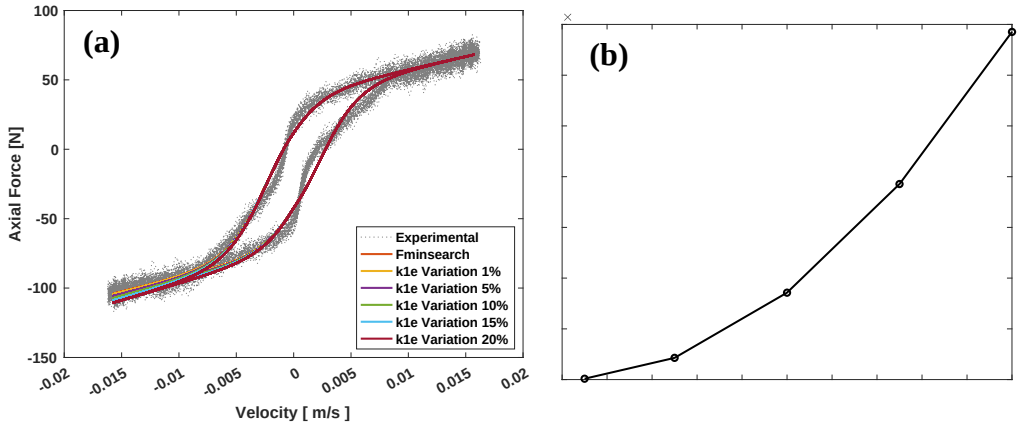

Figure 48 – Percentual variation of k_{1e} described on (a) F-V curve and (b) sensibility absolute error values of $|F_t - F_{to}|$ with k_{1e} variation

4.8.8 Parameters k_2 and k_3

Figure 49 provides insights into the analysis of the parameters k_2 and k_3. However, the lack of variation depicted in the figure indicates that changes in these parameters did not result in noticeable deviations or alterations in the system being studied. The absence of variation in the parameters k_2 and k_3 suggests that these specific parameters may not significantly influence the damping force or other relevant aspects of the system's behavior. Different parameters or factors in the analysis may substantially impact the overall performance or characteristics.

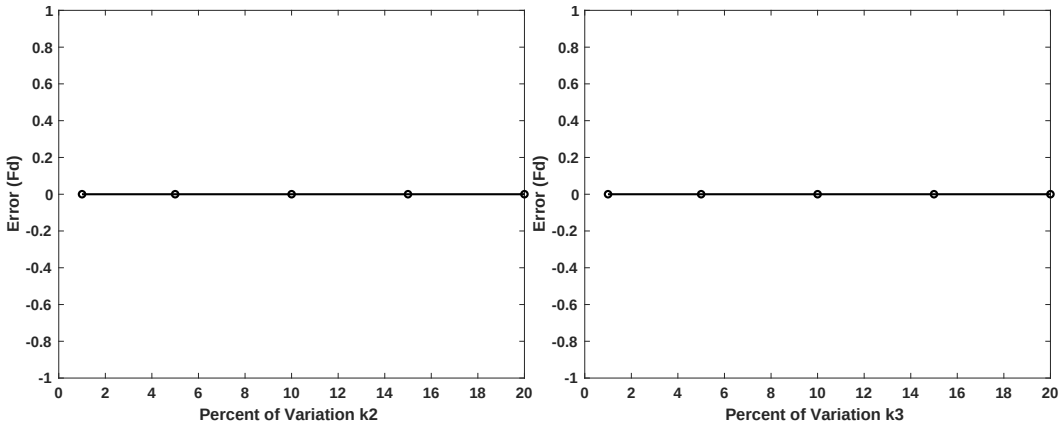

Figure 49 - Sensibility analysis by absolute error values of $|\boldsymbol{F_t} - \boldsymbol{F_{to}}|$ as a function of $\boldsymbol{f_0}$ for variation of physical parameters (a) $\boldsymbol{k_2}$, (b) $\boldsymbol{k_3}$.

4.8.9 Parameter k_4

Figure 50 and (b) provided the sensibility of f_t with the variation of the parameter k_4.

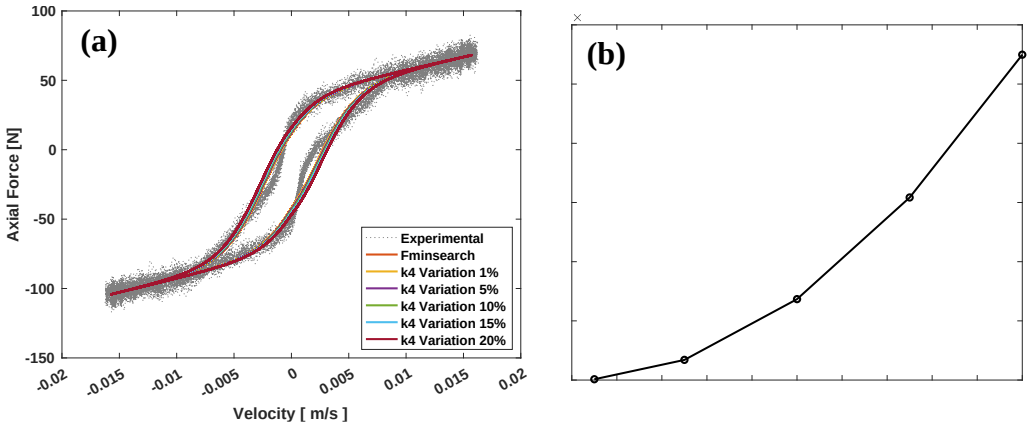

Figure 50 - Percentual variation of $\boldsymbol{k_4}$ described on (a) F-V curve and (b) sensibility absolute error values of $|\boldsymbol{F_t} - \boldsymbol{F_{to}}|$ with $\boldsymbol{k_4}$ variation

4.8.10 Parameter k_5

By analyzing the variations of the parameter $k_5$in Figure 51 and (b), it becomes evident that changes in k_5 significantly impact the damping force f_t. This implies that altering the value of k_5 leads to noticeable variations in the magnitude or behavior of the damping force within the system. Furthermore, the sensitivity of the parameter k_5 affects the vertical positioning of the hysteresis loop. By adjusting k_5, the entire

hysteresis loop can be shifted vertically, either higher or lower. This indicates that the parameter k_5 directly influences the overall position or level of the damping force and its relationship to the other variables or factors within the system.

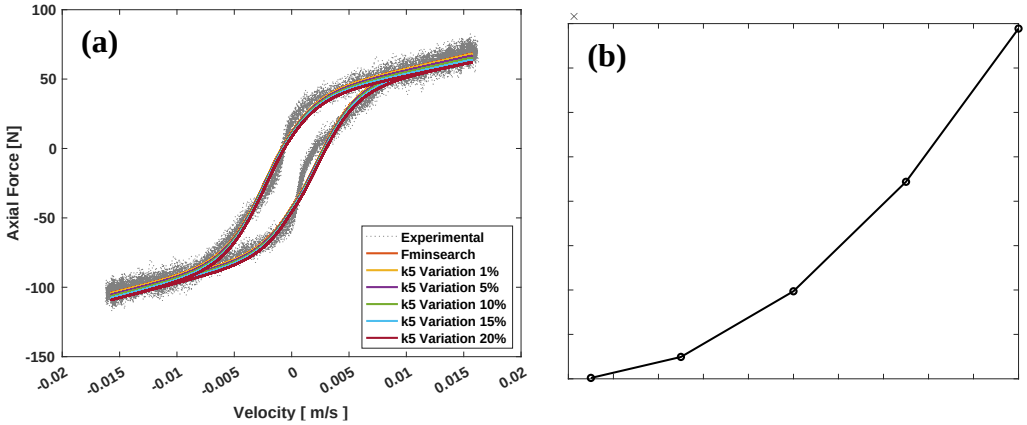

Figure 51 - Percentual variation of $\boldsymbol{k_5}$ described on (a) F-V curve and (b) sensibility absolute error values of $|\boldsymbol{F_t} - \boldsymbol{F_{to}}|$ with $\boldsymbol{k_5}$ variation

4.8.11 Parameter k_6

Figure 52 provides insights into the analysis of the parameter k_6. However, the figure indicates that variations in k_6 results in negligible changes or deviations in the system being studied. The low contribution of the parameter k_6 suggests that it has minimal impact on the damping force or other relevant aspects of the system's behavior. Different parameters or factors in the analysis are likely more influential in determining the overall performance or characteristics.

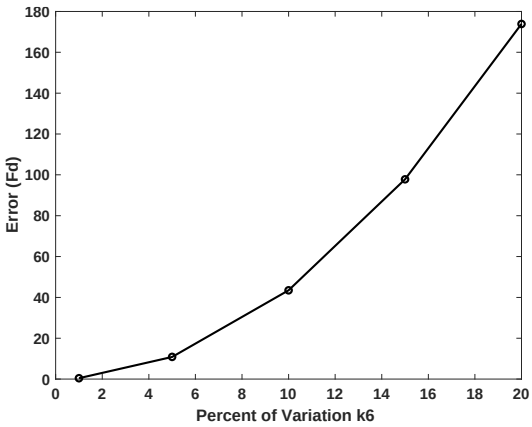

Figure 52 - Sensibility absolute error values of $|\boldsymbol{F_t} - \boldsymbol{F_{to}}|$ with $\boldsymbol{k_6}$ variation

Figure 53 - the evolution of the parameters $a_0, a_1, a_2 a_3$ and a_4. It is possible to visualize the evolution of the parameters graphically as the excitation current increases. However, despite the parameters identified using both DE and Nelder-Mead simplex techniques being close, it is not possible to conclude whether they tend to increase or decrease. This is because some parameters decrease when the current increases, while others vary slightly but increase.

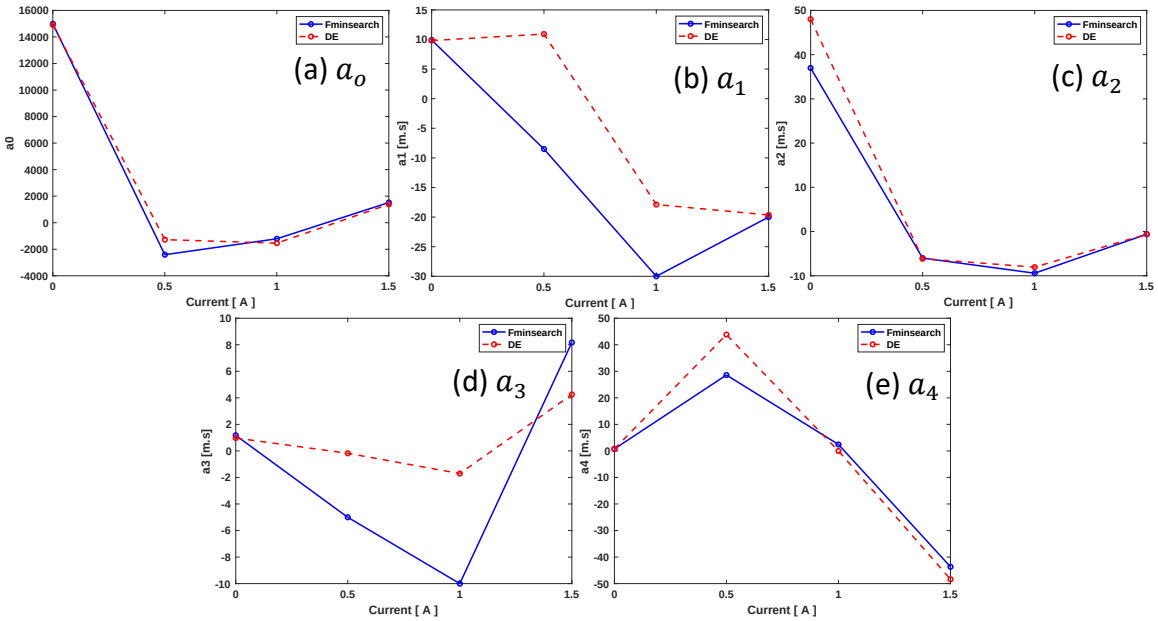

Figure *53* - Evolution of Hysteresis Parameters $\boldsymbol{a_0}$ to $\boldsymbol{a_4}$ as a function of current variation, with a stroke relative displacement of 2.5mm, obtained by Nelder-Mead simplex and DE minimization techniques

The statement Figure 54 says that when the excitation current was increased, the physical parameters (which describe the physical characteristics of the semi-active system) behaved in a non-content or predictable way. Some parameters decreased as the current increased, while others varied but tended to increase. On the other hand, the hysteresis parameters (which describe the relationship between the input and output signals of the identified system) behaved differently. These parameters either decreased or remained stable as the current increased, except for parameters k_2 and k_6, which did not decrease.

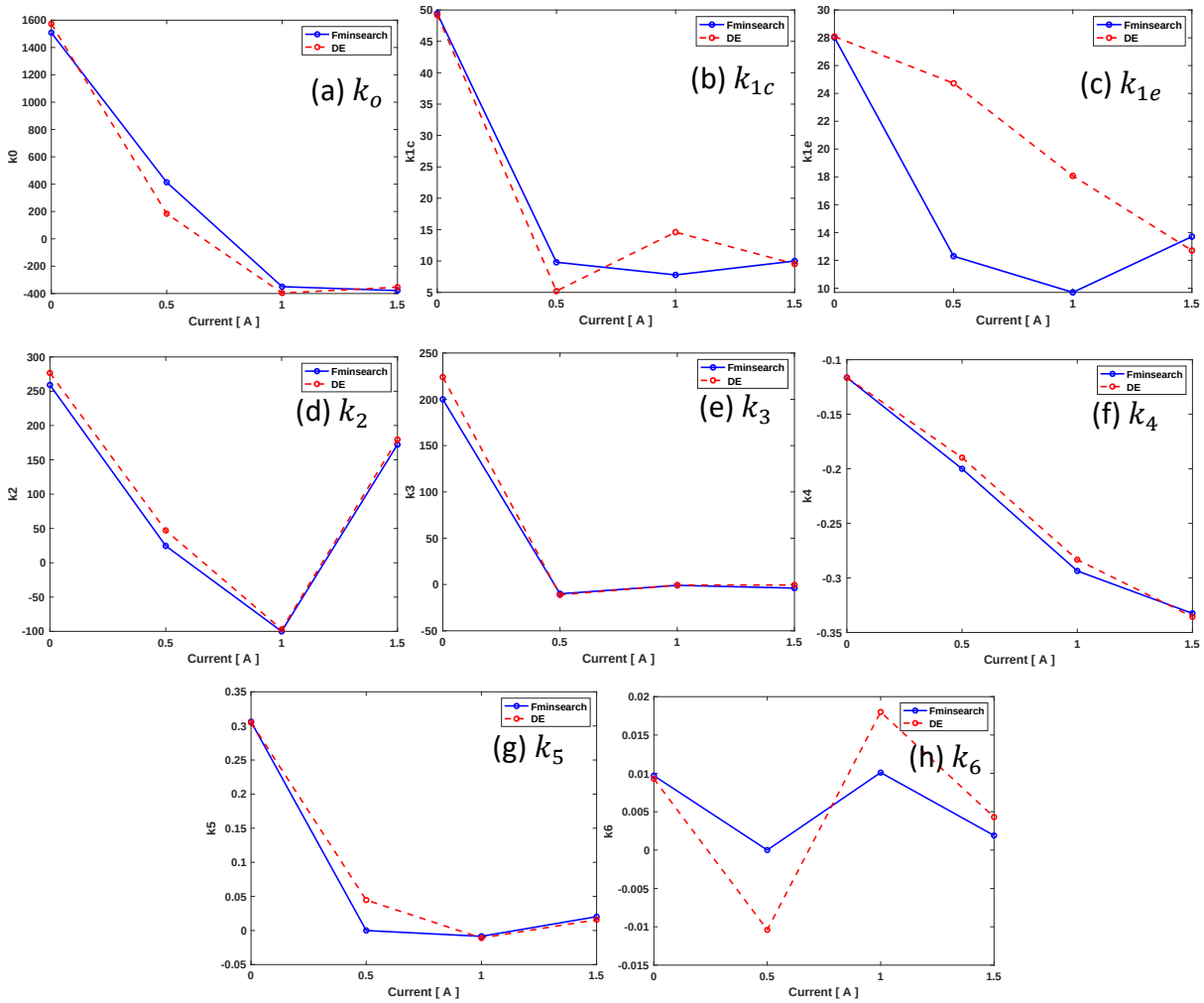

Figure *54* - Evolution of Hysteresis Parameters k_o to k_6 as a function of current variation, with a stroke relative displacement of 2.5mm, obtained by Nelder-Mead simplex and DE minimization techniques.

This suggests that the hysteresis behavior of the system is more predictable and less sensitive to changes in the excitation current than the system's physical characteristics. The fact that the parameters k_2 and k_6 did not decrease suggests that it may be particularly important in determining the system's behavior, even as the excitation current increases.

In order to assess the accuracy of the regression model, the residuals between the experimental and predicted responses are analyzed. This is done by examining normal probability plots and comparing the predicted response to the experimental data. When using the simplex method, implemented as the function "fminsearch" in

Matlab, the residual function (Figure 55) is found to be higher compared to the differential evolution algorithm. This indicates that the simplex method has a larger deviation between the predicted and experimental responses. In other words, the differential evolution algorithm yields a better fit between the model predictions and the actual data, resulting in lower residuals. This suggests that the differential evolution algorithm is more effective in optimizing the regression model and producing a closer match to the experimental results.

In the context of the analysis, several statistical parameters are considered. The statistical degrees of freedom, denoted as N, represent the number of independent observations in the data set.

The covariance matrix, represented as $\epsilon^T.\epsilon$, measures the variability and relationships between the residuals in the regression model. It provides valuable information about the dispersion and patterns of the residuals.

The objective function, denoted $S = S_{experimental} - S_{Identified}$ is a mathematical representation of the optimization problem being solved. It quantifies the discrepancy between the predicted and observed responses, aiming to minimize this difference.

Another parameter $C = \sum \frac{\Delta S}{S_{Identified}}$, represents the relative residual sum of squares of the objective function. It measures the proportion of the sum of squared residuals relative to the total sum of squares, providing insights into the goodness-of-fit of the regression model.

These statistical parameters play a crucial role in evaluating the performance and accuracy of the regression model. They help assess the variability, quality of fit, and overall effectiveness of the optimization techniques employed in the analysis.

The $relative\ error = \frac{S}{S_{Identified}} \rightarrow \epsilon_i = \frac{\Delta S_i}{S_{Identified}}$, is a measure used to quantify the difference between a computed or predicted value and the corresponding experimental value. It is typically calculated by taking the absolute difference between the identified value and the experimental value, divided by the absolute value of the identified value.

On the other hand, the second norm, also known as the Euclidean norm or L2 norm, $\|\epsilon\|_2 = \frac{1}{N}\sqrt{\epsilon^T.\epsilon} = \frac{1}{N}(C)^{\frac{1}{2}}$ is a mathematical concept used to measure the magnitude or length of a vector in a multi-dimensional space. In the context of error

analysis, the second norm is often applied to the vector of differences between identified and experimental values, providing a measure of the overall magnitude of the error.

By evaluating the relative error and the second norm, we can assess the accuracy and precision of the identified values in comparison to the experimental values. These metrics are commonly used in numerical analysis and optimization to quantify the quality of results and determine the level of agreement between identified and experimental values.

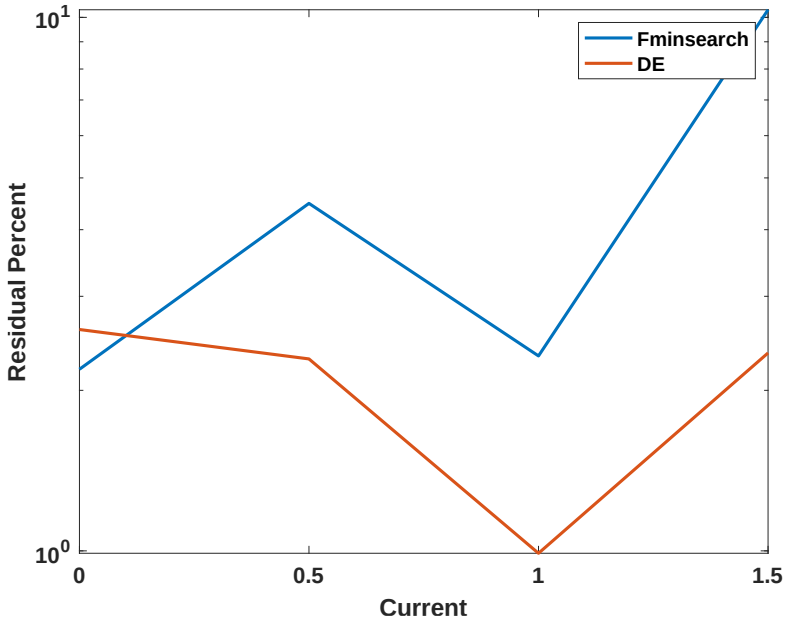

Figure 55 – *Percent of residue for currents of 0A, 0.5A, 1.0A, and 1.5A using Simplex and DE techniques.*

4.9 Sigmoid Model Parameters

The experimental results were approached and optimized using the Nelder-Mead simplex search method and differential evolution algorithm. Table 15 compares the parameters obtained by the two optimization methods; in this particular condition, the variation between the parameters obtained by the two techniques was relatively small; however, this did not occur in all cases; in some cases, the variation between the parameters comparing the two techniques was considerable. The difference in parameters is that while one technique identified the local minimum, the other located the global minimum of the function. To assess the sensitivity of the parameters, they

were subjected to variation rates of (1%, 5%, 10%, 15%, and 20%), it was observed that the physical parameters (I_0, I_1, a_2, a_3) did not change the force f_t when varied. Among the physical parameters, the parameter f_0 is the most sensitive since a minimal variation in it is capable of promoting significant changes in the force f_t.

Table 15 – Comparison of Physical Parameters, for a stroke damper harmonic excitation with 2.5 mm of displacement of 2.5mm to 1Hz.

	2.5 mm	$f_0\ (N)$	$I_0\ (amp)$	$I_1\ (amp)$	a_0	$a_1(m/s)^{-1}$	$a_2(amp)^{-1}$	$a_3(m/s)^{-1}$	$a_4(m/s)^{-1}$
Simplex	**0 A**	25,66	-1,00	0,72	14910	9,82	48,02	0,97	0,77
DE		25,63	-0,90	0,77	14989	9,91	36,98	1,18	0,75
Absolute Error	**1 Hz**	0,03	0,10	0,05	79	0,09	11,04	0,21	0,02

Table 16 presents a comparison between the hysteresis parameters obtained using the two optimization techniques. The parameters (k_2 e k_3) did not provide any change in the force f_t when varied. The parameter $k_{1\mathrm{c}}$ defines the angle, β_{hc} and the parameter $k_{1\mathrm{e}}$ defines the angle β_{he} represented in Fig. 2. The most sensitive hysteresis parameter is k_5, responsible for the vertical translation, that is, the parameter can shift the hysteresis loop upwards or downwards in the vertical direction.

A barplot (Figure *56*) was generated with the parameters obtained using the optimization techniques Nelder-Mead simplex search method and differential evolution (DE) and compared to values available in the literature (Santade 2017). The analysis indicates a significant correlation between the values, highlighting a strong relationship between the parameters.

Table 16 - Comparison of Physical Parameters, for a stroke damper harmonic excitation with 2.5 mm of displacement of 2.5mm to 1Hz.

	2.5 mm	k_0	k_{1c}	k_{1e}	k_2	k_3	k_4	k_5	k_6
Simplex	**0 A**	1573,46	49,24	28,09	276,67	224,04	-0,12	0,31	0,01
DE		1508,36	49,45	28,03	259,12	200,00	-0,12	0,31	0,01
Absolute Error	**1 Hz**	65,1	0,21	0,06	17,55	24,04	0,00	0,00	0,00

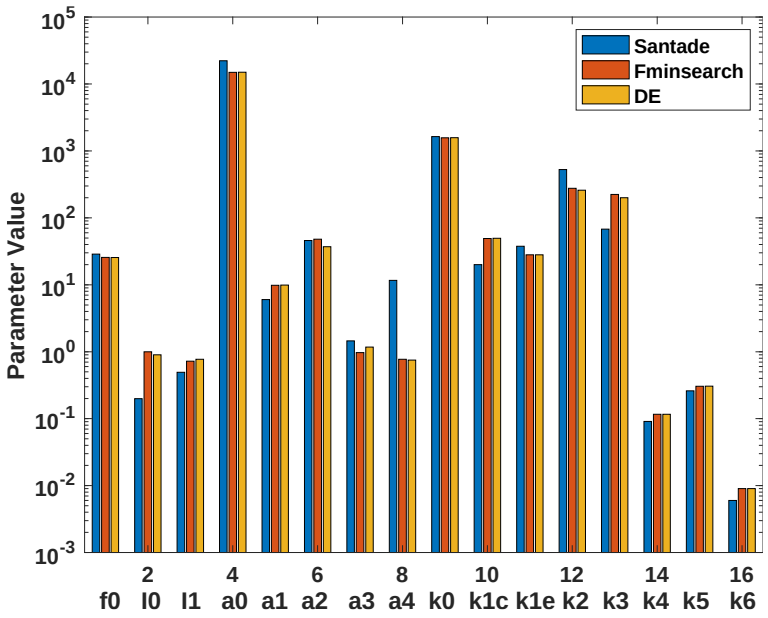

Figure 56 – Comparison of Physical and Hysteresis Parameter, by barplot, obtained by fminsearch and DE optimization algorithm per report to (Santade 2017).

In order to maintain a coherent narrative flow, the tables presenting identified parameters have been included in Appendix B. By relocating them to the appendix, the main text is able to progress smoothly without interruptions, while still providing readers with access to the detailed parameter information in an organized and accessible manner.

Figure 57 illustrates the comparison between parameters obtained using the Nelder-Mead simplex method and DE optimization algorithms. The hysteresis loops corresponding to these parameters are plotted for three different currents: 1.5 A, 1.0 A, and 0.5 A. The purpose of this comparison is to evaluate the effectiveness of both

optimization algorithms in determining the parameters that best describe the hysteresis behavior of the MR damper.

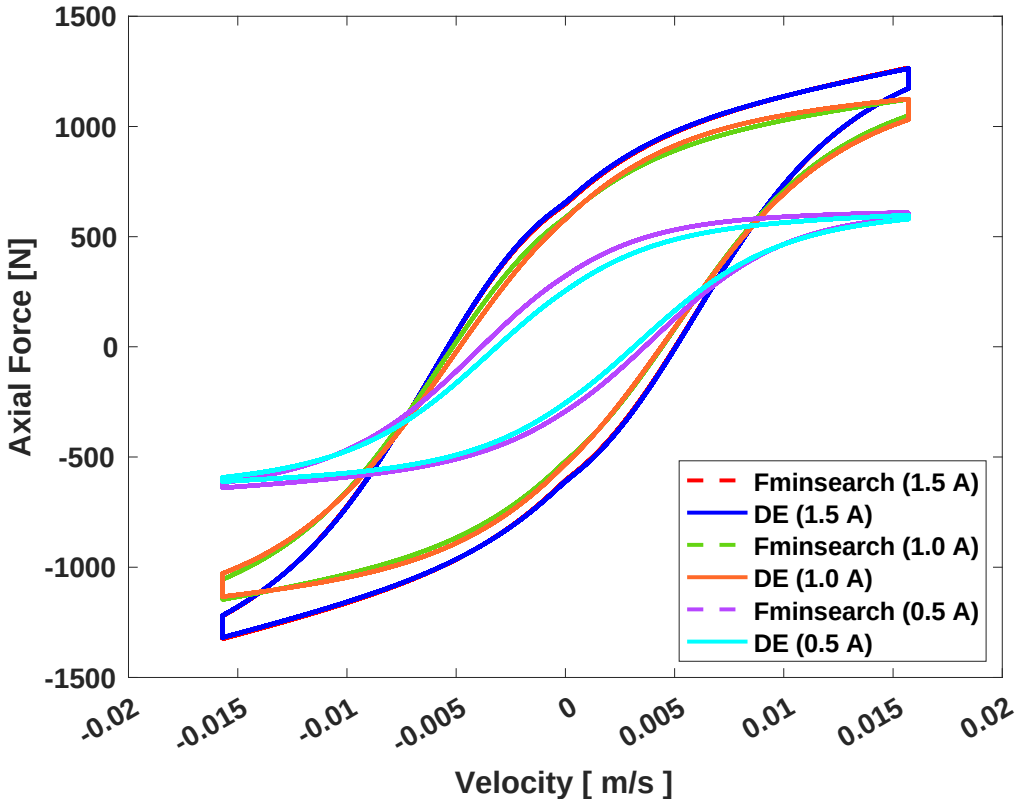

Figure 57 – Comparing Hysteresis Loop between Fminsearch and DE with the current variation of (1.5 A, 1.0 A, and 0.5 A)

Asymmetric characteristics were obtained over a constant current of 0 A (Damper's passive behavior), excitation frequency of (1 to 5 Hz), and displacement amplitude of (2.5mm – 7.5 mm), which are used to identify the model parameters. After optimization, the values of the obtained parameters were organized in Table 17. Under the working condition where the displacement is set to 2.5 mm, and the current is 0 A, the only manipulated variable is the frequency, which ranges from 1 Hz to 5 Hz. This means the displacement remains constant at 2.5 mm throughout the experiments, while the frequency is systematically adjusted. Data related to this experiment, including the physical constants and hysteresis parameters, are described in Table 17 (Appendix B). Table 18 (Appendix B) provides specific details on the hysteresis parameters observed during the tests. By keeping the displacement fixed and varying

only the frequency, researchers can analyze the impact of different frequencies within the 1 Hz to 5 Hz range on the system under this particular working condition.

Under the condition of a constant current of 0.5 A, a series of experiments were conducted to investigate the effects of varying frequencies and displacements. The frequency varied within the range of 1 to 5 Hz, while the displacement ranged from 2.5 mm to 7.5 mm. To gather data, multiple combinations of frequency and displacement were tested. Each combination represented a specific experimental condition. The results obtained from these experiments were recorded and organized in a series of tables, specifically Table 23 to Table 28.

Under the experimental conditions specified in Table 29 to Table 34, the current was fixed at 1 A, while the displacement varied between 2.5 mm and 7.5 mm, and the frequency ranged from 1 Hz to 5 Hz.

Table 35 to Table 40 present results for the working condition where the current is set to 1.5 A, while the displacement is varied between 2.5 mm to 7.5 mm, and the frequency ranges from 1 Hz to 5 Hz. However, it is important to note that certain parameters could not be identified for this specific working condition. During testing, when subjecting the system to maximum damping forces (achieved with an excitation current of 1.5 A) and high frequencies (in this case, 5 Hz), the universal testing machine (MTS) used was unable to maintain the displacement for a sinusoidal signal. Since the sigmoid model used in this study relies on a sinusoidal signal to determine parameters, some of them could not be determined due to this limitation of the machine in maintaining a sinusoidal signal at a frequency of 5 Hz. Therefore, in Table 35 to Table 40, certain parameters need to be identified or reported due to the limitation above in the experimental setup. It is crucial to consider this limitation when analyzing and interpreting the data from these tables for the specified working condition.

Table 23 to Table 40 depicted the parameters identified using the sigmoid model, which was obtained through the variation of both frequency and displacement in the context of the MR damper behavior while concurrently manipulating current. These tables provide crucial insights into the behavior of the MR damper under different operating conditions. The results obtained from these experiments indicate that the parametrized sigmoid model can effectively capture the observed symmetric and

asymmetric behavior exhibited by the MR damper. By analyzing the data presented in these tables, researchers can better understand how the identified parameters relate to the system's response under various combinations of frequency, displacement, and current. Furthermore, the information provided in these tables is valuable for adjusting and validating the parametrized model with experimental values. This allows researchers to refine and improve the model's accuracy, enhancing its ability to predict the behavior of the MR damper under different working conditions.

5 CONCLUSION

An objective function was optimized using the Nelder-Mead simplex search method and differential evolution algorithm to minimize normalized errors between experimental and identified data. The numerically parameterized model, based on the experimental behavior of the MR damper, successfully reproduced its nonlinear dynamic behavior using a sigmoid function. However, achieving an efficient parameter identification of the non-linear hysteretic parametrized sigmoid model was highly dependent on appropriate experimental methods. Initially, experiments using a hexagonal screw caused damage to the internal surface of the MR damper, resulting in clearances and imperfect fitting of the model. A fine-tuned pin was then designed to eliminate the clearances and improve the fit for the sigmoid model.

The F-V curve analysis for the 0A operating condition revealed that the MR damper exhibited an asymmetrical force response. However, the force behavior became symmetrical when a current was applied to the damper. This suggests that the current significantly impacts the MR damper's damping characteristics, influencing its force response.

Consistent with previous research, it was observed that increasing the excitation frequency had minimal effects on the damping force, indicating that the force remained relatively constant. However, the velocity increased dramatically with higher frequencies, suggesting a nonlinear relationship between force and velocity.

The relationship between stroke displacement and the dynamic response of the damper was examined. It was found that increasing the displacement resulted in higher force and velocity values. This highlights the sensitivity of the damper's response to changes in displacement and emphasizes the importance of considering stroke displacement in designing and controlling MR dampers.

The influence of temperature on the damping force was investigated, and it was observed that as the temperature increased to 71°C, the damping force decreased by approximately 26% compared to the baseline condition. This indicates that temperature significantly impacts the performance of MR dampers and should be carefully considered in their applications.

An error analysis was conducted on the experimental data, revealing a normal distribution of errors. This suggests that the errors in the data were random in nature, indicating that the experimental measurements were reliable and consistent.

The Differential Evolution optimization technique was employed to identify the parameters of the MR damper. It was observed that different parameter groups were obtained upon each algorithm initialization, indicating the initialization's influence on the optimization results. Parameters a0 and k2 exhibited the highest variance, suggesting that they have a significant impact on the performance and behavior of the MR damper.

Sensitivity analysis was performed to assess the impact of parameter variations on the system's response. Parameters f0, k5, k1c, and k1e were found to be the most sensitive, indicating that small changes in these parameters can lead to significant variations in the damping force. This highlights the importance of accurately determining and controlling these parameters in designing and optimizing MR dampers.

The identified parametrized sigmoid model using the Nelder-Mead simplex and DE optimization techniques showed a good correlation with each other and with the literature. The optimization process effectively captured the system's behavior and provided accurate parameter estimation, validating the reliability of the identified parameter values.

5.1 Further Works or Recommendations for Further Works

In this section, we outline potential avenues for further research and improvements to expand upon the findings and contributions of this master's dissertation.

a) **Correlation between Identified Parameters:** Explore the correlation between the parameters identified using the sigmoid and dynamic Bouc-Wen models. By comparing and analyzing the parameter values obtained from both models, a better understanding of the relationship between these models can be achieved, potentially leading to improved modeling and control strategies for MR dampers.

b) **Hysteresis Curve Analysis**: Investigate the hysteresis curves of the damping force versus velocity (F-V) for different current levels, specifically at 1A and 1.5A. Although the values were similar, examining the behavior under other proposed experimental conditions is important. This analysis can provide insights into how the current affects the hysteresis behavior of the MR damper, enabling a more comprehensive understanding of its dynamic response.

c) **Long-Term Experimentation:** Conduct long-term experiments to observe the effect of magnetic saturation over an extended period. By subjecting the MR damper to continuous operation, the study can explore the potential impact of magnetic saturation on damping performance and behavior. This investigation will provide valuable insights into the long-term stability and reliability of MR dampers, which is crucial for their practical applications.

REFERENCE LIST

Abdalaziz, Moustafa, Hossein Vatandoost, Ramin Sedaghati, and Subhash Rakheja. 2023. “Design and Experimental Characterization of a Bypass Magnetorheological Damper Featuring Variable Stiffness and Damping.” *Smart Materials and Structures* 32(3):035011. doi: 10.1088/1361-665X/ACB474.

Abdelkareem, Mohamed A. A., Lin Xu, Mohamed Kamal Ahmed Ali, Ahmed Elagouz, Jia Mi, Sijing Guo, Yilun Liu, and Lei Zuo. 2018. “Vibration Energy Harvesting in Automotive Suspension System: A Detailed Review.” *Applied Energy* 229:672–99. doi: 10.1016/J.APENERGY.2018.08.030.

Aboud, Wajdi S., Sallehuddin Mohamed Haris, and Yuzita Yaacob. 2014. “Advances in the Control of Mechatronic Suspension Systems.” *Journal of Zhejiang University: Science C* 15(10):848–60. doi: 10.1631/JZUS.C14A0027/METRICS.

Arnott ®. n.d. “Air Springs, Air Shocks, Air Struts & More | Arnott®.” Retrieved August 21, 2022 (https://www.arnottindustries.com/products?p=2&product_type=721).

Attivissimo, F., A. Cataldo, L. Fabbiano, and N. Giaquinto. 2011. “Systematic Errors and Measurement Uncertainty: An Experimental Approach.” *Measurement* 44(9):1781–89. doi: 10.1016/J.MEASUREMENT.2011.07.011.

Beer, Randall D. 2008. “The Dynamics of Brain-Body-Environment Systems: A Status Report.” *Handbook of Cognitive Science* 99–120. doi: 10.1016/B978-0-08-046616-3.00006-2.

Çeşmeci, Şevki, and Tahsin Engin. 2010. “Modeling and Testing of a Field-Controllable Magnetorheological Fluid Damper.” *International Journal of Mechanical Sciences* 52(8):1036–46. doi: 10.1016/J.IJMECSCI.2010.04.007.

Chen, H., Z. Y. Liu, and P. Y. Sun. 2005. “Application of Constrained H∞ Control to Active Suspension Systems on Half-Car Models.” *Journal of Dynamic Systems, Measurement, and Control* 127(3):345–54. doi: 10.1115/1.1985442.

Chen, Xiaoliang, Liyou Xu, Shuai Zhang, Sixia Zhao, and Kui Liu. 2022. “Parameter Identification of the Bouc-Wen Model for the Magnetorheological Damper Using Fireworks Algorithm.” *Journal of Mechanical Science and Technology* 36(5):2213–24. doi: 10.1007/S12206-022-0405-2/METRICS.

Chevrolet ®. 2023. “Novo Camaro 2023 - Carro Esportivo 0km | Chevrolet Brasil.” Retrieved May 26, 2023 (https://www.chevrolet.com.br/esportivos/novo-camaro?ppc=GOOGLE_700000001717310_71700000101066709_587000080772538 97_p73448073016&&&gclid=CjwKCAjw1MajBhAcEiwAagW9MVHu3SB9HjPETIdHP3G_iCv9jNwJkwwfnlmLg9MYzvaCTP3lJkjB4xoCyAsQAvD_BwE&gclsrc=aw.ds).

Coelho. 2012. “Fundamentos, Potencialidades e Aplicações de Algoritmos Evolutivos | Galoá Proceedings.” Retrieved May 26, 2023 (https://proceedings.science/series/23/proceedings_non_indexed/8).

Deng, Huaxia, Jialei Deng, Rui Yue, al -, Moustafa Abdalaziz, Hossein Vatandoost, Ramin Sedaghati, and Subhash Rakheja. 2023. “Design and Experimental Characterization of a Bypass Magnetorheological Damper Featuring Variable Stiffness and Damping.” *Smart Materials and Structures* 32(3):035011. doi: 10.1088/1361-665X/ACB474.

Deng, Zhijun, Bo Shi, Dongping Wei, al -, Kelsey B. Hatzell, Jens Eller, Yury Gogotsi, Tianyu Tang, Shujing Sha, Chenhao Pan, and Hang Li. 2023. “Sliding Mode

Control of Vehicle Semi-Active Suspension System Based on Magnetorheological Damper." *Journal of Physics: Conference Series* 2459(1):012085. doi: 10.1088/1742-6596/2459/1/012085.

Desai, Rangaraj Madhavrao, Mohibb E. Hussain Jamadar, Hemantha Kumar, Sharnappa Joladarashi, S. C. Rajasekaran, and G. Amarnath. 2019. "Evaluation of a Commercial MR Damper for Application in Semi-Active Suspension." *SN Applied Sciences* 1(9):1–10. doi: 10.1007/S42452-019-1026-Y/FIGURES/12.

Dixon, John C. 2007. "The Shock Absorber Handbook: Second Edition." *The Shock Absorber Handbook: Second Edition* 1–415. doi: 10.1002/9780470516430.

Du, Xiu Mei, Miao Yu, Jie Fu, You Xiang Peng, Hui Feng Shi, and Hua Zhang. 2018. "H∞ Control for a Semi-Active Scissors Linkage Seat Suspension with Magnetorheological Damper:" *Https://Doi.Org/10.1177/1045389X18778340* 30(5):708–21. doi: 10.1177/1045389X18778340.

Eslaminasab, Nima. n.d. "Development of a Semi-Active Intelligent Suspension System for Heavy Vehicles."

Ferrari ®. n.d. "Line up: The Ferrari Official Car Range 2022." Retrieved August 21, 2022 (https://www.ferrari.com/en-EN/auto/car-range).

Fischer, Daniel, and Rolf Isermann. 2004. "Mechatronic Semi-Active and Active Vehicle Suspensions." *Control Engineering Practice* 12(11):1353–67. doi: 10.1016/J.CONENGPRAC.2003.08.003.

Ford ®. n.d. "2022 Ford Mustang Sports Car | Handling Features." Retrieved August 21, 2022 (https://www.ford.com/cars/mustang/features/handling/).

Fu, Bin, Rocco Libero Giossi, Rickard Persson, Sebastian Stichel, Stefano Bruni, and Roger Goodall. 2020. "Active Suspension in Railway Vehicles: A Literature Survey." *Railway Engineering Science 2020 28:1* 28(1):3–35. doi: 10.1007/S40534-020-00207-W.

Gavin, H. P., R. D. Hanson, and F. E. Filisko. 1996. "Electrorheological Dampers, Part I: Analysis and Design." *Journal of Applied Mechanics* 63(3):669–75. doi: 10.1115/1.2823348.

Glaser, Radek, Vincent Caccese, Mohsen Shahinpoor, D. H. Wang, W. H. Liao, Mohammad Meftahul Ferdaus, M. M. Rashid, and M. I. Bhuiyan. 2016. "Magneto-Rheological Defects and Failures: A Review." *IOP Conference Series: Materials Science and Engineering* 114(1):012101. doi: 10.1088/1757-899X/114/1/012101.

Goodarzi, Avesta, and Amir Khajepour. 2017. "Vehicle Suspension System Technology and Design." *Vehicle Suspension System Technology and Design*. doi: 10.1007/978-3-031-01494-9.

Guo, Shuqi, Shaopu Yang, and Cunzhi Pan. 2016. "Dynamic Modeling of Magnetorheological Damper Behaviors:" *Http://Dx.Doi.Org/10.1177/1045389X06055860* 17(1):3–14. doi: 10.1177/1045389X06055860.

Gysen, B L J, Bart L J Gysen, Johannes J. H. Paulides, Jeroen L. G. Janssen, and Elena A. Lomonova. 2010. "Active Electromagnetic Suspension System for Improved Vehicle Dynamics." *IEEE Transactions on Vehicular Technology* 59(3):1156–63. doi: 10.1109/TVT.2009.2038706.

Hamby, D. M. 1994. "A Review of Techniques for Parameter Sensitivity Analysis of Environmental Models." *Environmental Monitoring and Assessment* 32(2):135–54. doi: 10.1007/BF00547132/METRICS.

Huang, Yanqiu, Jingjing Pei, Peter V. Nielsen, Francis Bonthoux, Sullivan Lechene, Francois xavier Keller, Songheng Wu, Chunwen Xu, and Zhixiang Cao. 2021. "Experimental Techniques." *Industrial Ventilation Design Guidebook: Volume 2: Engineering Design and Applications, Second Edition* 185–277. doi: 10.1016/B978-0-12-816673-4.00004-3.

Hyniova, Katerina, Antonin Stribrsky, Jaroslav Honcu, and Ales Kruczek. 2009. "Active Suspension System –Energy Control." *IFAC Proceedings Volumes* 42(19):146–52. doi: 10.3182/20090921-3-TR-3005.00027.

Issa, Mohamed, and Anas Samn. 2022. "Passive Vehicle Suspension System Optimization Using Harris Hawk Optimization Algorithm." *Mathematics and Computers in Simulation* 191:328–45. doi: 10.1016/J.MATCOM.2021.08.016.

Jin, Tianhe, Zhiming Liu, Shuaishuai Sun, Zunsong Ren, Lei Deng, Bo Yang, Matthew Daniel Christie, and Weihua Li. 2020a. "Development and Evaluation of a Versatile Semi-Active Suspension System for High-Speed Railway Vehicles." *Mechanical Systems and Signal Processing* 135. doi: 10.1016/J.YMSSP.2019.106338.

Jin, Tianhe, Zhiming Liu, Shuaishuai Sun, Zunsong Ren, Lei Deng, Bo Yang, Matthew Daniel Christie, and Weihua Li. 2020b. "Development and Evaluation of a Versatile Semi-Active Suspension System for High-Speed Railway Vehicles." *Mechanical Systems and Signal Processing* 135:106338. doi: 10.1016/J.YMSSP.2019.106338.

Joshua Robert, J., P. Senthil Kumar, S. Tushar Nair, D. H. Sharne Moni, and B. Swarneswar. 2022. "Fuzzy Control of Active Suspension System Based on Quarter Car Model." *Materials Today: Proceedings* 66:902–8. doi: 10.1016/J.MATPR.2022.04.575.

Kanarachos, Stratis, Dzmitry Savitski, Nikos Lagaros, and Michael E. Fitzpatrick. 2018. "Automotive Magnetorheological Dampers: Modelling and Parameter Identification Using Contrast-Based Fruit Fly Optimisation." *Soft Computing* 22(24):8131–49. doi: 10.1007/S00500-017-2757-6.

Karkoub, Mansour A., and Mohamed Zribi. 2007. "Active/Semi-Active Suspension Control Using Magnetorheological Actuators." *Http://Dx.Doi.Org/10.1080/00207720500436344* 37(1):35–44. doi: 10.1080/00207720500436344.

Kim, Hyung Tae, An Mok Jeong, Hyo Young Kim, Jong Wook An, Cheol Ho Kim, Kyung Chan Jin, and Seung Bok Choi. 2018. "Lateral Vibration Control of a Precise Machine Using Magneto-Rheological Mounts Featuring Multiple Directional Damping Effect." *Smart Materials and Structures* 27(3):037001. doi: 10.1088/1361-665X/AAAD9E.

Krauze, Piotr. 2013. "Comparison of Control Strategies in a Semi-Active Suspension System of the Experimental ATV:" *Http://Dx.Doi.Org/10.1260/0263-0923.32.1-2.67* 32(1–2):67–80. doi: 10.1260/0263-0923.32.1-2.67.

Kumar, James Sathya, P. Sam Paul, Girish Raghunathan, and Divin George Alex. 2019. "A Review of Challenges and Solutions in the Preparation and Use of Magnetorheological Fluids." *International Journal of Mechanical and Materials Engineering* 14(1):1–18. doi: 10.1186/S40712-019-0109-2/FIGURES/5.

Kumar, Jitender, and Gian Bhushan. 2022. "Improvement in Ride Comfort and Vehicle Stability Using Hybrid Semi-Active Suspension System." *Journal of The Institution*

of Engineers (India): Series C 103(5):1133–42. doi: 10.1007/S40032-022-00855-3/FIGURES/21.

Lagarias, Jeffrey C., James A. Reeds, Margaret H. Wright, and Paul E. Wright. 2006. "Convergence Properties of the Nelder--Mead Simplex Method in Low Dimensions." *Https://Doi.Org/10.1137/S1052623496303470* 9(1):112–47. doi: 10.1137/S1052623496303470.

Lamborghini ®. n.d. "Lamborghini Aventador S | Lamborghini.Com." Retrieved August 21, 2022 (https://www.lamborghini.com/en-en/history/aventador-s).

Land Rover ®. n.d. "Land Rover 4x4 Cars and Luxury SUV British Design | Land Rover MENA." Retrieved August 21, 2022 (https://www.landrover-me.com/en/index.html).

Latunde, Tolulope, and Olabode Matthias Bamigbola. 2018. "Parameter Estimation and Sensitivity Analysis of an Optimal Control Model for Capital Asset Management." *Advances in Fuzzy Systems* 2018. doi: 10.1155/2018/4756520.

Li, Guojie, and Ze Biao Yang. 2020. "Modelling and Analysis of a Magnetorheological Damper with Nonmagnetized Passages in Piston and Minor Losses." *Shock and Vibration* 2020. doi: 10.1155/2020/2052140.

Li, W. H., G. Z. Yao, G. Chen, S. H. Yeo, and F. F. Yap. 2000. "Testing and Steady State Modeling of a Linear MR Damper under Sinusoidal Loading." *Smart Materials and Structures* 9(1):95. doi: 10.1088/0964-1726/9/1/310.

Liao, Yingying, Yongqiang Liu, and Shaopu Yang. 2019. "Semiactive Control of High-Speed Railway Vehicle Suspension Systems with Magnetorheological Dampers." *Shock and Vibration* 2019. doi: 10.1155/2019/5279380.

Liu, Hui, Hongbin Gu, and Dawei Chen. 2008. "Application of High-Speed Solenoid Valve to the Semi-Active Control of Landing Gear." *Chinese Journal of Aeronautics* 21(3):232–40. doi: 10.1016/S1000-9361(08)60030-8.

Liu, Rong, and Qiu Sheng Liu. 2014. "Non-Modal Stability in Hagen-Poiseuille Flow of a Bingham Fluid." *Physics of Fluids* 26(1):014102. doi: 10.1063/1.4861025.

Liu, Xiaoyuan, Roger Goodall, and Simon Iwnicki. 2020. "A Direct Control Approach for Automatic Steering and Stability of Motorized Independently-Rotating Wheels." *Lecture Notes in Mechanical Engineering* 24–30. doi: 10.1007/978-3-030-38077-9_3/COVER.

Lobato, Fran Sérgio. 2008. "Otimização Multi-Objetivo Para o Projeto de Sistemas de Engenharia."

LORD ®. n.d. "How Does an MR Damper Work? | LORD Corp." Retrieved August 19, 2022 (https://www.lord.com/products-and-solutions/active-vibration-control/industrial-suspension-systems/how-does-mr-damper-work).

Lord Corporation. 2023. "LORD Corporation, RD 8041-1 Damper." Retrieved April 11, 2023 (http://www.lordfulfillment.com/upload/DS7016.pdf).

Lu, Hongwei, Zhongming Xu, Kaizhan Gao, Zhifei Zhang, Zhi Li, and Jujiang Xie. 2020. "A New Invertible Model of Magnetorheological Damper Based on Sigmoid Function." *Smart Materials and Structures* 29(11):115026. doi: 10.1088/1361-665X/ABB0A1.

Marcu, Sorin, Dinel Popa, Nicolae Doru Stănescu, and Nicolae Pandrea. 2017. "Model for the Study of Active Suspensions." *IOP Conference Series: Materials Science and Engineering* 252(1):012032. doi: 10.1088/1757-899X/252/1/012032.

Mitra, Anirban C., G. R. Kiranchand, Tanushri Soni, and Nilotpal Banerjee. 2016. "Design of Experiments for Optimization of Automotive Suspension System Using

Quarter Car Test Rig." *Procedia Engineering* 144:1102–9. doi: 10.1016/J.PROENG.2016.05.071.

Mohajer Rahbari, N., B. Farahmand Azar, S. Talatahari, and H. Safari. 2013. "Semi-Active Direct Control Method for Seismic Alleviation of Structures Using MR Dampers." *Structural Control and Health Monitoring* 20(6):1021–42. doi: 10.1002/STC.1515.

Murata, Satoshi. 2011. "Vehicle Dynamics Innovation with In-Wheel Motor." *SAE International*.

Muthalif, Asan GA, Banna Kasemi, and Mahbub Rashid. 2017. "Semi-Active Vibration Control Using Experimental Model of Magnetorheological Damper with Adaptive F-PID Controller Rovision; Robotic Navigation Aid for Visually Impaired People Using FLC-ORCA View Project Wireless Power Transfer Using Conical and Spiral Coils View Project." *Smart Structures and Systems* 20(1):85–97. doi: 10.12989/sss.2017.20.1.085.

Narayan, S., Ali Sulaiman Alsagri, and Vipul Gupta. 2019. "The Design and Analysis of Hybrid Automotive Suspension System." *International Journal of Mechanical and Production Engineering Research and Development* 9(4):637–42. doi: 10.24247/IJMPERDAUG201963.

Negash, Birhan Abebaw, Wonhee You, Jinho Lee, and Kwansup Lee. 2020. "Parameter Identification of Bouc-Wen Model for Magnetorheological (MR) Fluid Damper by a Novel Genetic Algorithm." *Advances in Mechanical Engineering* 12(8). doi: 10.1177/1687814020950546.

Nguyen, Duc Ngoc, and Tuan Anh Nguyen. 2023. "The Dynamic Model and Control Algorithm for the Active Suspension System." *Mathematical Problems in Engineering* 2023:1–9. doi: 10.1155/2023/2889435.

Oh, Jong Seok, and Seung Bok Choi. 2019. "Ride Quality Control of a Full Vehicle Suspension System Featuring Magnetorheological Dampers with Multiple Orifice Holes." *Frontiers in Materials* 6. doi: 10.3389/FMATS.2019.00008.

Omar, Mahmoud, M. M. El-kassaby, and Walid Abdelghaffar. 2017. "A Universal Suspension Test Rig for Electrohydraulic Active and Passive Automotive Suspension System." *Alexandria Engineering Journal* 56(4):359–70. doi: 10.1016/J.AEJ.2017.01.024.

Riazi, Behnam. 2021. "Scholarship at UWindsor Scholarship at UWindsor Electronic Theses and Dissertations Theses, Dissertations, and Major Papers Design and Investigation of a Semi-Active Suspension System in Design and Investigation of a Semi-Active Suspension System in Automotive Applications Automotive Applications."

Rosli, Rosmazi, and Zamri Mohamed. 2020. "Optimization of Modified Bouc–Wen Model for Magnetorheological Damper Using Modified Cuckoo Search Algorithm:" *Https://Doi.Org/10.1177/1077546320951383* 27(17–18):1956–67. doi: 10.1177/1077546320951383.

Santade. 2017. "Análise Dinâmica de Amortecedores Não Lineares Assimétricos, Com Histerese e Sujeitos a Folga e Avaliação Do Efeito Temperatura." Retrieved October 4, 2022 (https://repositorio.unesp.br/handle/11449/151680).

Sassi, Sadok, Abdelmonaam Sassi, Khaled Cherif, and Faris Tarlochan. 2018. "Magnetorheological Damper with External Excitation for More Efficient Control of Vehicles' Dynamics:" *Https://Doi.Org/10.1177/1045389X18781038* 29(14):2919–32. doi: 10.1177/1045389X18781038.

Savaresi, Sergio, Charles Poussot-Vassal, Cristiano Spelta, Olivier Sename, and Luc Dugard. 2010. “Semi-Active Suspension Control Design for Vehicles.” *Semi-Active Suspension Control Design for Vehicles*. doi: 10.1016/C2009-0-63839-3.

Senator ®. n.d. “HSV / Senator Signature.” Retrieved August 21, 2022 (https://www.hsv.com.au/see/senatorsignature/).

Silva et al. 2023. “Parameter Identification of Bouc-Wen Model for MR Damper.” *Proceedings of the XIX International Symposium on Dynamic Problems of Mechanics*. doi: 10.26678/ABCM.DINAME2023.DIN2023-0119.

Soliman, A. M. A., and M. M. S. Kaldas. 2019. “Semi-Active Suspension Systems from Research to Mass-Market – A Review:” *Https://Doi.Org/10.1177/1461348419876392* 40(2):1005–23. doi: 10.1177/1461348419876392.

Soliman, A. M. A., and M. M. S. Kaldas. 2021. “Semi-Active Suspension Systems from Research to Mass-Market – A Review.” *Journal of Low Frequency Noise Vibration and Active Control* 40(2):1005–23. doi: 10.1177/1461348419876392/FORMAT/EPUB.

Spaggiari, A., D. Castagnetti, N. Golinelli, E. Dragoni, and G. Scirè Mammano. 2019. “Smart Materials: Properties, Design and Mechatronic Applications.” *Proceedings of the Institution of Mechanical Engineers, Part L: Journal of Materials: Design and Applications* 233(4):734–62. doi: 10.1177/1464420716673671.

SpencerJr., B. F., S. J. Dyke, M. K. Sain, and J. D. Carlson. 1997. “Phenomenological Model for Magnetorheological Dampers.” *Journal of Engineering Mechanics* 123(3):230–38. doi: 10.1061/(ASCE)0733-9399(1997)123:3(230).

Storn, Rainer, and Kenneth Price. 1997a. “Differential Evolution - A Simple and Efficient Heuristic for Global Optimization over Continuous Spaces.” *Journal of Global Optimization* 11(4):341–59. doi: 10.1023/A:1008202821328/METRICS.

Storn, Rainer, and Kenneth Price. 1997b. “Differential Evolution - A Simple and Efficient Heuristic for Global Optimization over Continuous Spaces.” *Journal of Global Optimization* 11(4):341–59. doi: 10.1023/A:1008202821328/METRICS.

Stribrsky, Antonin, Katerina Hyniova, Jaroslav Honcu, and Ales Kruczek. 2007. “Energy Recuperation in Automotive Active Suspension Systems with Linear Electric Motor.” *2007 Mediterranean Conference on Control and Automation, MED*. doi: 10.1109/MED.2007.4433870.

Talatahari, Siamak, and Nima Mohajer Rahbari. 2015. “Enriched Imperialist Competitive Algorithm for System Identification of Magneto-Rheological Dampers.” *Mechanical Systems and Signal Processing* 62–63:506–16. doi: 10.1016/J.YMSSP.2015.03.020.

Tanifuji, Katsuya, Satoshi Koizumi, and R. H. Shimamune. 2002. “Mechatronics in Japanese Rail Vehicles: Active and Semi-Active Suspensions.” *Control Engineering Practice* 10(9):999–1004. doi: 10.1016/S0967-0661(01)00165-4.

Theunissen, Johan, Antonio Tota, Patrick Gruber, Miguel Dhaens, and Aldo Sorniotti. 2021a. “Preview-Based Techniques for Vehicle Suspension Control: A State-of-the-Art Review.” *Annual Reviews in Control* 51:206–35. doi: 10.1016/J.ARCONTROL.2021.03.010.

Theunissen, Johan, Antonio Tota, Patrick Gruber, Miguel Dhaens, and Aldo Sorniotti. 2021b. “Preview-Based Techniques for Vehicle Suspension Control: A State-of-the-Art Review.” *Annual Reviews in Control* 51:206–35. doi: 10.1016/J.ARCONTROL.2021.03.010.

Tsioptsias, Naoum, Antuela Tako, and Stewart Robinson. 2016. “Model Validation and Testing in Simulation: A Literature Review.” doi: 10.4230/OASIcs.SCOR.2016.6.
Turnip, Arjon, Keum-Shik Hong, and Seonghun Park. 2008. “Control of a Semi-Active MR-Damper Suspension System: A New Polynomial Model.” *IFAC Proceedings Volumes* 41(2):4683–88. doi: 10.3182/20080706-5-KR-1001.00788.
Viana, Felipe Antonio Chegury. 2008. “Surrogate Modeling Techniques and Heuristic Optimization Methods Applied to Design and Identification Problems.”
Vikhar, Pradnya A. 2017. “Evolutionary Algorithms: A Critical Review and Its Future Prospects.” *Proceedings - International Conference on Global Trends in Signal Processing, Information Computing and Communication, ICGTSPICC 2016* 261–65. doi: 10.1109/ICGTSPICC.2016.7955308.
Vivas-Lopez, Carlos A., Diana Hernández-Alcantara, Ruben Morales-Menendez, Ricardo A. Ramírez-Mendoza, and Horacio Ahuett-Garza. 2015. “Method for Modeling Electrorheological Dampers Using Its Dynamic Characteristics.” *Mathematical Problems in Engineering* 2015. doi: 10.1155/2015/905731.
Wang, D. H., and W. H. Liao. 2011. “Magnetorheological Fluid Dampers: A Review of Parametric Modelling.” *Smart Materials and Structures* 20(2):023001. doi: 10.1088/0964-1726/20/2/023001.
Wang, Mingxiang, Hui Pang, Jibo Luo, and Minhao Liu. 2023. “On an Enhanced Back Propagation Neural Network Control of Vehicle Semi-Active Suspension with a Magnetorheological Damper.” *Transactions of the Institute of Measurement and Control* 45(3):512–23. doi: 10.1177/01423312221118224/ASSET/IMAGES/LARGE/10.1177_01423312221118224-FIG14.JPEG.
Wang, Yu, Shihpin Lin, Hiroshi Tajima, and Yoshihiro Suda. 2020. “Assessment of Curve Passing Performance and Active Steering Control of Railway Vehicle with Independently Rotating Wheels Using Negative Tread Conicity.” *Lecture Notes in Mechanical Engineering* 785–92. doi: 10.1007/978-3-030-38077-9_91/COVER.
Wang, Zhirui, Alex Radin, and Campbell Laird. 1989. “Influence of Frequency on the Actual Testing Load of Hydraulic Mechanical Testing Machines.” *Journal of Testing and Evaluation* 17(3):167–71. doi: 10.1520/JTE11107J.
Wang1, En Rong, Xiao Qing Ma2, S. Rakhela2, and C. Y. Su2. 2003. “Modelling the Hysteretic Characteristics of a Magnetorheological Uid Damper.”
Yaakub, S. F., S. H. Yahaya, F. Ahmad, M. S. Salleh, and A. R. M. Warikh. 2020. “A Comprehensive Review on the Related Models in Magneto-Rheological Automobile Suspension System.” *International Journal of Engineering Research and Technology* 13(7):1700–1708. doi: 10.37624/IJERT/13.7.2020.1700-1708.
Yamin, Ahmad Hafizal Mohd, Mat Hussin Ab Talib, Intan Zaurah Mat Darus, and Nur Safwati Mohd Nor. 2022. “MAGNETO-RHEOLOGICAL (MR) DAMPER – PARAMETRIC MODELLING AND EXPERIMENTAL VALIDATION FOR LORD RD 8040-1.” *Jurnal Teknologi* 84(2):27–34. doi: 10.11113/JURNALTEKNOLOGI.V84.16611.
Yang, Shaopu, Yiwei Zhao, Yongqiang Liu, Yingying Liao, and Peng Wang. 2022. “A New Semi-Active Control Strategy on Lateral Suspension Systems of High-Speed Trains and Its Application in HIL Test Rig.” *Https://Doi.Org/10.1080/00423114.2022.2081221* 61(5):1317–44. doi: 10.1080/00423114.2022.2081221.

Yang, Yang, Zhao Dong Xu, Yan Wei Xu, and Ying Qing Guo. 2020. “Analysis on Influence of the Magnetorheological Fluid Microstructure on the Mechanical Properties of Magnetorheological Dampers.” *Smart Materials and Structures* 29(11):115025. doi: 10.1088/1361-665X/ABADD2.

Yao, G. Z., F. F. Yap, G. Chen, W. H. Li, and S. H. Yeo. 2002. “MR Damper and Its Application for Semi-Active Control of Vehicle Suspension System.” *Mechatronics* 12(7):963–73. doi: 10.1016/S0957-4158(01)00032-0.

Zhang, Shuguang, Wenku Shi, and Zhiyong Chen. 2021. “Modeling and Parameter Identification of MR Damper Considering Excitation Characteristics and Current.” *Shock and Vibration* 2021. doi: 10.1155/2021/6691650.

Zhao, Junjie, Pengfei Liu, Dingxin Leng, Haoyu Zhan, Guangrui Luan, Donghong Ning, and Jianqiang Yu. 2023. “Prescribed Performance Control-Based Semi-Active Vibration Controller for Seat Suspension Equipped with an Electromagnetic Damper.” *Vibration 2023, Vol. 6, Pages 303-318* 6(1):303–18. doi: 10.3390/VIBRATION6010019.

MR DAMPER SUPPORT TECHNICAL DRAWING

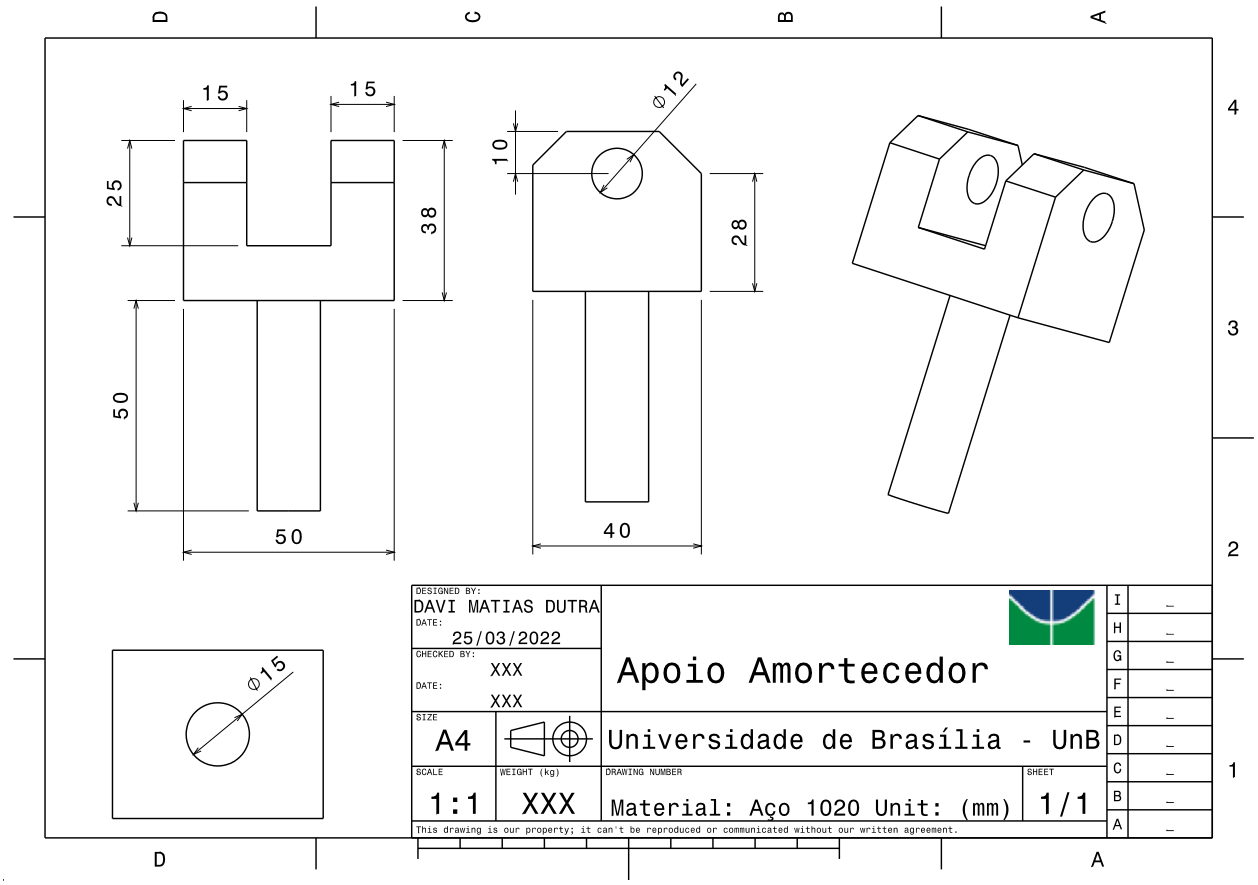

Figure 58 - MR Damper Support Technical Drawing

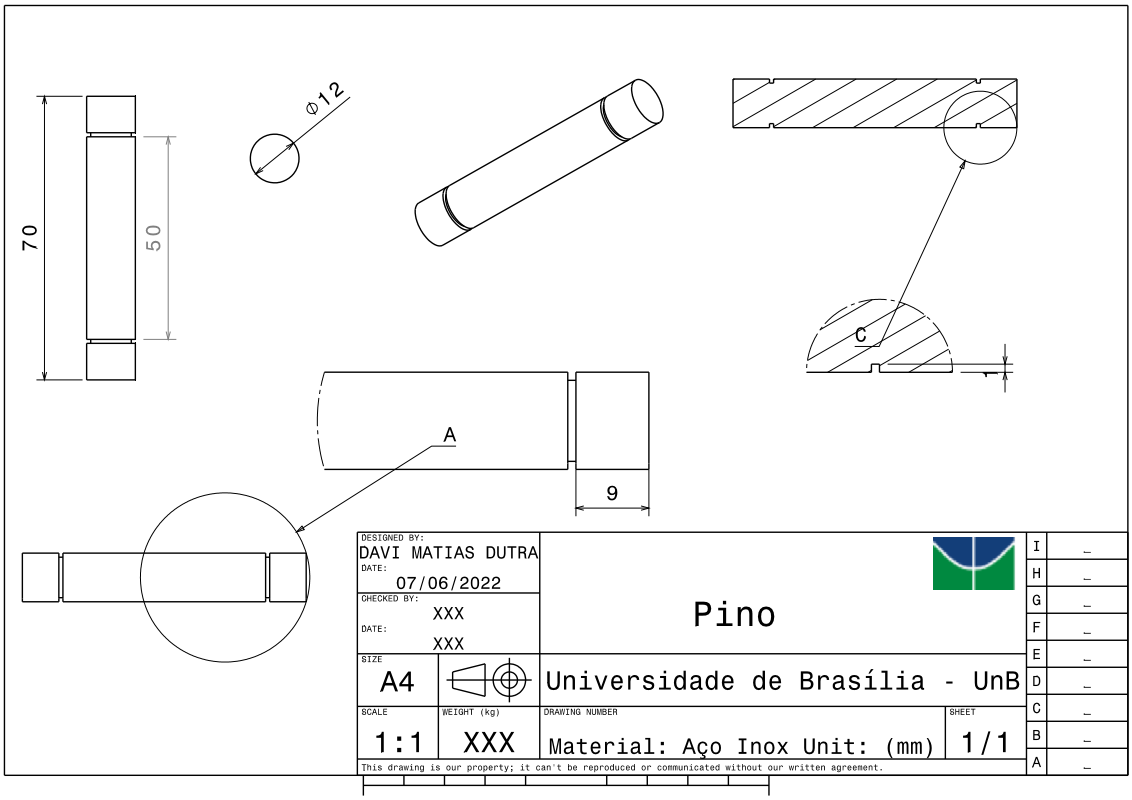

Figure *59* - MR Damper Pin Support Technical Drawing

EXPERIMENTAL RESULTS FITTING

For instance, for the simulation case presented here (identified result) compared with experimental points, understanding and analysis of the effect of increasing the excitation frequency are important in designing and implementing the semi-active suspension system. Figure 60 to Figure 61 present the nonlinear behavior of the MR damper behaving as a passive damper, i.e., without excitation current. Increasing the frequency, it can be seen that the force and velocity reach higher values.

Figure 60 to Figure 67 present the nonlinear behavior of the MR damper behaving as a passive damper, i.e., without excitation current. Increasing the frequency, it also can be seen that the force and velocity reach higher values. When comparing the displacement increase, it is possible to conclude that the compressive damping force has been shifted to higher values.

Figure 68 to Figure 75 present the nonlinear behavior of the MR damper behaving as a semi-active damper, with 0.5 A of excitation current. Increasing the frequency, it also can be seen that the force and velocity reach higher values. When comparing the displacement increase, it is possible to conclude that the compressive damping force has been shifted to higher values.

Figure 76 to Figure 83 present the nonlinear behavior of the MR damper behaving as a semi-active damper, with 1.0 A of excitation current. Increasing the frequency, it also can be seen that the force and velocity reach higher values. When comparing the displacement increase, it is possible to conclude that the compressive damping force has been shifted to higher values.

Figure 84 to Figure 90 presents the nonlinear behavior of the MR damper behaving as a semi-active damper, with 1.5 A of excitation current. Increasing the frequency, it also can be seen that the force and velocity reach higher values. When comparing the displacement increase, it is possible to conclude that the compressive damping force has been shifted to higher values.

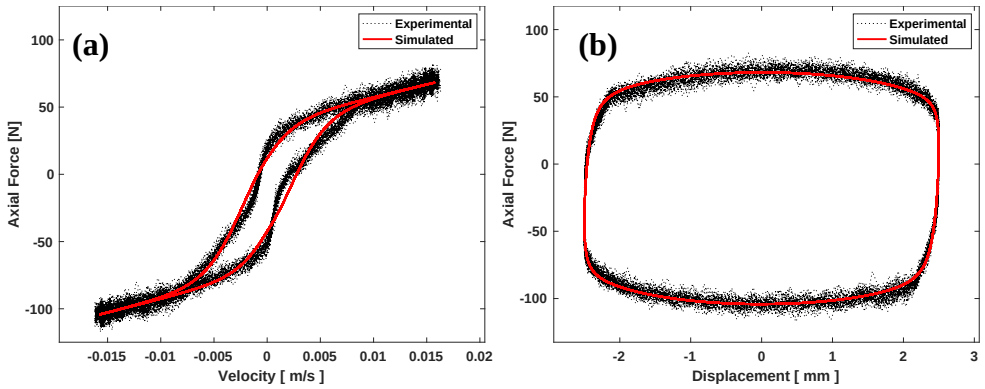

Figure 60 - (a) Force vs Displacement (2.5 mm) (b) Force vs Velocity [Current (0 A), and Excitation Frequency 1 Hz]

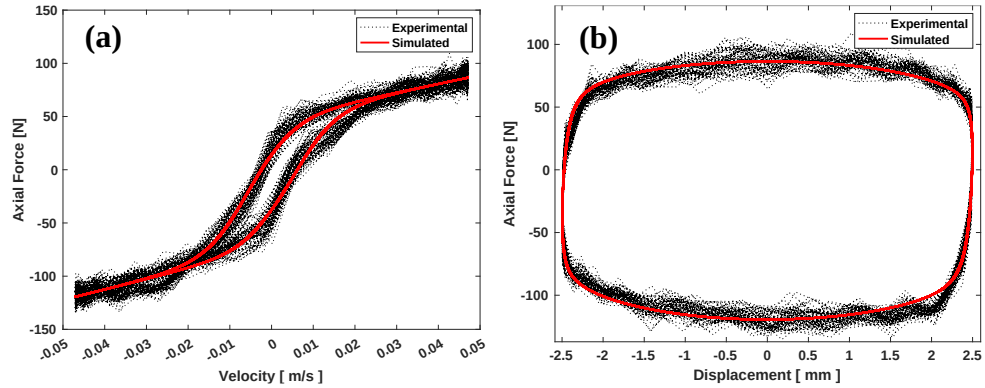

Figure 61 - (a) Force vs Displacement (2.5 mm) (b) Force vs Velocity Current (0 A), and Excitation Frequency 3 Hz

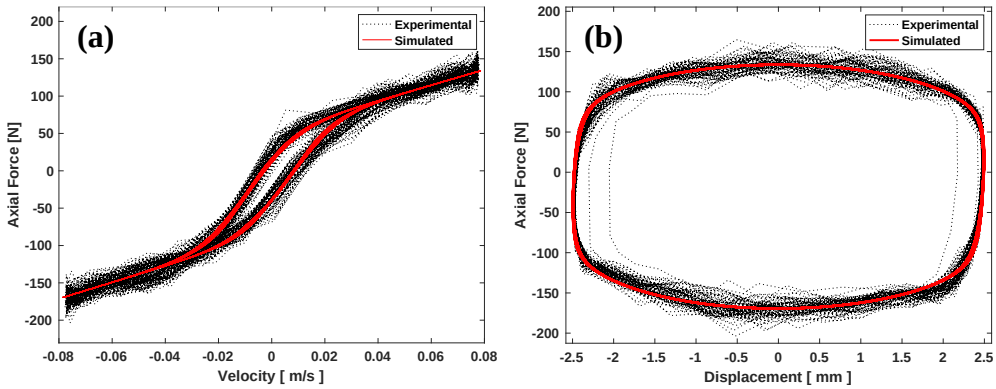

Figure 62 - (a) Force vs Displacement (2.5 mm) (b) Force vs Velocity [Current (0 A), and Excitation Frequency 5 Hz]

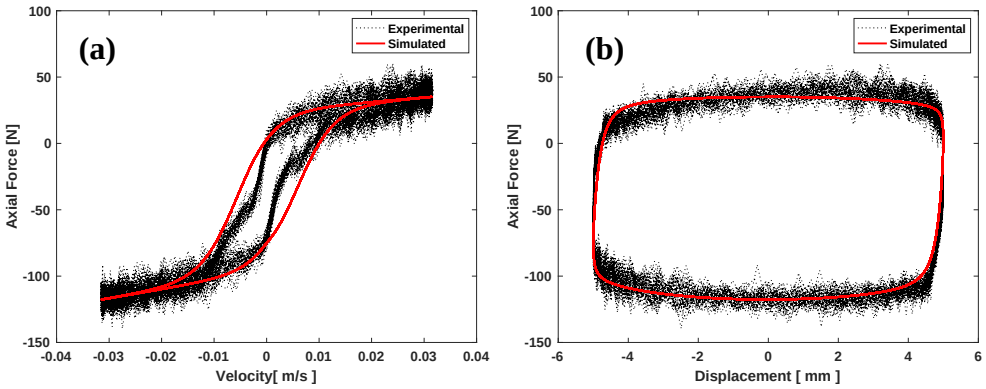

Figure 63 - (a) Force vs Displacement (5.0 mm) (b) Force vs Velocity [Current (0 A), and Excitation Frequency 1 Hz]

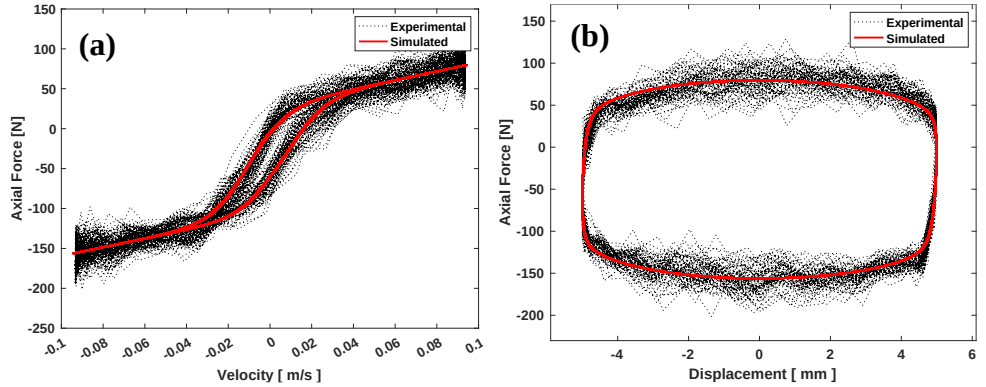

Figure 64 - *(a) Force vs Displacement (5.0 mm) (b) Force vs Velocity [Current (0 A), and Excitation Frequency 3 Hz]*

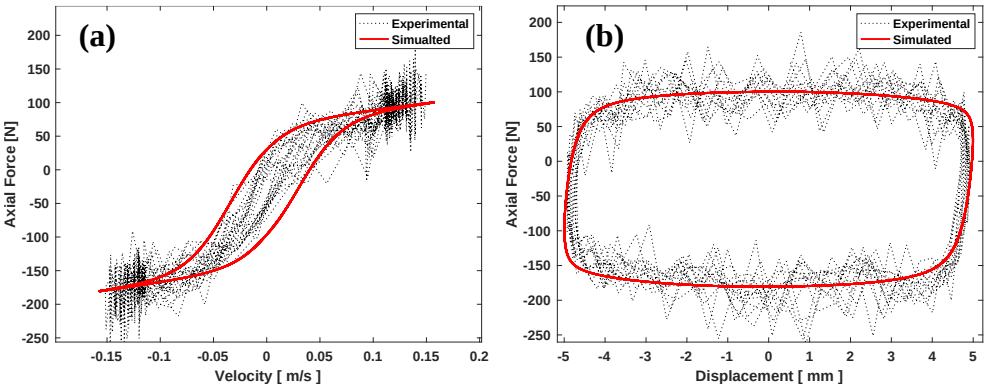

Figure 65 - (a) Force vs Displacement (5.0 mm) (b) Force vs Velocity [Current (0 A), and Excitation Frequency 5 Hz]

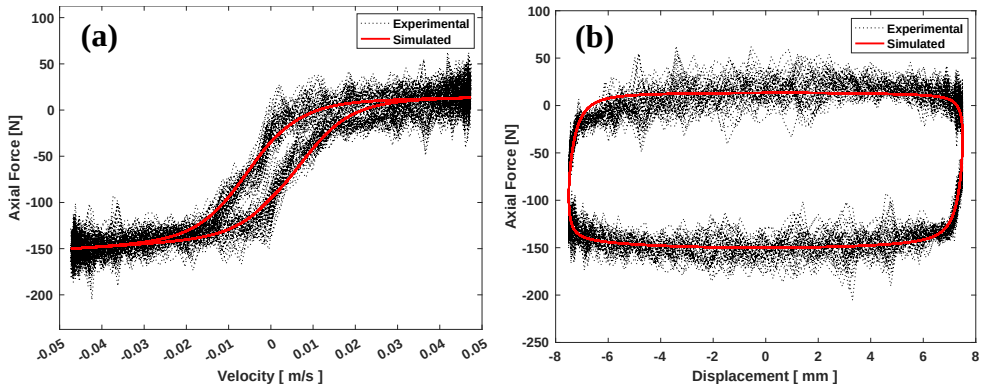

Figure 66 - (a) Force vs Displacement (7.5 mm) (b) Force vs Velocity [Current (0 A), and Excitation Frequency 1 Hz]

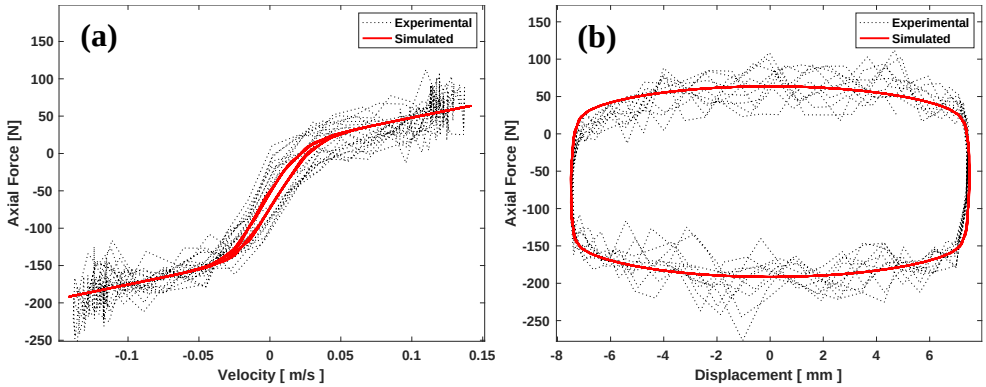

Figure 67 - (a) Force vs Displacement (7.5 mm) (b) Force vs Velocity [Current (0 A), and Excitation Frequency 3 Hz]

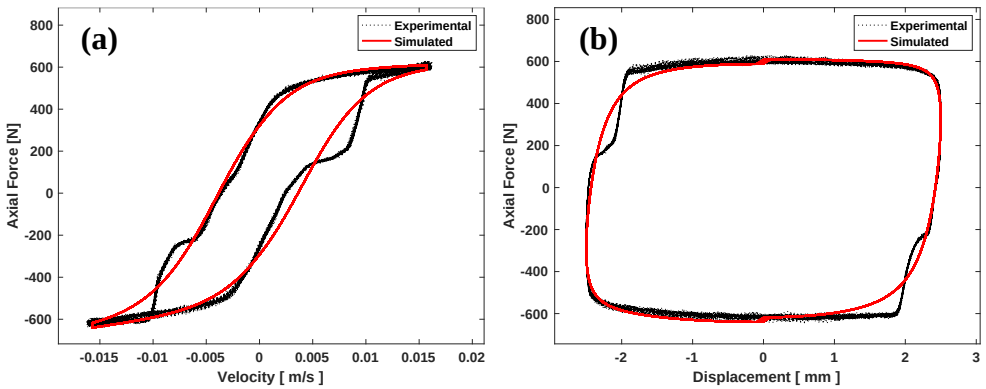

Figure 68 - (a) Force vs Displacement (2.5 mm) (b) Force vs Velocity [Current (0.5 A), and Excitation Frequency 1 Hz]

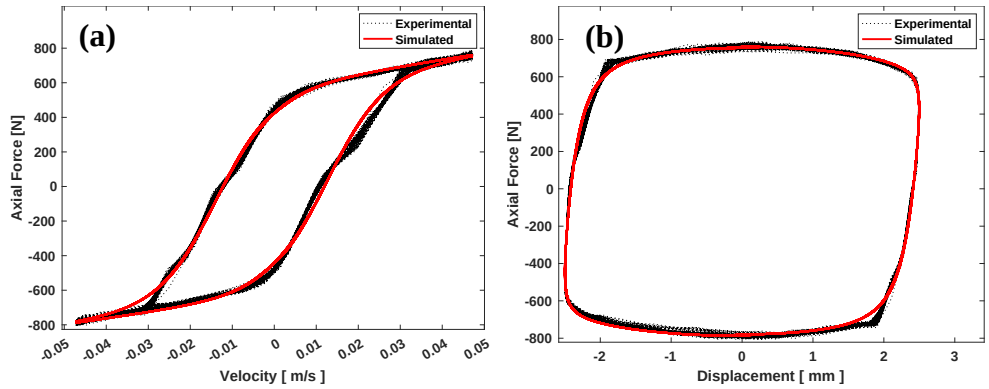

Figure 69 - (a) Force vs Displacement (2.5 mm) (b) Force vs Velocity [Current (0.5 A), and Excitation Frequency 3 Hz]

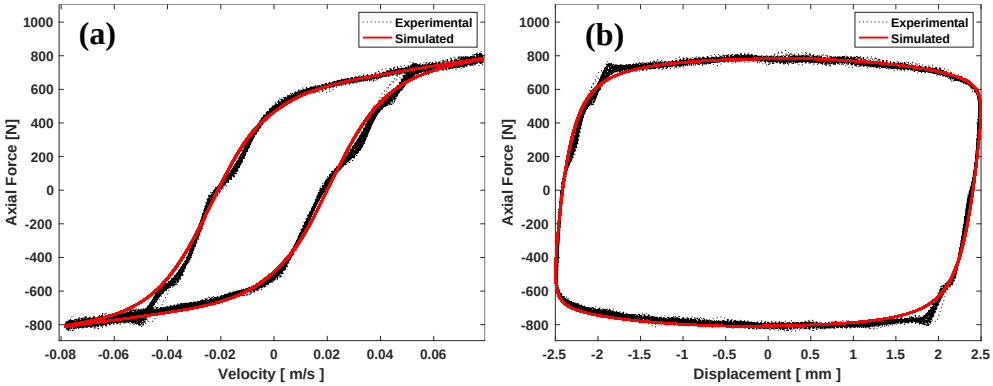

Figure 70 - (a) Force vs Displacement (2.5 mm) (b) Force vs Velocity [Current (0.5 A), and Excitation Frequency 5 Hz]

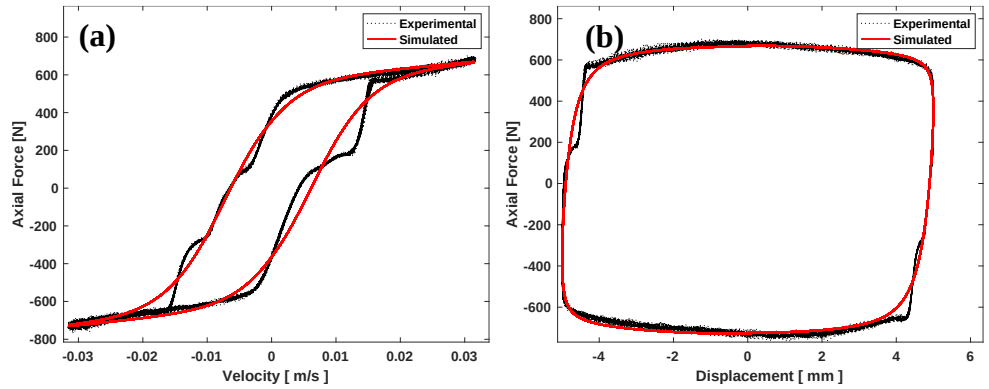

Figure 71 - (a) Force vs Displacement (5.0 mm) (b) Force vs Velocity [Current (0.5 A), and Excitation Frequency 1 Hz]

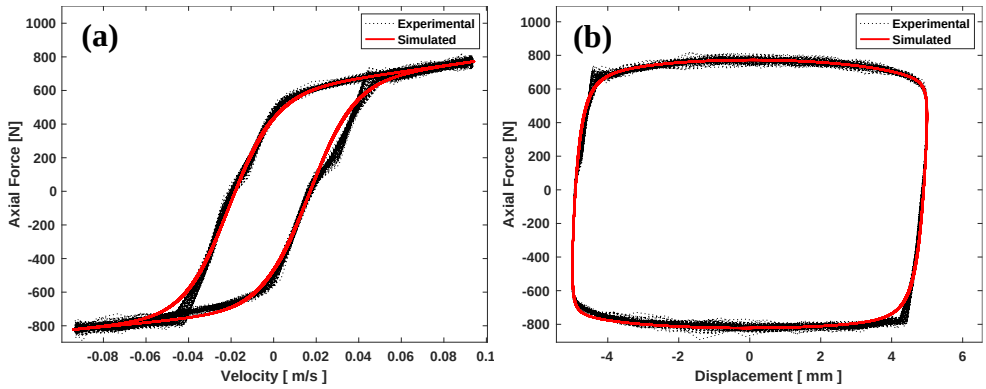

Figure 72 - (a) Force vs Displacement (5.0 mm) (b) Force vs Velocity [Current (0.5 A), and Excitation Frequency 3 Hz]

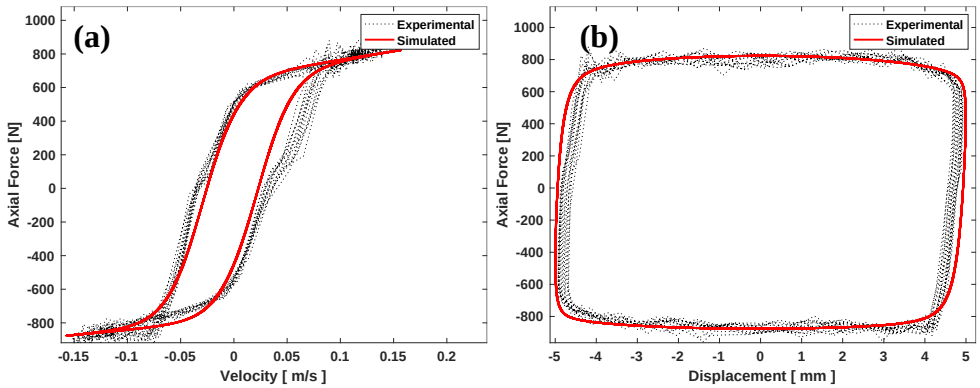

Figure 73 - (a) Force vs Displacement (5.0 mm) (b) Force vs Velocity [Current (0.5 A), and Excitation Frequency 5 Hz]

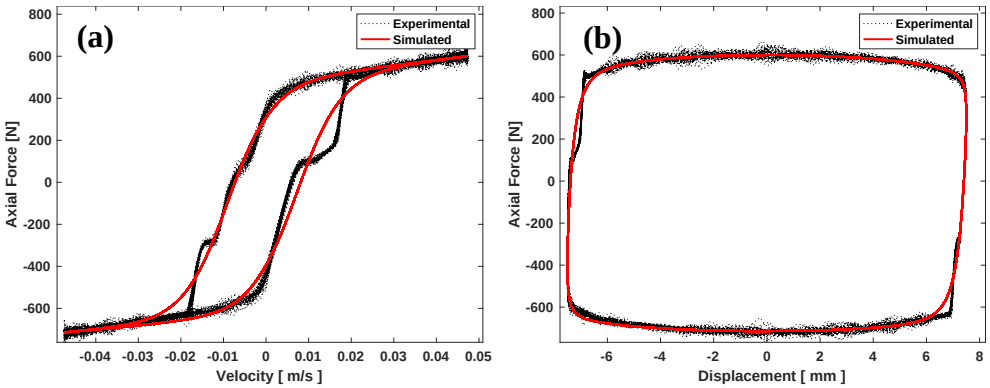

Figure 74 - (a) Force vs Displacement (7.5 mm) (b) Force vs Velocity [Current (0.5 A), and Excitation Frequency 1 Hz]

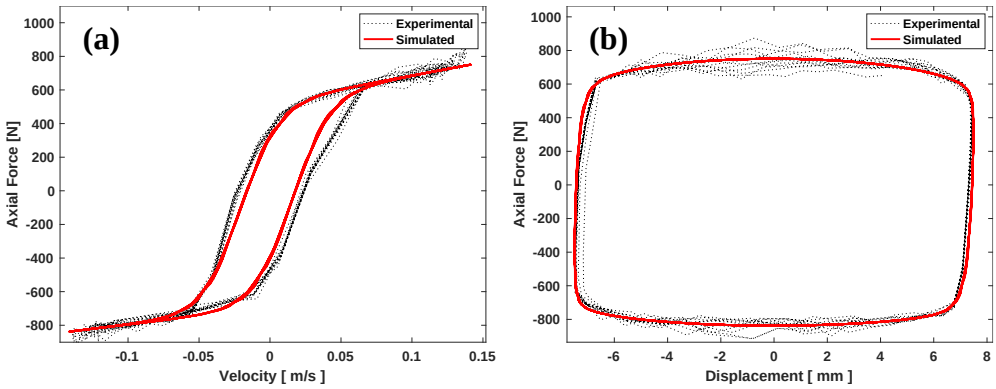

Figure 75 - (a) Force vs Displacement (7.5 mm) (b) Force vs Velocity [Current (0.5 A), and Excitation Frequency 3 Hz]

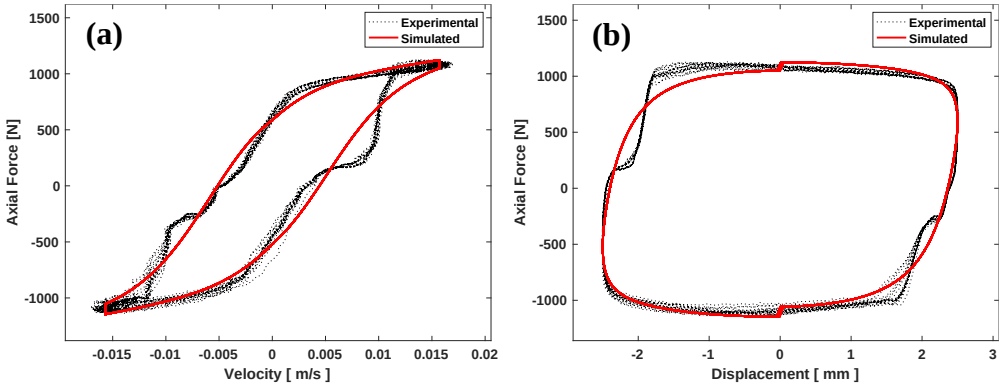

Figure 76 - (a) Force vs Displacement (2.5 mm) (b) Force vs Velocity [Current (1.0 A), and Excitation Frequency 1 Hz]

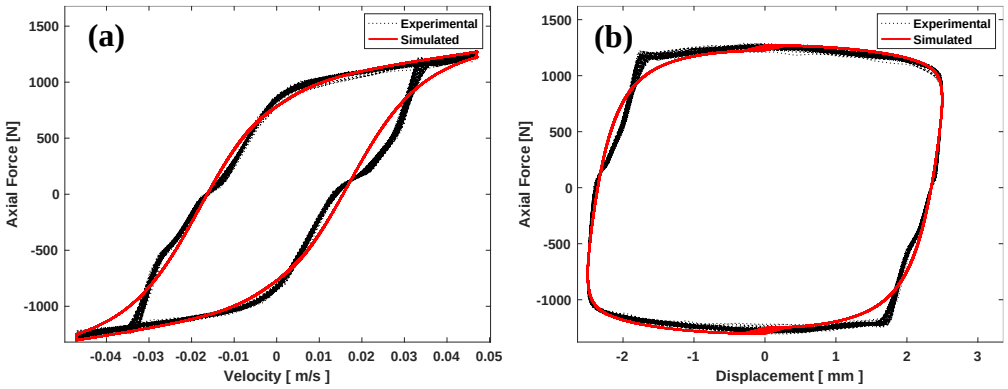

Figure 77 - (a) Force vs Displacement (2.5 mm) (b) Force vs Velocity [Current (1.0 A), and Excitation Frequency 3 Hz]

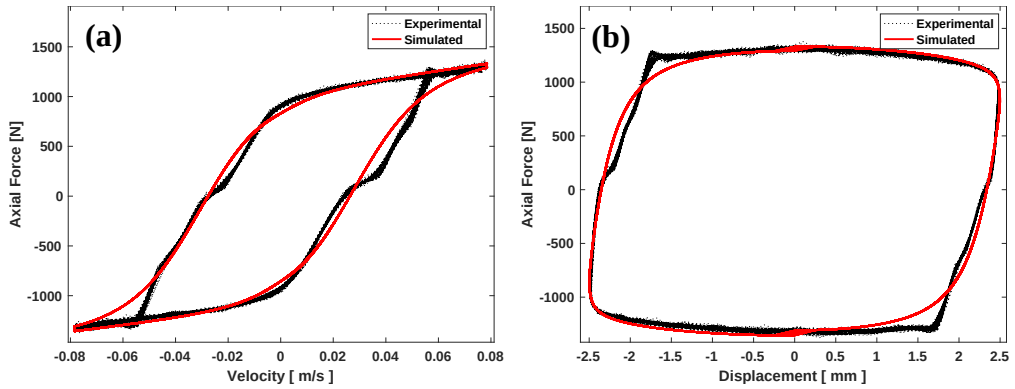

Figure 78 - (a) Force vs Displacement (2.5 mm) (b) Force vs Velocity [Current (1.0 A), and Excitation Frequency 5 Hz]

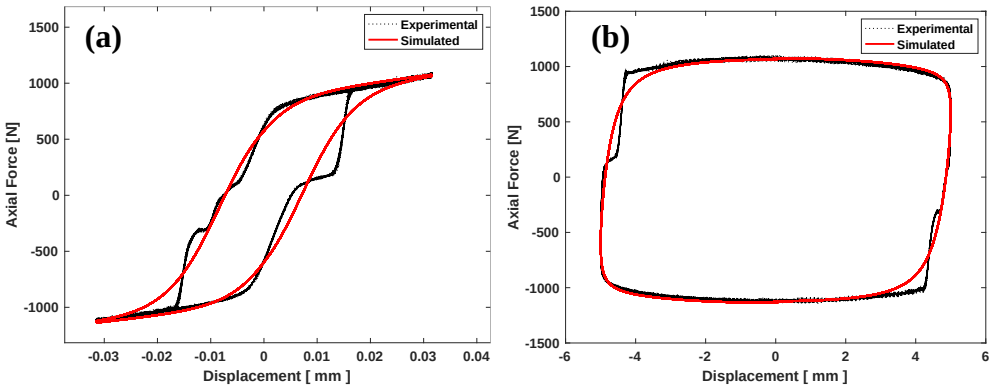

Figure 79 - (a) Force vs Displacement (5.0 mm) (b) Force vs Velocity [Current (1.0 A), and Excitation Frequency 1 Hz]

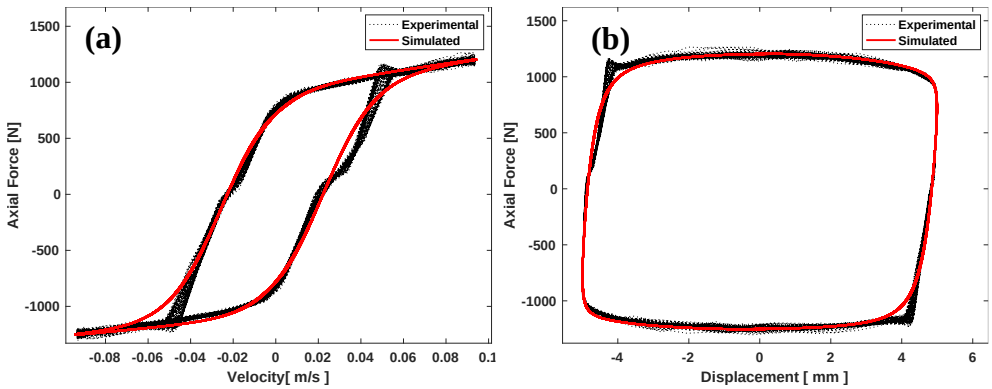

Figure 80 - (a) Force vs Displacement (5.0 mm) (b) Force vs Velocity [Current (1.0 A), and Excitation Frequency 3 Hz]

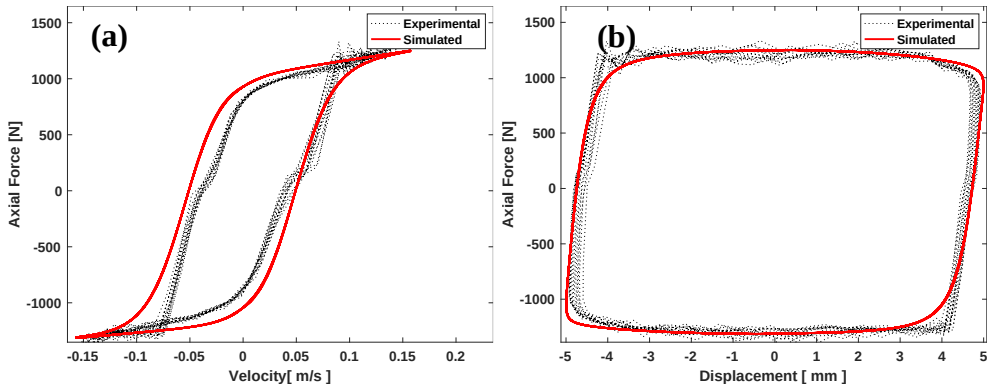

Figure 81 - (a) Force vs Displacement (5.0 mm) (b) Force vs Velocity [Current (1.0 A), and Excitation Frequency 5 Hz]

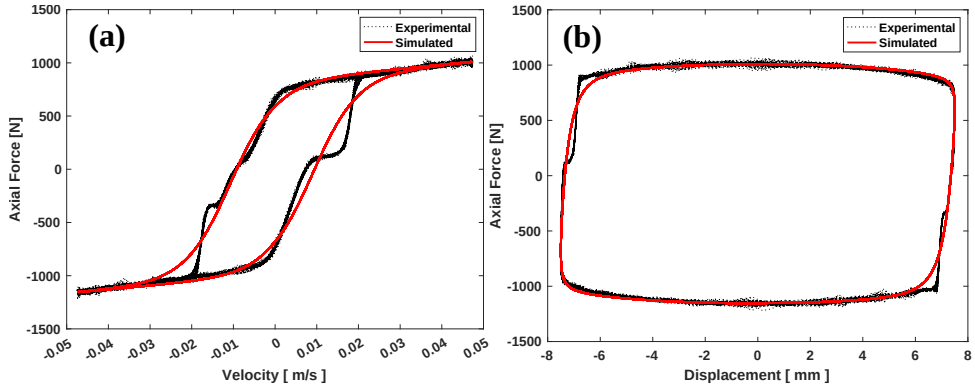

Figure 82 - *(a) Force vs Displacement (7.5 mm) (b) Force vs Velocity* [Current (1.0 A), and Excitation Frequency 1 Hz]

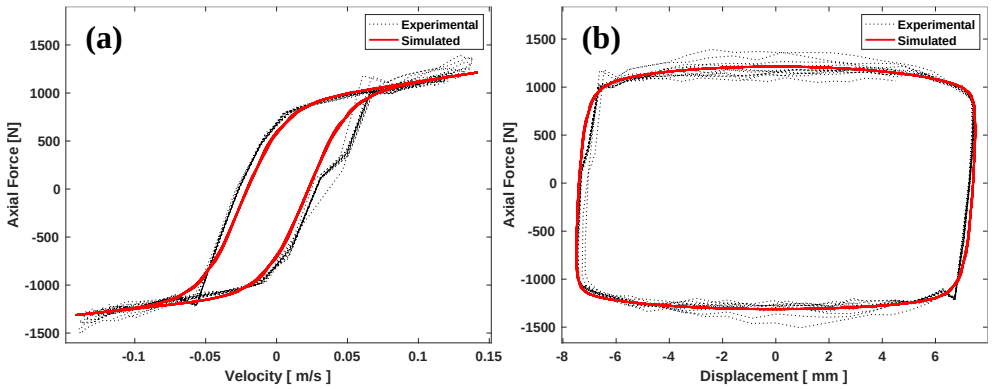

Figure 83 - *(a) Force vs Displacement (7.5 mm) (b) Force vs Velocity* [Current (1.0 A), and Excitation Frequency 3 Hz]

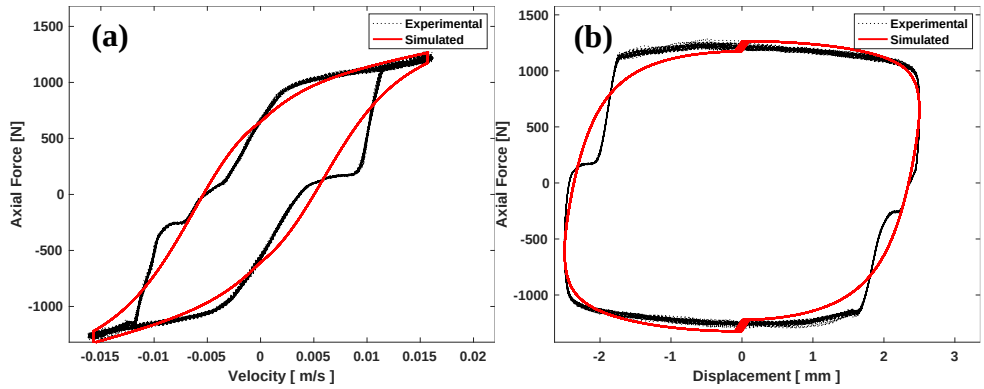

Figure 84 - (a) Force vs Displacement (2.5 mm) (b) Force vs Velocity [Current (1.5 A), and Excitation Frequency 1 Hz]

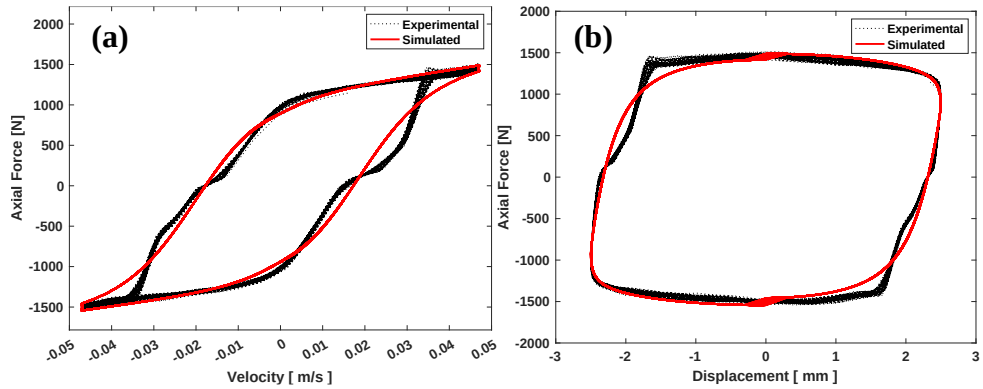

Figure 85 - (a) Force vs Displacement (2.5 mm) (b) Force vs Velocity [Current (1.5 A), and Excitation Frequency 3 Hz]

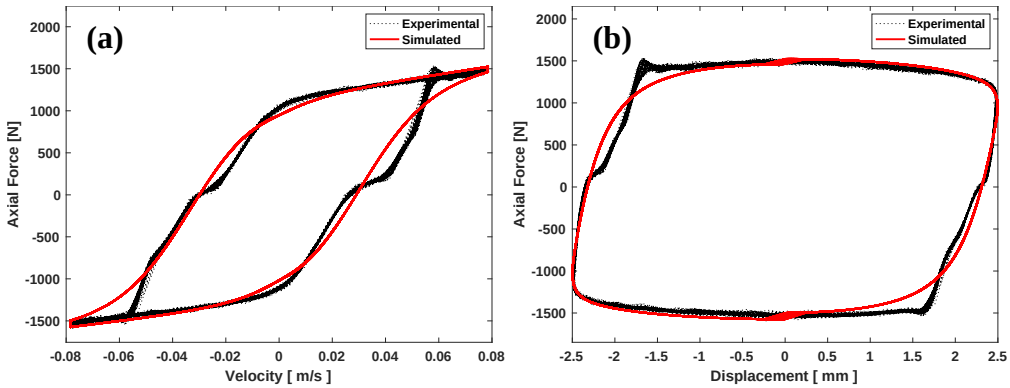

Figure 86 - (a) Force vs Displacement (2.5 mm) (b) Force vs Velocity [Current (1.5 A), and Excitation Frequency 5 Hz]

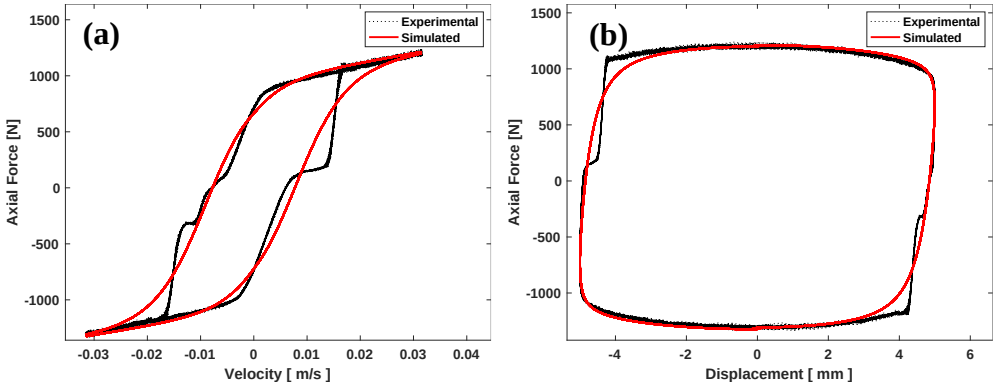

Figure 87 - (a) Force vs Displacement (5.0 mm) (b) Force vs Velocity [Current (1.5 A), and Excitation Frequency 1 Hz]

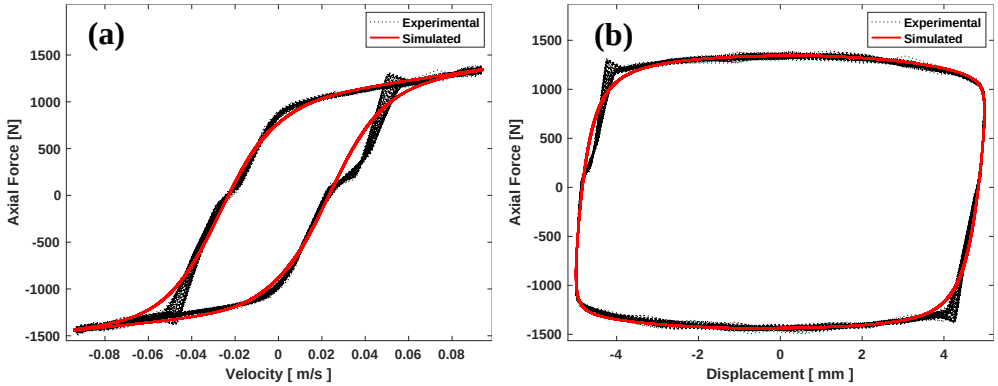

Figure 88 - (a) Force vs Displacement (5.0 mm) (b) Force vs Velocity [Current (1.5 A), and Excitation Frequency 3 Hz]

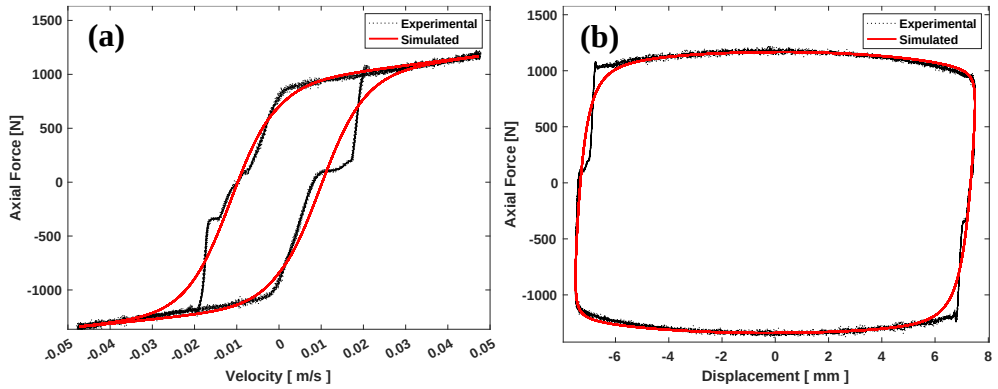

Figure 89 - (a) Force vs Displacement (7.5 mm) (b) Force vs Velocity [Current (1.5 A), and Excitation Frequency 1 Hz]

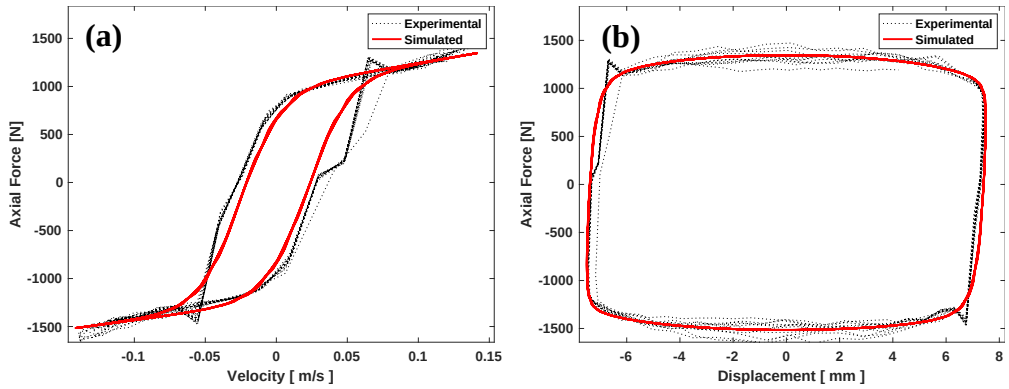

Figure 90 - (a) Force vs Displacement (7.5 mm) (b) Force vs Velocity [Current (1.5 A), and Excitation Frequency 3 Hz]

IDENTIFIED PARAMETERS

Table 17 - *Physical Constants (Displacement 2.5 mm and 0 A)*

	2.5 mm	$f_0\ (N)$	$I_0\ (amp)$	$I_1\ (amp)$	a_0	$a_1(m/s)^{-1}$	$a_2(amp)^{-1}$	$a_3(m/s)^{-1}$	$a_4(m/s)^{-1}$
fmisearch	**0 A**	25,6619	-0,9991	0,7249	14910,6454	9,8158	48,0249	0,9731	0,7677
DE	**1 Hz**	25,6345	-0,8972	0,7714	14989,5266	9,9074	36,9818	1,1754	0,751
Absolute Error		**0,027**	**0,102**	**0,047**	**78,881**	**0,092**	**11,043**	**0,202**	**0,017**

	2.5 mm	$f_0\ (N)$	$I_0\ (amp)$	$I_1\ (amp)$	a_0	$a_1(m/s)^{-1}$	$a_2(amp)^{-1}$	$a_3(m/s)^{-1}$	$a_4(m/s)^{-1}$
fmisearch	**0 A**	3,3953	0,5086	0,2722	-347,4239	60,0024	0,00008	1,0343	2,5304
DE	**3 Hz**	3,392	0,4936	0,2513	-347,4698	60	0	1	2,7283
Absolute Error		**0,003**	**0,015**	**0,021**	**0,046**	**0,002**	**0,000**	**0,034**	**0,198**

	2.5 mm	$f_0\ (N)$	$I_0\ (amp)$	$I_1\ (amp)$	a_0	$a_1(m/s)^{-1}$	$a_2(amp)^{-1}$	$a_3(m/s)^{-1}$	$a_4(m/s)^{-1}$
fmisearch	**0 A**	2,3721	-0,1681	0,3336	-401,8866	42,3131	0,0065	2,5193	0,1756
DE	**5 Hz**	4,7491	0,4917	0,1616	-350	52,3218	0	-0,5	0,0463
Absolute Error		**2,377**	**0,660**	**0,172**	**51,887**	**10,009**	**0,007**	**3,019**	**0,129**

Table 18 - *Hysteresis Parameters (Displacement 2.5 mm and 0 A)*

	2.5 mm	k_0	k_{1c}	k_{1e}	k_2	k_3	k_4	k_5	k_6
fmisearch	**0 A**	1573,4645	49,2355	28,0918	276,6692	224,0376	-0,1164	0,3051	0,0093
DE	**1 Hz**	1508,359	49,454	28,0276	259,1192	200	-0,1164	0,3062	0,0097
Absolute Error		**65,106**	**0,218**	**0,064**	**17,550**	**24,038**	**0,000**	**0,001**	**0,000**

	2.5 mm	k_0	k_{1c}	k_{1e}	k_2	k_3	k_4	k_5	k_6
fmisearch	**0 A**	-55,9593	19,1875	14,8895	0,00092	-6,453	-0,0928	0,2106	0,0049
DE	**3 Hz**	-55,8583	19,548	14,9938	0	-7,0449	-0,0895	0,2128	0,0055
Absolute Error		**0,101**	**0,360**	**0,104**	**0,001**	**0,592**	**0,003**	**0,002**	**0,001**

	2.5 mm	k_0	k_{1c}	k_{1e}	k_2	k_3	k_4	k_5	k_6
fmisearch	**0 A**	-47,2822	20,0135	13,1864	-0,003	16,4732	-0,0777	0,2302	0,0118
DE	**5 Hz**	-56,1618	17,1619	13,3585	21,6745	-2,9774	-0,0894	0,2098	0,0043
Absolute Error		**8,880**	**2,852**	**0,172**	**21,678**	**19,451**	**0,012**	**0,020**	**0,008**

Table 19 - *Physical Constants (Displacement 5.0 mm and 0 A)*

	5.0 mm	$f_0\ (N)$	$I_0\ (amp)$	$I_1\ (amp)$	a_0	$a_1(m/s)^{-1}$	$a_2(amp)^{-1}$	$a_3(m/s)^{-1}$	$a_4(m/s)^{-1}$
fmisearch	**0 A**	29,6255	0,6455	0,1814	-920,6681	1,1534	30,2999	-3,0912	5,3455
DE		29,9595	0,5	0,2049	-901,7662	1,2484	24,3987	-3,4362	6,2339
Absolute Error	**1 Hz**	**0,334**	**0,146**	**0,024**	**18,902**	**0,095**	**5,901**	**0,345**	**0,888**

	5.0 mm	$f_0\ (N)$	$I_0\ (amp)$	$I_1\ (amp)$	a_0	$a_1(m/s)^{-1}$	$a_2(amp)^{-1}$	$a_3(m/s)^{-1}$	$a_4(m/s)^{-1}$
fmisearch	**0 A**	10,6497	0,1089	0,4123	-478,8665	17,5909	0,0249	-6,0363	-0,0167
DE		11,1337	0,079	-1,2207	-261,6497	18,891	-1,8743	4,6889	0
Absolute Error	**3 Hz**	**0,484**	**0,030**	**1,633**	**217,217**	**1,300**	**1,899**	**10,725**	**0,017**

	5.0 mm	$f_0\ (N)$	$I_0\ (amp)$	$I_1\ (amp)$	a_0	$a_1(m/s)^{-1}$	$a_2(amp)^{-1}$	$a_3(m/s)^{-1}$	$a_4(m/s)^{-1}$
fmisearch	**0 A**	13,1578	-2,0354	10,7986	17,6142	12,4518	-2,0509	5,7049	5,6586
DE		13,9475	-1,9676	15	17,4394	13,1127	-1,9739	13,5673	10
Absolute Error	**5 Hz**	**0,790**	**0,068**	**4,201**	**0,175**	**0,661**	**0,077**	**7,862**	**4,341**

Table 20 - *Hysteresis Parameters (Displacement 2.5 mm and 0 A)*

	5.0 mm	k_0	k_{1c}	k_{1e}	k_2	k_3	k_4	k_5	k_6
fmisearch	**0 A**	-132,6445	16,4691	8,3742	34,0324	9,1374	-0,1683	0,5951	0
DE		-132,2764	15	8,2248	46,8741	8,8788	-0,1683	0,5871	0
Absolute Error	**1 Hz**	**0,368**	**1,469**	**0,149**	**12,842**	**0,259**	**0,000**	**0,008**	**0,000**

	5.0 mm	k_0	k_{1c}	k_{1e}	k_2	k_3	k_4	k_5	k_6
fmisearch	**0 A**	-50,6659	19,8732	5,1113	8,0089	32,2462	-0,0766	0,5837	0,0216
DE		-39,0015	8	4,2651	35,3051	-43,8664	-0,0777	0,4376	0
Absolute Error	**3 Hz**	**11,664**	**11,873**	**0,846**	**27,296**	**76,113**	**0,001**	**0,146**	**0,022**

	5.0 mm	k_0	k_{1c}	k_{1e}	k_2	k_3	k_4	k_5	k_6
fmisearch	**0 A**	-4,1041	7,2563	3,9698	576,4257	1222,9115	-0,1781	0,3556	0,0186
DE		-3,7027	4,6859	3,2941	676,8255	700	-0,1657	0,305	0,0142
Absolute Error	**5 Hz**	**0,401**	**2,570**	**0,676**	**100,400**	**522,912**	**0,012**	**0,051**	**0,004**

Table 21 - *Physical Constants (Displacement 7.5 mm and 0 A)*

	7.5 mm	$f_0\ (N)$	$I_0\ (amp)$	$I_1\ (amp)$	a_0	$a_1(m/s)^{-1}$	$a_2(amp)^{-1}$	$a_3(m/s)^{-1}$	$a_4(m/s)^{-1}$
fmisearch	**0 A**	13,9565	3,3217	144,5684	-36,2256	30,441	-1418,0483	521,9166	13,4778
DE		13,995	2,8756	146,4299	-35,9536	30,4799	-1556,4617	497,795	13,4885
Absolute Error	**1 Hz**	**0,038**	**0,446**	**1,862**	**0,272**	**0,039**	**138,413**	**24,122**	**0,011**

	7.5 mm	$f_0\ (N)$	$I_0\ (amp)$	$I_1\ (amp)$	a_0	$a_1(m/s)^{-1}$	$a_2(amp)^{-1}$	$a_3(m/s)^{-1}$	$a_4(m/s)^{-1}$
fmisearch	**0 A**	36,9584	1,1972	15,9384	10,0302	-0,1287	11,1264	-1,4908	-5,4115
DE		39,7856	3,4133	15	10	-0,0794	11,6943	-0,7426	-3,943
Absolute Error	**3 Hz**	**2,827**	**2,216**	**0,938**	**0,030**	**0,049**	**0,568**	**0,748**	**1,469**

	7.5 mm	$f_0\ (N)$	$I_0\ (amp)$	$I_1\ (amp)$	a_0	$a_1(m/s)^{-1}$	$a_2(amp)^{-1}$	$a_3(m/s)^{-1}$	$a_4(m/s)^{-1}$
fmisearch	**0 A**	48,5887	-19,504	52,4888	15,6563	-0,3815	-9,9161	-56,3861	3,1763
DE		41,1451	2,7895	4,8102	10	0,6562	-12,3317	-15	4,2263
Absolute Error	**5 Hz**	**7,444**	**22,294**	**47,679**	**5,656**	**1,038**	**2,416**	**41,386**	**1,050**

Table 22 - *Hysteresis Parameters (Displacement 7.5 mm and 0 A)*

	7.5 mm	k_0	k_{1c}	k_{1e}	k_2	k_3	k_4	k_5	k_6
fmisearch	**0 A**	-25,7645	22,3601	3,9908	4692,1982	6290,5804	-0,1116	0,8814	-0,0028
DE		-25,7595	24,2509	3,6873	4000	5074,6564	-0,111	0,8843	0
Absolute Error	**1 Hz**	0,005	1,891	0,304	692,198	1215,924	0,001	0,003	0,003

	7.5 mm	k_0	k_{1c}	k_{1e}	k_2	k_3	k_4	k_5	k_6
fmisearch	**0 A**	-6,3974	17,8639	1,3244	1312,2442	11,5663	-0,01986	0,8647	0,01253
DE		-6,2371	11,5596	1,3831	-304,2792	5,2786	-0,0236	0,796	0,0092
Absolute Error	**3 Hz**	**0,160**	**6,304**	**0,059**	**1616,523**	**6,288**	**0,004**	**0,069**	**0,003**

	7.5 mm	k_0	k_{1c}	k_{1e}	k_2	k_3	k_4	k_5	k_6
fmisearch	**0 A**	-1,9371	0,929	2,5525	-784,1384	-260,5154	-0,3236	0,4939	-0,1206
DE		-2,6492	14,8761	1,8139	-78,1658	-20	-0,2914	0,7211	0
Absolute Error	**5 Hz**	**0,712**	**13,947**	**0,739**	**705,973**	**240,515**	**0,032**	**0,227**	**0,121**

Table 23 - *Physical Constants (Displacement 2.5 mm and 0.5 A)*

	2.5 mm	$f_0\ (N)$	$I_0\ (amp)$	$I_1\ (amp)$	a_0	$a_1(m/s)^{-1}$	$a_2(amp)^{-1}$	$a_3(m/s)^{-1}$	$a_4(m/s)^{-1}$
fmisearch	**0 A**	13,355	0,02	-0,1997	-1276,2485	10,9136	-6,1439	-0,1785	43,844
DE		22,8	-0,1	5	-2411,5	-8,5	-6	-5	28,6
Absolute Error	**1 Hz**	**9,445**	**0,120**	**5,200**	**1135,252**	**19,414**	**0,144**	**4,822**	**15,244**

	2.5 mm	$f_0\ (N)$	$I_0\ (amp)$	$I_1\ (amp)$	a_0	$a_1(m/s)^{-1}$	$a_2(amp)^{-1}$	$a_3(m/s)^{-1}$	$a_4(m/s)^{-1}$
fmisearch	**0 A**	10,0413	0,2057	1,1787	1011,098	-9,2809	4,8845	-9,0976	8,1576
DE		9,9914	0,205	0,8663	992,9712	-8,749	4,9745	-10	7,7142
Absolute Error	**3 Hz**	**0,050**	**0,001**	**0,312**	**18,127**	**0,532**	**0,090**	**0,902**	**0,443**

	2.5 mm	$f_0\ (N)$	$I_0\ (amp)$	$I_1\ (amp)$	a_0	$a_1(m/s)^{-1}$	$a_2(amp)^{-1}$	$a_3(m/s)^{-1}$	$a_4(m/s)^{-1}$
fmisearch	**0 A**	8,5352	-0,2657	0,8499	-265,5703	-20,2994	7,0697	8,9875	8,1642
DE		8,6868	-0,2791	0,8877	-258,4893	-19,8431	7,1568	10	8,8824
Absolute Error	**5 Hz**	**0,152**	**0,013**	**0,038**	**7,081**	**0,456**	**0,087**	**1,013**	**0,718**

Table 24 - *Hysteresis Parameters (Displacement 2.5 mm and 0.5 A)*

	2.5 mm	k_0	k_{1c}	k_{1e}	k_2	k_3	k_4	k_5	k_6
fmisearch	**0 A**	183,8416	5,2105	24,7304	47,1201	-11,2777	-0,1897	0,0447	-0,0104
DE		413,9	9,8	12,3	24,5	-10	-0,2	0	0
Absolute Error	**1 Hz**	**230,058**	**4,590**	**12,430**	**22,620**	**1,278**	**0,010**	**0,045**	**0,010**

	2.5 mm	k_0	k_{1c}	k_{1e}	k_2	k_3	k_4	k_5	k_6
fmisearch	**0 A**	120,1364	10,0054	8,1781	148,92	7,3218	-0,2564	0,04	0,0141
DE		118,6437	10	7,3233	150	8,8805	-0,2547	0,0502	0,0168
Absolute Error	**3 Hz**	**1,493**	**0,005**	**0,855**	**1,080**	**1,559**	**0,002**	**0,010**	**0,003**

	2.5 mm	k_0	k_{1c}	k_{1e}	k_2	k_3	k_4	k_5	k_6
fmisearch	**0 A**	21,5153	7,9887	6,0157	-86,8191	5,507	-0,2612	-0,048	0,0196
DE		22,1482	6,7911	5,1717	-87,4556	5,4942	-0,2594	-0,0469	0,0202
Absolute Error	**5 Hz**	**0,633**	**1,198**	**0,844**	**0,636**	**0,013**	**0,002**	**0,001**	**0,001**

Table 25 - *Physical Constants (Displacement 5.0 mm and 0.5 A)*

	5.0 mm	$f_0\ (N)$	$I_0\ (amp)$	$I_1\ (amp)$	a_0	$a_1(m/s)^{-1}$	$a_2(amp)^{-1}$	$a_3(m/s)^{-1}$	$a_4(m/s)^{-1}$
fmisearch	**0 A**	16,8288	0,591	0,7688	-10,0621	0,6226	-1,6971	-8,1993	-14,6664
DE		16,8748	0,5961	0,7706	-10	0,6146	-1,7017	-8,2487	-15
Absolute Error	**1 Hz**	**0,046**	**0,005**	**0,002**	**0,062**	**0,008**	**0,005**	**0,049**	**0,334**

	5.0 mm	$f_0\ (N)$	$I_0\ (amp)$	$I_1\ (amp)$	a_0	$a_1(m/s)^{-1}$	$a_2(amp)^{-1}$	$a_3(m/s)^{-1}$	$a_4(m/s)^{-1}$
fmisearch	**0 A**	6,9723	-0,4024	3,9965	4293,5162	4,5957	-4,6364	-33,5663	-4,5612
DE		5,6512	-0,3565	0,9755	2500	2	-3,2872	10	6,8574
Absolute Error	**3 Hz**	**1,321**	**0,046**	**3,021**	**1793,516**	**2,596**	**1,349**	**43,566**	**11,419**

	5.0 mm	$f_0\ (N)$	$I_0\ (amp)$	$I_1\ (amp)$	a_0	$a_1(m/s)^{-1}$	$a_2(amp)^{-1}$	$a_3(m/s)^{-1}$	$a_4(m/s)^{-1}$
fmisearch	**0 A**	20,1464	0,5946	-0,9116	-2490,129	-0,2784	-1,5091	7,0114	8,3585
DE		20	0,5806	-1	-2500	-0,2704	-1,6136	7,7121	8,9641
Absolute Error	**5 Hz**	**0,146**	**0,014**	**0,088**	**9,870**	**0,008**	**0,105**	**0,701**	**0,606**

Table 26 - *Hysteresis Parameters (Displacement 5.0 mm and 0.5 A)*

	5.0 mm	k_0	k_{1c}	k_{1e}	k_2	k_3	k_4	k_5	k_6
fmisearch	**0 A**	-30,3898	3,3457	3,342	140,5533	10,0263	-0,2021	-0,0436	0,0156
DE		-30,4074	3,129	3,6721	140,7609	10	-0,2004	-0,0393	0,0162
Absolute Error	**1 Hz**	**0,018**	**0,217**	**0,330**	**0,208**	**0,026**	**0,002**	**0,004**	**0,001**

	5.0 mm	k_0	k_{1c}	k_{1e}	k_2	k_3	k_4	k_5	k_6
fmisearch	**0 A**	451,5344	1,9368	1,0986	-75,5504	-6,6065	-0,1871	0,0809	0,0227
DE		255,1377	3,9718	5	-134,8579	1,9139	-0,1998	0,0234	0
Absolute Error	**3 Hz**	**196,397**	**2,035**	**3,901**	**59,308**	**8,520**	**0,013**	**0,058**	**0,023**

	5.0 mm	k_0	k_{1c}	k_{1e}	k_2	k_3	k_4	k_5	k_6
fmisearch	**0 A**	-263,4564	5,7221	2,8734	-134,5452	-0,7388	-0,1602	0,0822	0,0253
DE		-277,1413	5	2,3553	-135,3305	-0,7944	-0,1554	0,0728	0,0232
Absolute Error	**5 Hz**	**13,685**	**0,722**	**0,518**	**0,785**	**0,056**	**0,005**	**0,009**	**0,002**

Table 27 - *Physical Constants (Displacement 7.5 mm and 0.5 A)*

	7.5 mm	$f_0\ (N)$	$I_0\ (amp)$	$I_1\ (amp)$	a_0	$a_1(m/s)^{-1}$	$a_2(amp)^{-1}$	$a_3(m/s)^{-1}$	$a_4(m/s)^{-1}$
fmisearch	**0 A**	57,466	-9,6048	0,8527	990,7987	45,7139	-10,1378	-8,5264	-1,4579
DE		57,3634	-9,1735	0,8483	991,3431	45,6873	-9,6336	-8,4224	-1,5371
Absolute Error	**1 Hz**	**0,103**	**0,431**	**0,004**	**0,544**	**0,027**	**0,504**	**0,104**	**0,079**

	7.5 mm	$f_0\ (N)$	$I_0\ (amp)$	$I_1\ (amp)$	a_0	$a_1(m/s)^{-1}$	$a_2(amp)^{-1}$	$a_3(m/s)^{-1}$	$a_4(m/s)^{-1}$
fmisearch	**0 A**	8,4749	-42,4761	-0,3266	-3441,085	30,2105	0,1796	12,746	13,1961
DE		8,6574	-10	-0,8656	-4000	30	9,4317	9,4929	12,3846
Absolute Error	**3 Hz**	**0,183**	**32,476**	**0,539**	**558,914**	**0,211**	**9,252**	**3,253**	**0,811**

	7.5 mm	$f_0\ (N)$	$I_0\ (amp)$	$I_1\ (amp)$	a_0	$a_1(m/s)^{-1}$	$a_2(amp)^{-1}$	$a_3(m/s)^{-1}$	$a_4(m/s)^{-1}$
fmisearch	**0 A**	9,4367	-33,4192	0,3725	7072,4184	16,6357	-1,161	11,4772	3,2693
DE		10	-6,7938	1	4000	16,1014	-10	5,357	6,4739
Absolute Error	**5 Hz**	**0,563**	**26,625**	**0,628**	**3072,418**	**0,534**	**8,839**	**6,120**	**3,205**

Table 28 - *Hysteresis Parameters (Displacement 7.5 mm and 0.5 A)*

	7.5 mm	k_0	k_{1c}	k_{1e}	k_2	k_3	k_4	k_5	k_6
fmisearch	**0 A**	86,1568	4,953	2,8168	-86,5839	-5,2597	-0,163	0,1313	0,0199
DE		85,3701	5	2,8825	-87,9637	-5,0043	-0,1638	0,132	0,0198
Absolute Error	**1 Hz**	**0,787**	**0,047**	**0,066**	**1,380**	**0,255**	**0,001**	**0,001**	**0,000**

	7.5 mm	k_0	k_{1c}	k_{1e}	k_2	k_3	k_4	k_5	k_6
fmisearch	**0 A**	-303,3774	19,291	9,5091	-161,4035	-0,5731	-0,2481	0,1354	0,0192
DE		-350	15	10	-84,4376	-4,7401	-0,1414	0,1019	0
Absolute Error	**3 Hz**	**46,623**	**4,291**	**0,491**	**76,966**	**4,167**	**0,107**	**0,034**	**0,019**

	7.5 mm	k_0	k_{1c}	k_{1e}	k_2	k_3	k_4	k_5	k_6
fmisearch	**0 A**	636,7583	5,40003	4,1027	-208,3809	-19,9968	-0,3014	0,1295	-0,0386
DE		326,9108	15	10	-100	-8,7761	-0,2398	0,1605	0
Absolute Error	**5 Hz**	**309,848**	**9,600**	**5,897**	**108,381**	**11,221**	**0,062**	**0,031**	**0,039**

Table 29 - *Physical Constants (Displacement 2.5 mm and 1.0 A)*

	2.5 mm	$f_0\ (N)$	$I_0\ (amp)$	$I_1\ (amp)$	a_0	$a_1(m/s)^{-1}$	$a_2(amp)^{-1}$	$a_3(m/s)^{-1}$	$a_4(m/s)^{-1}$
fmisearch	**0 A**	6,624	-0,168	0,969	-1541,4195	-17,8797	-8,038	-1,7045	-0,0248
DE	**1 Hz**	6,5206	-0,2941	0,8328	-1212,1847	-30	-9,4154	-10	2,4302
Absolute Error		**0,103**	**0,126**	**0,136**	**329,235**	**12,120**	**1,377**	**8,296**	**2,455**

	2.5 mm	$f_0\ (N)$	$I_0\ (amp)$	$I_1\ (amp)$	a_0	$a_1(m/s)^{-1}$	$a_2(amp)^{-1}$	$a_3(m/s)^{-1}$	$a_4(m/s)^{-1}$
fmisearch	**0 A**	28,9067	0,0469	0,959	-4870,146	2,1133	0,6168	-6,4475	45,039
DE	**3 Hz**	30	0,0585	1	-4000	1,9951	0,6324	-10	42,2761
Absolute Error		**1,093**	**0,012**	**0,041**	**870,146**	**0,118**	**0,016**	**3,553**	**2,763**

	2.5 mm	$f_0\ (N)$	$I_0\ (amp)$	$I_1\ (amp)$	a_0	$a_1(m/s)^{-1}$	$a_2(amp)^{-1}$	$a_3(m/s)^{-1}$	$a_4(m/s)^{-1}$
fmisearch	**0 A**	13,3321	0,8331	0,9776	101,0989	-9,9742	-2,2515	-8,1764	9,9027
DE	**5 Hz**	13,3472	0,8389	1	100	-8,821	-2,2525	-8,4067	9,9468
Absolute Error		**0,015**	**0,006**	**0,022**	**1,099**	**1,153**	**0,001**	**0,230**	**0,044**

Table 30 - *Hysteresis Parameters (Displacement 2.5 mm and 1.0 A)*

	2.5 mm	k_0	k_{1c}	k_{1e}	k_2	k_3	k_4	k_5	k_6
fmisearch	**0 A**	-396,3713	14,6026	18,0758	-97,2071	-0,5992	-0,2833	-0,01093	0,018
DE	**1 Hz**	-350	7,78	9,6956	-100	-0,9278	-0,2936	-0,0085	0,0101
Absolute Error		**46,371**	**6,823**	**8,380**	**2,793**	**0,329**	**0,010**	**0,002**	**0,008**

	2.5 mm	k_0	k_{1c}	k_{1e}	k_2	k_3	k_4	k_5	k_6
fmisearch	**0 A**	-844,6408	45,8311	48,6343	105,6248	-32,0906	-0,318	0,00065	0,0102
DE	**3 Hz**	-800	25,3561	31,5754	107,8727	-40	-0,3315	-0,0006	0,0072
Absolute Error		**44,641**	**20,475**	**17,059**	**2,248**	**7,909**	**0,014**	**0,001**	**0,003**

	2.5 mm	k_0	k_{1c}	k_{1e}	k_2	k_3	k_4	k_5	k_6
fmisearch	**0 A**	3,4594	8,1213	6,4508	-460,3568	-8,5108	-0,343	0,0335	0,0189
DE	**5 Hz**	3,5517	8,7165	6,0067	-457,7227	-8,5301	-0,3423	0,0376	0,0169
Absolute Error		**0,092**	**0,595**	**0,444**	**2,634**	**0,019**	**0,001**	**0,004**	**0,002**

Table 31 - *Physical Constants (Displacement 5.0 mm and 1.0 A)*

	5.0 mm	$f_0\ (N)$	$I_0\ (amp)$	$I_1\ (amp)$	a_0	$a_1(m/s)^{-1}$	$a_2(amp)^{-1}$	$a_3(m/s)^{-1}$	$a_4(m/s)^{-1}$
fmisearch	**0 A**	29,6255	0,6455	0,1814	-920,6681	1,1534	30,2999	-3,0912	5,3455
DE		29,9595	0,5	0,2049	-901,7662	1,2484	24,3987	-3,4362	6,2339
Absolute Error	**1 Hz**	**0,334**	**0,146**	**0,024**	**18,902**	**0,095**	**5,901**	**0,345**	**0,888**

	5.0 mm	$f_0\ (N)$	$I_0\ (amp)$	$I_1\ (amp)$	a_0	$a_1(m/s)^{-1}$	$a_2(amp)^{-1}$	$a_3(m/s)^{-1}$	$a_4(m/s)^{-1}$
fmisearch	**0 A**	10,6497	0,1089	0,4123	-478,8665	17,5909	0,0249	-6,0363	-0,0167
DE		11,1337	0,079	-1,2207	-261,6497	18,891	-1,8743	4,6889	0
Absolute Error	**3 Hz**	**0,484**	**0,030**	**1,633**	**217,217**	**1,300**	**1,899**	**10,725**	**0,017**

	5.0 mm	$f_0\ (N)$	$I_0\ (amp)$	$I_1\ (amp)$	a_0	$a_1(m/s)^{-1}$	$a_2(amp)^{-1}$	$a_3(m/s)^{-1}$	$a_4(m/s)^{-1}$
fmisearch	**0 A**	13,1578	-2,0354	10,7986	17,6142	12,4518	-2,0509	5,7049	5,6586
DE		13,9475	-1,9676	15	17,4394	13,1127	-1,9739	13,5673	10
Absolute Error	**5 Hz**	**0,790**	**0,068**	**4,201**	**0,175**	**0,661**	**0,077**	**7,862**	**4,341**

Table 32 - *Hysteresis Parameters (Displacement 5.0 mm and 1.0 A)*

	5.0 mm	k_0	k_{1c}	k_{1e}	k_2	k_3	k_4	k_5	k_6
fmisearch	**0 A**	-132,6445	16,4691	8,3742	34,0324	9,1374	-0,1683	0,5951	0
DE		-132,2764	15	8,2248	46,8741	8,8788	-0,1683	0,5871	0
Absolute Error	**1 Hz**	**0,368**	**1,469**	**0,149**	**12,842**	**0,259**	**0,000**	**0,008**	**0,000**

	5.0 mm	k_0	k_{1c}	k_{1e}	k_2	k_3	k_4	k_5	k_6
fmisearch	**0 A**	-50,6659	19,8732	5,1113	8,0089	32,2462	-0,0766	0,5837	0,0216
DE		-39,0015	8	4,2651	35,3051	-43,8664	-0,0777	0,4376	0
Absolute Error	**3 Hz**	**11,664**	**11,873**	**0,846**	**27,296**	**76,113**	**0,001**	**0,146**	**0,022**

	5.0 mm	k_0	k_{1c}	k_{1e}	k_2	k_3	k_4	k_5	k_6
fmisearch	**0 A**	-4,1041	7,2563	3,9698	576,4257	1222,9115	-0,1781	0,3556	0,0186
DE		-3,7027	4,6859	3,2941	676,8255	700	-0,1657	0,305	0,0142
Absolute Error	**5 Hz**	**0,401**	**2,570**	**0,676**	**100,400**	**522,912**	**0,012**	**0,051**	**0,004**

Table 33 - *Physical Constants (Displacement 7.5 mm and 1.0 A)*

	7.5 mm	$f_0\ (N)$	$I_0\ (amp)$	$I_1\ (amp)$	a_0	$a_1(m/s)^{-1}$	$a_2(amp)^{-1}$	$a_3(m/s)^{-1}$	$a_4(m/s)^{-1}$
fmisearch	**0 A**	58,9993	11,0539	5,1908	109,3486	50,9355	-0,3835	-6,9848	5,5349
DE		59,9195	11,1631	3,7058	132,956	50	-0,409	-10	4,7631
Absolute Error	**1 Hz**	**0,920**	**0,109**	**1,485**	**23,607**	**0,935**	**0,026**	**3,015**	**0,772**

	7.5 mm	$f_0\ (N)$	$I_0\ (amp)$	$I_1\ (amp)$	a_0	$a_1(m/s)^{-1}$	$a_2(amp)^{-1}$	$a_3(m/s)^{-1}$	$a_4(m/s)^{-1}$
fmisearch	**0 A**	47,3781	-18,1367	-2,1385	-3371,553	21,1848	0,5506	-6,8914	13,9636
DE		46,2045	-15	-5	-3000	21,3637	6,0457	-10	15
Absolute Error	**3 Hz**	**1,174**	**3,137**	**2,862**	**371,553**	**0,179**	**5,495**	**3,109**	**1,036**

	7.5 mm	$f_0\ (N)$	$I_0\ (amp)$	$I_1\ (amp)$	a_0	$a_1(m/s)^{-1}$	$a_2(amp)^{-1}$	$a_3(m/s)^{-1}$	$a_4(m/s)^{-1}$
fmisearch	**0 A**	46,296	0,4224	-1,0237	0,0043	11,564	-19,4095	-33,9762	8,9902
DE		60	8,9141	-5	1553,8023	10,4793	-7,5002	-10	8,7615
Absolute Error	**5 Hz**	**13,704**	**8,492**	**3,976**	**1553,798**	**1,085**	**11,909**	**23,976**	**0,229**

Table 34 - *Hysteresis Parameters (Displacement 7.5 mm and 1.0 A)*

	7.5 mm	k_0	k_{1c}	k_{1e}	k_2	k_3	k_4	k_5	k_6
fmisearch	**0 A**	-8,7308	5,9892	4,6294	-62,6504	4,5873	-0,1981	0,0873	0,0172
DE		-7,5822	8,6742	7,4046	-64,7773	5,1341	-0,2071	0,0805	0,0121
Absolute Error	**1 Hz**	**1,149**	**2,685**	**2,775**	**2,127**	**0,547**	**0,009**	**0,007**	**0,005**

	7.5 mm	k_0	k_{1c}	k_{1e}	k_2	k_3	k_4	k_5	k_6
fmisearch	**0 A**	-328,9064	18,4291	10,5664	-156,6766	9,3526	-0,1538	0,0991	0,0135
DE		-297,4245	17,4562	14,6865	-100	20	-0,1531	0,0632	0
Absolute Error	**3 Hz**	**31,482**	**0,973**	**4,120**	**56,677**	**10,647**	**0,001**	**0,036**	**0,014**

	7.5 mm	k_0	k_{1c}	k_{1e}	k_2	k_3	k_4	k_5	k_6
fmisearch	**0 A**	-4,2437	16,6544	16,3655	-193,2744	0,5326	-0,3042	0,0685	-0,054
DE		-153,0738	20	15	-60,5428	-20	-0,2515	0,1292	0
Absolute Error	**5 Hz**	**148,830**	**3,346**	**1,366**	**132,732**	**20,533**	**0,053**	**0,061**	**0,054**

Table 35 - *Physical Constants (Displacement 2.5 mm and 1.5 A)*

	2.5 mm	$f_0\ (N)$	$I_0\ (amp)$	$I_1\ (amp)$	a_0	$a_1(m/s)^{-1}$	$a_2(amp)^{-1}$	$a_3(m/s)^{-1}$	$a_4(m/s)^{-1}$
fmisearch	**0 A**	14,5939	-1,5	0,8918	1387,3688	-19,6472	-0,6091	4,2536	-48,3863
DE	**1 Hz**	15	-1,351	4,0736	1521,5	-20	-0,6089	8,1728	-43,6564
Absolute Error		**0,406**	**0,149**	**3,182**	**134,131**	**0,353**	**0,000**	**3,919**	**4,730**

	2.5 mm	$f_0\ (N)$	$I_0\ (amp)$	$I_1\ (amp)$	a_0	$a_1(m/s)^{-1}$	$a_2(amp)^{-1}$	$a_3(m/s)^{-1}$	$a_4(m/s)^{-1}$
fmisearch	**0 A**	9,7955	0,4354	0,8346	150,9803	50,167	-4,9613	0,704	44,285
DE	**3 Hz**	9,9917	0,4345	0,8577	150	50	-4,9364	0,7541	45,535
Absolute Error		**0,196**	**0,001**	**0,023**	**0,980**	**0,167**	**0,025**	**0,050**	**1,250**

	2.5 mm	$f_0\ (N)$	$I_0\ (amp)$	$I_1\ (amp)$	a_0	$a_1(m/s)^{-1}$	$a_2(amp)^{-1}$	$a_3(m/s)^{-1}$	$a_4(m/s)^{-1}$
fmisearch	**0 A**	12,0907	0,9011	-0,0067	77,6908	5,5674	2,1342	0,1672	9,345
DE	**5 Hz**	3,0358	-0,6747	1	88,1339	0,0472	4,3561	0,3951	1,7923
Absolute Error		**9,055**	**1,576**	**1,007**	**10,443**	**5,520**	**2,222**	**0,228**	**7,553**

Table 36 - *Hysteresis Parameters (Displacement 2.5 mm and 1.5 A)*

	2.5 mm	k_0	k_{1c}	k_{1e}	k_2	k_3	k_4	k_5	k_6
fmisearch	**0 A**	-353,556	9,535	12,7113	179,6432	-0,5571	-0,3356	0,01582	0,0043
DE	**1 Hz**	-378,1301	10	13,7047	172,2363	-3,9066	-0,3325	0,0203	0,0019
Absolute Error		**24,574**	**0,465**	**0,993**	**7,407**	**3,350**	**0,003**	**0,004**	**0,002**

	2.5 mm	k_0	k_{1c}	k_{1e}	k_2	k_3	k_4	k_5	k_6
fmisearch	**0 A**	5,1367	58,3436	47,6644	-88,8607	-3,2251	-1,0055	0,0422	0,02
DE	**3 Hz**	5	60	48,6269	-87,6466	-3,1531	-1	0,0394	0,0155
Absolute Error		**0,137**	**1,656**	**0,962**	**1,214**	**0,072**	**0,006**	**0,003**	**0,005**

	2.5 mm	k_0	k_{1c}	k_{1e}	k_2	k_3	k_4	k_5	k_6
fmisearch	**0 A**	0,1257	8,7951	6,2511	314,9802	-2,983	-0,4715	0,0537	0,0234
DE	**5 Hz**	-1	7,8382	3,6344	194,693	-5	-1	0,1126	0,0279
Absolute Error		**1,126**	**0,957**	**2,617**	**120,287**	**2,017**	**0,529**	**0,059**	**0,005**

Table 37 - *Physical Constants (Displacement 5.0 mm and 1.5 A)*

	5.0 mm	$f_0\ (N)$	$I_0\ (amp)$	$I_1\ (amp)$	a_0	$a_1(m/s)^{-1}$	$a_2(amp)^{-1}$	$a_3(m/s)^{-1}$	$a_4(m/s)^{-1}$
fmisearch	**0 A**	1,7145	-0,0015	0,9534	217,9941	-5,3391	1,97	-0,0458	11,9741
DE	**1 Hz**	1,7496	-0,0056	0,9225	206,2941	-5,3188	2,06	-0,0371	17,2276
Absolute Error		**0,035**	**0,004**	**0,031**	**11,700**	**0,020**	**0,090**	**0,009**	**5,254**

	5.0 mm	$f_0\ (N)$	$I_0\ (amp)$	$I_1\ (amp)$	a_0	$a_1(m/s)^{-1}$	$a_2(amp)^{-1}$	$a_3(m/s)^{-1}$	$a_4(m/s)^{-1}$
fmisearch	**0 A**	4,0532	0,6629	-0,1745	79,6552	-9,2728	-3,6794	0,264	7,0678
DE	**3 Hz**	4,1431	0,6467	-0,2689	77,9003	-7,6813	-3,8521	0,2688	5
Absolute Error		**0,090**	**0,016**	**0,094**	**1,755**	**1,592**	**0,173**	**0,005**	**2,068**

Table 38 - *Hysteresis Parameters (Displacement 5.0 mm and 1.5 A)*

	5.0 mm	k_0	k_{1c}	k_{1e}	k_2	k_3	k_4	k_5	k_6
fmisearch	**0 A**	0,4675	12,6939	10,2487	711,4982	-4,7924	-0,2275	0,0649	0,0199
DE	**1 Hz**	0,375	10	10	719,1883	-4,7335	-0,2261	0,0461	0,0128
Absolute Error		**0,093**	**2,694**	**0,249**	**7,690**	**0,059**	**0,001**	**0,019**	**0,007**

	5.0 mm	k_0	k_{1c}	k_{1e}	k_2	k_3	k_4	k_5	k_6
fmisearch	**0 A**	-0,414	6,5777	3,7692	-2430,5846	-4,817	-0,467	0,088	0,0224
DE	**3 Hz**	-0,3951	7	5	-2197,9	-3,7304	-0,3771	0,1	0,0421
Absolute Error		**0,019**	**0,422**	**1,231**	**232,685**	**1,087**	**0,090**	**0,012**	**0,020**

Table 39 - *Physical Constants (Displacement 7.5 mm and 1.5 A)*

	7.5 mm	$f_0\ (N)$	$I_0\ (amp)$	$I_1\ (amp)$	a_0	$a_1(m/s)^{-1}$	$a_2(amp)^{-1}$	$a_3(m/s)^{-1}$	$a_4(m/s)^{-1}$
fmisearch	**0 A**	6,634	-0,1917	-0,289	-37,2851	0,1162	2,4914	0,1553	-5,5404
DE	**1 Hz**	5	-0,1788	-1	-15	3,5366	4,5344	0,2295	3,9599
Absolute Error		**1,634**	**0,013**	**0,711**	**22,285**	**3,420**	**2,043**	**0,074**	**9,500**

	7.5 mm	$f_0\ (N)$	$I_0\ (amp)$	$I_1\ (amp)$	a_0	$a_1(m/s)^{-1}$	$a_2(amp)^{-1}$	$a_3(m/s)^{-1}$	$a_4(m/s)^{-1}$
fmisearch	**0 A**	5,6551	0,00006	-0,0996	3521,1391	18,806	4,2912	-2,627	11,6694
DE	**3 Hz**	7	-0,3	0	3491,6	14,6	4,9	-1,6	8,2
Absolute Error		**1,345**	**0,300**	**0,100**	**29,539**	**4,206**	**0,609**	**1,027**	**3,469**

Table 40 - *Hysteresis Parameters (Displacement 7.5 mm and 1.5 A)*

	7.5 mm	k_0	k_{1c}	k_{1e}	k_2	k_3	k_4	k_5	k_6
fmisearch	**0 A**	-17,0379	4,0717	2,6228	-137,1178	-11,1536	-0,6046	-0,1054	0,0184
DE		-19,7769	9,5467	5	-130,9403	-6,1686	-0,4599	0,1231	0
Absolute Error	**1 Hz**	**2,739**	**5,475**	**2,377**	**6,177**	**4,985**	**0,145**	**0,229**	**0,018**

	7.5 mm	k_0	k_{1c}	k_{1e}	k_2	k_3	k_4	k_5	k_6
fmisearch	**0 A**	326,3898	13,2878	8,4861	23,7982	3,9404	0,1405	0,109	0,01126
DE		-337	8,6	4,5	21,1	-0,4	-0,1	0,1	0
Absolute Error	**3 Hz**	**663,390**	**4,688**	**3,986**	**2,698**	**4,340**	**0,241**	**0,009**	**0,011**

Appendix D - .....

ALGORITHM ROUTINES FOR MR DAMPER ANALYSIS

```
%.....
% Hysteretic Damping Behavior - MR Damper
% - Experiment with 0—1.5 A - Passive Behavior (Sinusoidal Wave)
%
% Author: Davi Matias Dutra da Silva
%%.....

% clear memory
clear all; close all; clc

%% Load Experiment Data

load('MR_Damper.mat')

%% Defining Variables

displacement1 =  MR_0A_2_5mm_1Hz (:,2);
axial_force1 =  100.00 + 1000*MR_0A_2_5mm_1Hz (:,1);
time1 = MR_0A_2_5mm_1Hz  (:,3);

%% Calculating Velocity

dt1 = time1(2)-time1(1);
velocity1 = zeros(1,length(displacement1));
velocity1(1) = (displacement1(2)-displacement1(1))/dt1;
velocity1(2:end-1) = ...
(displacement1(3:end)-displacement1(1:end-2))/(2*dt1);
velocity1(end) = (displacement1(end)-displacement1(end-1))/(dt1);

%% Sine Wave Equation - Displacement Optimization (Fminsearch)
% Frequency 1 Hz, Amplitude 2.5 mm I = 0A

% Parameters Definition

 a = 2.5;          % Amplitude (mm)
 f= 1.0;          % Frequency (Hz)
 phi = 4.4810;     % Phase

x0 = [a, f, phi];

% Parameters Definition

time_1 = time1(3000:10000);
displacement_1 = displacement1(3000:10000);
axial_force_1 = axial_force1(3000:10000);
velocity_1=velocity1(3000:10000);

% Replacing Variables in the Theoretical Equation for Displacement

theo_displacement1 = (x0(1)*sin(2*pi*x0(2)*time_1+x0(3)));

error_displacement = erro_sin(x0,displacement_1,time_1);

figure()

plot(time_1,displacement_1,'b-',time_1,theo_displacement1,'r--',time_1,error_displacement,'k:')
```

```
options = optimset('PlotFcns',@optimplotfval);

[xe,fval] = fminsearch(@(x) norm(erro_sin(x,displacement_1,time_1)),x0,options);

theo_displacement_e1 = (x0(1)*sin(2*pi*x0(2)*time_1+x0(3)));
error_te = erro_sin(xe,displacement_1,time_1);

figure(1)
plot(time_1,displacement_1,'b-',time_1,theo_displacement_e1,'r--',time_1,error_te,'k:')
%% Asymmetric Model

% SANTADE VALUES
%x = [f0 I0 I1 a0 a1 a2 a3 a4 k0 k1c k1e k2 k3 k4 k5 k6] ;
%x = [28.7 -0.199 0.492 22247 6.02 -45.8 1.450 11.65 1638 19.99 37.71 527.6 -67.9 -0.091 -0.260 0.006];

A0 = 2.5/1000 ; % Amplitude (mm)
f = 1;          % Frequency (Hz)
phi = 4.4809;   % Phase
t1 =  time_1 ;

%% Cálculo Velocidade e Força

t1 =  time_1 ;
d1 =  A0*sin(2*pi*f*t1+phi) ;                % Displacement
v1 =  A0*(2*pi*f)*cos(2*pi*f*t1+phi)  ;      % Velocity
a1 = -A0*(2*pi*f)^2*sin(2*pi*f*t1+phi) ;     % Acceleration

x = [  25.6619050296050       -0.999122025295741          0.724851411855189          14910.6454776751
          9.81575303306505 48.0248995672128 0.973123238651358          0.767702794870205
          1573.46450443553 49.2354996261320 28.0917580638950 276.669171418703 224.037622632523 -
0.116357912445695          0.305083070147038          0.00934067044941964];

Fd_i0_1Hz = mrf_sigmoid(x,d1,v1,a1,t1,Iref);    % Theoretical Force

error_force = erro_fd(x,axial_force_1,d1,v1,a1,time_1,Iref);

plot(time_1,axial_force_1,'b-',time_1,Fd_i0_1Hz,'r--',time_1,error_force,'k:')

options = optimset('PlotFcns',@optimplotfval);

[xef,fval] = fminsearch(@(x) norm(erro_fd(x,axial_force_1,d1,v1,a1,time_1,Iref)),x,options);

theo_force_e1 = mrf_sigmoid(xef,d1,v1,a1,t1,Iref);
error_fte = erro_fd(xef,axial_force_1,d1,v1,a1,time_1,Iref);

figure(1)
plot(time_1,axial_force_1,'b-',time_1,theo_force_e1,'r--',time_1,error_fte,'k:')

%% Testing for Santade Parameters

x = [28.7 -0.199 0.492 22247 6.02 -45.8 1.450 11.65 1638 19.99 37.71 527.6 -67.9 -0.091 0.260 0.006];

theo_force_2 = mrf_sigmoid(x,d1,v1,a1,t1,Iref) ;

theo_force1 = mrf_sigmoid(xef,d1,v1,a1,t1,Iref) ;

figure(1)
plot(time_1,d1_filtro1,'b-',time_1,theo_force1,'r--',time_1,axial_force_1)

figure(2)
plot(velocity_1/1000,d1_filtro1,'b:',v1,theo_force_e1,'r--',v1,theo_force_2,'b-',velocity_1/1000,axial_force_1)
```

```
%% Ploting Grafic

figure(1)
plot(time_1,axial_force_1,'b-',time_1,theo_force_e1,'r--')

figure(2)
plot(velocity_1/1000,axial_force_1,'b:',v1,theo_force_e1,v1,theo_force_2)
xlabel('Velocity [ m/s ]')
ylabel('Axial Force [N]')
legend('Experimental','Simulated')

figure(3)
plot(displacement_1,axial_force_1,'b:',theo_displacement_e1,theo_force_e1)
xlabel('Displacement [ mm ]')
ylabel('Axial Force [N]')
legend('Experimental','Simulated')


function Fd = mrf_sigmoid(x,d,v,a,t,Iref)
%MRF_SIGMOID Summary of this function goes here

% Passive Damper k4 = 0 (vh=0)
% (Symmetric f-v Model) k5=k6=0 and k1c=k1e
% vm = amplitude * frequency

f0 = x(1);
I = Iref;   % Corrente Elétrica de Excitação
I0 = x(2);  % Bias
I1 = x(3);
a0 = x(4);
a1 = x(5);
a2 = x(6);
a3 = x(7);
a4 = x(8);
k0 = x(9);
k1c = x(10);
k1e = x(11);
k2 = x(12);
k3 = x(13);
k4 = x(14);
k5 = x(15);
k6 = x(16);

%vm = max(v);
vm = sqrt((v.*v)-a.*d) ;

Fd = zeros(size(t));
for i=1:length(d)
   alph = a0/(1+k0*vm(i));
   kve   = k1e*exp(-a4*vm(i));
   kvc   = k1c*exp(-a4*vm(i));

   const21 = k2/(1+exp(-1*a2*(I+I0)));
   const22 = k2/(1+exp(-1*a2*I0));
   const31 = k3/(1+exp(-1*a3*(I+I1))) ;
   const32 = k3/(1+exp(-1*a3*I1)) ;

   vd(i) = k6*vm(i);
   vh(i) = sign(a(i))*k4.*vm(i)*(1+const31-const32);

   ft(i) = f0*(1+exp(a1*vm(i)))*(1+const21-const22);
   fd(i) = k5*ft(i);
```

```
    aux = ft(i)* ( ...
        (1-exp(-1*alph*(v(i)+vh(i)+vd(i))))/ ...
        (1+exp(-1*alph*(v(i)+vh(i)+vd(i)))) - fd(i) ;
    if (v(i)>=0)
        Fd(i) = aux*(1+(kvc*abs(v(i))));
    else
        Fd(i) = aux*(1+(kve*abs(v(i))));
    end
%
end

function error_force = erro_fd(x,force,d,v,a,t,lref)
theo_force = mrf_sigmoid(x,d,v,a,t,lref);
error_force = theo_force - force;

end
```